Fibre Optic Network Supporting High Speed Transmission in the Square Kilometre Array, South Africa

By Rotich, Enoch Kirwa

Submitted in partial fulfilment of the requirements for the degree of

Philosophiae Doctor

in the faculty of Science at

Nelson Mandela Metropolitan University (NMMU).

March 2015.

Promoter

Prof. Tim Gibbon

Co-promoters

Prof. Andrew Leitch

Dr. Romeo Gamatham

Dedication

This thesis is dedicated to my family.

"Keep your face on the light source and you will never see your shadow"

Declaration

I, *Enoch Kirwa Rotich*

Student number: *212238523*,

hereby declare that this thesis for Ph.D award is my own work and has not been previously submitted for assessment in any University for any award.

Signature .....  ....

Date .....11/03/2015.....

Acknowledgement

Terming it as a long academic trek is an obvious statement but perhaps I would erroneously convince myself that it was short because I was not a lone ranger, I wouldn't have made it on my own. The presence and valuable assistance of several people made the trek less painful and shorter. Firstly, I wish to extend my sincere gratitude to my promoter Prof. Tim Gibbon for his careful, responsible concern, straight talk, guidance, positive criticisms during my study. My co – promoters; Prof. Andrew Leitch and Dr. Romeo Gamatham, thank you so much for your time, positive suggestions and all the assistance towards this work. Am also grateful to Physics department fraternity and NMMU at large for giving me an opportunity to undertake my Ph.D. studies. Thanks to Alta Beer for her excellent services she offered to optical fibre research unit (OFRU). My former supervisors Dr. Waswa and Dr. Amolo, thanks for your moulding. Prof Xianbin Yu (DTU), thanks for your advice during your NMMU visit.

I sincerely acknowledge the research funding and support from: Telkom, Dartcom, Infinera, Ingoma Communication Services, CSIR-NLC, NRF, THRIP, OFS, ALC, Cisco, and above all scholarship funding from SKA/NRF South Africa. Thanks for making my dream a reality!

To my family, saying thank you may not be enough but I hope that it conveys the message of my heart. Your precious time, prayers, sacrifice, inspiration, guidance and all kinds of support is sincerely appreciated. Wayne Kibish and Livia, thank you so much for constantly remembering and reminding them to pray for me.

I am deeply indebted to my OFRU colleagues and other friends; Chabata, Wassin, Boiyo, Kourouma, Kwarikunda, Dr. Okello, Okullo, Simiyu, Okerio, John, Sister Ann, Kampire, Juliet, Tereziah, Jane, Makatleho, Fefe & Lucien, thanks for being there whenever. To Okello, Kwarikunda and Chabata, the routine morning/evening trainings made us 'younger'. I live to remember that.Your company was valuable. To my other friends Agnes, Dr. Mathabo, Prof. Berit, Dr. Sseviirri, Dr. Muguro, Dr. Munji, Dr. Ireeta, Dr. Okullo, Dr. Bosire & family, St. James church and an endless list of friends wherever. Your help, constant check on social media, stimulating suggestions, steadfast love, support and encouragement was valuable. I may not mention everyone by name but I appreciate *whatever*, *whoever*, *wherever* and *whenever* I needed to keep going. I appreciate each one's contribution in a special way. I thank S. Wassin, H. Kourouma and SKA engineers (R. Julie, R. Siebrits, S. Malan and H. Kriel) for their assistance on the measurements co-executed during my research

study. To each of the above, I extend my deepest appreciation and their extreme generosity will be remembered always.

Now unto him that is able to do exceeding abundantly above all that we ask or think, according to the power that worketh in us be the Glory (Eph. 3:20). He said, "Let there be light," and there was light and He saw it was good (Gen. 1:3). And so it was, just 3×10^8 m/s changed things. Thank you God for the care, love, kindness, mercies, protection and guidance.

"*Kongoi kot mising, Asanteh sana, Enkosi, Siyabonga, Dankie, Thank you*"

Enoch Kirwa Rotich Kipnoo,
March 2015.

Contents

List of Figures

List of Tables

Abstract

This thesis provides in-depth information on the high speed optical transport requirements for the Square Kilometre Array. The stringent data rates as well as timing and synchronization requirements are dealt with respect to the optical fibre technology. Regarding the data transport, we draw a clear comparison between a typical telecommunication access network and a telescope network. Invoking simulations and experiments on the field and laboratory test bed, we successfully implement a suitable telescope network using vertical cavity surface emitting laser (VCSEL) technology.

Polarization effects on the KAT-7 telescope network, an operational prototype for the SKA is studied so as to estimate the expected effect in the MeerKAT telescope with transmission distances $\leq 12\ km$. The study further relates the obtained values to the expected impact on the distribution of the time and frequency reference in the MeerKAT array. Clock stability depends on the differential group delay (DGD) and polarization stability. On a 10.25 km link that includes the riser cable a DGD of 62.1 fs was attained. This corresponds to a polarization mode dispersion (PMD) coefficient of 19.4 $fs/km^{1/2}$. This is a low PMD value considering telecommunication network. The PMD value is within the allowed budget in the telescope network. However, this may not be the case at longer baselines extending to over 1000 km as expected in SKA 2. The fibre's deployment contribution to the DGD is measured by comparing the deployed fibre to the undeployed of equal lengths. On the 10.25 km deployed single mode fibre, the maximum and mean DGDs measured were 217.7 fs and 84.8 fs respectively. The undeployed fibre of similar type and equal length, gave a maximum and minimum DGDs of 58.6 fs and 36.3 fs respectively. The deployment is seen to increase the maximum and minimum DGDs by factors of 3.7 and 2.3 respectively. This implies that fibre deployment is very critical in ensuring the birefringence is minimized. Polarization fluctuation recorded a maximum of 180^o during the 15 hour real time astronomer use of the antenna. To ascertain the contribution of the riser cable, state of polarization (SOP) of the buried section of the single mode fibre in the link was established. A maximum SOP change of 14^o over 15 hour monitoring was measured. From the stability realized on the buried section of the fibre, the change in polarization is contributed by the riser cable. The fluctuation in polarization can cause the phase of a clock signal to drift between the birefringent axes by an equal amount corresponding to DGD. We experimentally demonstrate how polarization stabilization can be

attained using the polarization maintaining fibre.

We also demonstrate the applicability of VCSEL technology in the SKA unidirectional data flow especially for shorter baselines $< 100\ km$. The VCSEL is a low cost light source with attractive advantages such as low power consumption, high speed capabilities and wavelength tuneability. This work entails the use of traditional amplitude modulation commonly known as non-return-to-zero (NRZ) on-off keying (OOK) because of its simplicity and cost. For the MeerKAT typical distances, we show that even in a worst case scenario, the use of VCSEL on different fibres in MeerKAT distance is achievable. Using the impairment reduction approach, we successfully manage to achieve transmission distance beyond MeerKAT. Several in-line dispersion compensation mechanisms in telecommunication have been successfully employed. The work focused on the use of negative dispersion fibre to mitigate the chromatic dispersion effects in the optical fibre. The inverse dispersion fibre (IDF) is proposed for compensation in the conventional zero dispersion wavelength fibres, G.652 that are used at the third window. Similarly, the chromatic dispersion compensation of non-zero dispersion shifted fibre (NZDSF) is experimentally demonstrated using negative dispersion submarine reduced slope (SRS), G. 655 (-). With dispersion management, we demonstrate how transmissions beyond MeerKAT baselines can be achieved error free.

A systematic investigation of the use of distributed Raman amplification to overcome the attenuation losses is provided. High on-off gains of up to 15 dB, 8 dB and 5 dB for bidirectional, forward and backward pumping respectively is achieved on a 25 km Raman optimized NZDSF-Reach fibre. Combined dispersion mitigation technique and low noise distributed Raman amplification, up to about 80 km transmission was achieved on a 4.25 $Gbps$ modulated VCSEL using a single pump. Using bidirectional pumping, more than 100 km of transmission was achieved error free. The high gains enhance the VCSEL transmission distance. We further suggest a novel way of using the Raman pump to distribute the clock signal while amplifying the data signal streaming the astronomical data from the remote placed telescope receivers.

In summary, the work presented in this thesis has demonstrated the potential use of VCSEL technology for data collection in the telescope array. We have studied the optical effects and mitigation so as to improve the clock and data transmission. This work is relevant and valuable in providing SKA with VCSELs, an option for extremely high network performance at reasonable costs.

KEYWORDS: *MeerKAT, square kilometre array, vertical cavity surface emitting laser, chromatic dispersion, polarization, Raman amplification, clock distribution, optical fibre network, transmission.*

List of acronyms

AA – Aperture array
ADC - Analogue to digital converter
ALMA - Atacama large millimetre array
AlGaAs – Aluminum gallium arsenide
APD – Avalanche photodiode
ASC - Antenna service container
ASKAP - Australian square kilometre array pathfinder
AWG – Arrayed waveguide grating
BER – Bit error rate
BERT - Bit error rate tester
BPSK - Binary phase shift keying
BTJ - Buried tunnel junction
CC - Computing container
CD – Chromatic dispersion
CW - Continuous wave
DBR - Distributed Bragg reflectors
DC – Direct current
DCF - Dispersion compensating fibre
DFB – Distributed feedback
DGD - Differential group delay
DOP - Degree of polarization
DRA - Distributed Raman amplification
DWDM - Dense wavelength division multiplexing
EAM – Electro absorption modulator
EDFA - Erbium doped fibre amplifier
EEL - Edge emitting lasers
ER –Extinction ratio
EVLA - Expanded very large array
EVN - European very large baseline interferometric network
FBG - Fibre Bragg grating

FP – Fabry-Perot
FSK - Frequency shift keying
FTTX - Fibre to the home/premise/building/node/hut
FUT - Fibre under test
FWM - Four-wave mixing
GaAs – Gallium arsenide
GaAlAs – Gallium aluminum arsenide
GaInAs – Gallium indium arsenide
GVD - Group-velocity dispersion
IDF - Inverse dispersion fibre
IEC - International electrotechnical commission
InAlAs – Indium-aluminum-arsenide
InAlGaAs – Indium aluminum gallium arsenide
InGaAsP – Indium gallium arsenide phosphide
InP – Indium phosphide
InPGaAs – Indium phosphide gallium arsenide
IM – Intensity modulation
ITU–T - International telecommunications union
LASER – Light amplification by stimulated emission of radiation
LDC – Laser diode controller
LED – Light emitting diode
$LiNbO_3$ – Lithium niobate
MERLIN - Multi-element radio linked interferometer network
MMF – Multimode fibre
MZM – Machzehnder modulator
NRZ – Non-return-to-zero
NZDSF - Non-zero dispersion shifted fibre
NZDSF-RS - Non-zero dispersion shifted fibre reduced slope
NZDSF-SRS - Non-zero dispersion shifted fibre submarine reduced slope
OLT – Optical line terminal
ONU - Optical network unit
OSNR - Optical signal to noise ratio
OTDR - Optical time domain reflectometer
PAM - Pulse amplitude modulation
PC – Polarization controller
PIN – Positive intrinsic negative
PMD - Polarization mode dispersion
PMF - Polarization maintaining fibre

PPG – Programmable pattern generator
QAM - Quadrature amplitude modulation
QPSK - Quadrature phase shift keying
QW – Quantum well
RDS - Relative dispersion slope
RF - Radio frequency
RFI - Radio frequency interference
ROSA - Receive optical sub-assembly
RZ – Return-to-zero
SBS - Stimulated Brillouine scattering
SKA - Square kilometre array
SMF – Single mode fibre
SOA - Semiconductor optical amplifier
SOP – State of polarization
SPM - Self-phase modulation
SRS - Stimulated Raman scattering
TDM – Time division multiplexing
TFR - Time and frequency reference
TOSA - Transmit optical sub-assembly
VCSEL - Vertical cavity surface emitting laser
WDM-PON - Wavelength division multiplexed passive optical network
XPM - Cross-phase modulation
ZDSF - Zero dispersion shifted fibre
ZDW - Zero dispersion wavelength

Chapter 1

Introduction

Tremendous evolution of optical communication and communication systems in the past century has been remarkable. This has been fostered by the ever-growing demand for bandwidths. Commercial deployment of optical fibres started in 1980s [1], the high demand enhanced fibre manufacturing technologies, development in semiconductor lasers as well as optical detectors. During this period, America for instance, had systems that operated at 90 $Mbps$. This meant each single mode fibre could simultaneously transmit only 1300 voice channels at a time. The 10 $Gbps$ optical systems improved this simultaneous voice channels by a factor of 100. The current use of dense wavelength division multiplexing (DWDM) systems translated the terabit per second transmission to over 13 million simultaneous calls over a single fibre [2]. In essence, the internet is expanding at an unprecedented rate because of the increasing number of users. Fibre to the home/premise/building/node (FTTX) which has taken shape in Asian, European and American countries entail day to day businesses, academics and individual users relying on the high speed networks to undertake their daily activities. With high demand, continuous research to develop technologies that meet the intended data rates has been inevitable. Issues relating to capacity, sensitivity and implementation in telecommunication have been overcome using modulation and multiplexing techniques. Improvement in capacity and reach relies on increase in spectral efficiency, increase in total available bandwidth and reduction in signal impairments accumulated per unit distance [3]. Spectral efficiency can be improved by using techniques that transmit more bits per symbol [4-6] but this is limited by noise and other distortions thus reducing sensitivity per bit. To overcome the sensitivity issue while achieving high spectral efficiency, use of flexible networks have been proposed [7-9]. Due to complexity and cost of advanced techniques of pushing the transmission limit, impairment reduction and use of low noise amplifiers to reduce the noise levels are key to increasing transmission capacity as well as reach in conventional methods. The developments in capacity has seen the transition from 10 G to 40 G, 40 G to 100 G, 100 G to 500 G and currently towards achieving 1 T systems. This remarkable progress is vital to major scientific projects such as astronomy.

The need to transmit enormous data rates in astronomy related projects demands efficient high speed technologies over the transmission lengths. In the past years, astronomy has relied on microwave free space technologies and coaxial copper cables for shorter transmissions or magnetic tapes for antennas distributed across continents particularly interferometers. The bandwidth of microwave systems is restricted to about 30 MHz by regulation and/or costs while copper cables are limited to about 2 km by attenuation and bandwidth of approximately 100 MHz at these distances. Magnetic tape can accommodate only up to 1 $Gbps$. Tape recording further introduce time lag between observation and correlation [10]. Recently, the fibre optic transmission is progressively replacing the old methods of transmission in astronomy except at densely populated areas where difficulty is experienced in fibre deployment due to existing infra-structure.

Fibre optic transmission exceeds the performance of other media of transmission because of the following: Firstly, an optical fibre has a higher speed and bandwidth. Speed refers to per channel data rate while bandwidth relates to the large carrying capacity. Bandwidth is the total data flow realized from the using multiple channels in an optical fibre. Fibre optic networks operate at high speeds. For instance, record transmissions achieved are 1.05 $Pbps$ over 52.4 km [11, 12], 305 $Tbps$ over 10.1 km [13], 102.3 $Tbps$ over 240 km [14], 31 $Tbps$ over 7200 km [15]. The largest operating submarine cable is the Russian optical trans arctic submarine cable system (ROTACS) at 60 $Tbps$. It connects Russia to China and Japan. Optical fibre is also immune to electromagnetic interference. It has greater resistance to electromagnetic noise and interference such as radios, motors or other nearby cables. Fibres are non-conductive, non-radiative and non-inductive. Maintenance of an optical fibre link is cheaper. Fibre optic cables costs much less to maintain though initial cost is higher. It consumes low power. Lastly, optical fibres have low losses of about 0.2 dB/km. Therefore, signals can be transmitted for longer distances without needing to be re-generated or amplifed.

Square Kilometre Array (SKA) project is of no exception in the optical fibre demand. In fact, optical fibre links form the backbone of the SKA. An optical fibre network is preferred to other media of transmission because of the above merits. To start with is the enormous data rates that are expected to stream from receptors, this requires sufficient transmission rate in addition to the bandwidth. Immunity to interference is a perfect feature suited for radio frequency interference (RFI) free environment for accurate instrument operation in the array. Regarding transmission distance, different baselines extending up to 3000 km require a low loss medium for effective transmission. The very large baseline interferometry (VLBI) linking countries and continents also require efficient means of transmission of the astronomical data. The low cost of maintenance of fibre optic cables is ideal for the SKA's magnitude.

This thesis investigates the optical technology choice suitable and appropriate for the typical SKA transmission distances especially the MeerKAT distances and beyond. Vertical cavity surface emitting laser (VCSEL) high speed transmission technology is proposed because they

are extremely cost effective, low power consuming, high bandwidth, wavelength tuneable, directly modulated and energy efficient at low drive currents and suitable for relatively short transmission distances among other advantages. Optical effects such as chromatic dispersion and polarization mode dispersion over the typical distances on different fibre types is investigated. The study demonstrates the use of negative dispersion fibre to curb the chromatic dispersion issue and improve the transmission reach. Polarization mode dispersion is a challenge in the accurate and stable distribution of the time and frequency reference (TFR) in the array. This work characterizes the deployed KAT-7 fibre network in the Karoo, South Africa so as to estimate for the expected polarization effects in the MeerKAT TFR. This is important due to the needs of the astronomers in the instrument use. Raman amplification which is attractive due to its low noise levels, high bandwidth and high gain is experimentally studied. The different pumping schemes are analysed in a laboratory optical fibre test bed. The backward pumping is implemented so as to achieve bi-directional transmission. It was used to demonstrate how a Raman pump can be used to transmit clock signal while simultaneously amplifying the digitized astronomical data.

1.1 Outline of the Thesis

This thesis is organized as follows; Chapter 1 introduces the growth of optical fibre communication and its application in the major science projects such as astronomy. Chapter 2 gives an overview of SKA with available technologies and system requirements for data and time and frequency reference (TFR) transport. It reviews the existing telescope related projects in the world. In chapter 3, state of the art of the VCSEL technology, its advantages as well as its assembly is covered. Modulation methods, optical fibres types and receivers are discussed. It further introduces the various optical effects relevant to optical network performance. These include fibre attenuation, linear (dispersion) and nonlinear processes (Raman processes) in the fibre. Chapters 4 to 7 give the findings on the various simulation and experiments performed both in the field and the laboratory. Chapter 4 gives details regarding polarization effects in the KAT-7 telescope network. It points out the differential group delay (DGD) which is a measure of polarization mode dispersion (PMD) in an optical fibre. Chapter 5 presents the characterization of VCSELs, optimization of the transmitter-pair, comparison of receivers and VCSEL driving techniques. The transmissions are narrowed to typical MeerKAT distances. Chapter 6 provides the details of chromatic dispersion in the fibre, its measurement and compensation techniques. Chapter 7 discusses Raman amplification and its use in the VCSEL technology to improve the transmission reach. Chapter 8 summarizes the findings of this thesis. It is then followed by appendices and references.

Chapter 2

Square Kilometre Array and other related projects in the world

2.1 The birth of SKA, its construction and the scientific purpose

The Square Kilometre Array (SKA) concept arose for the first time in 1991. It was not until 2000 that the first agreement between the different international groups was signed.

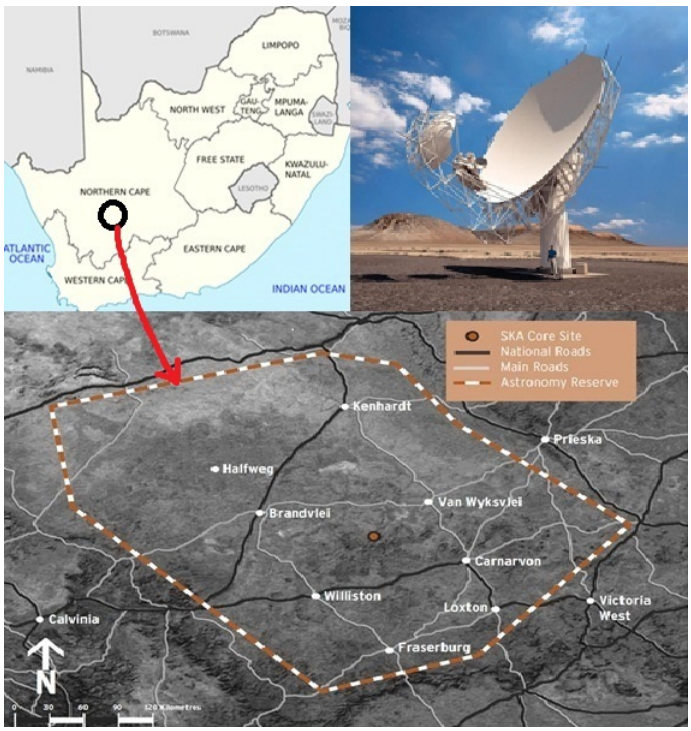

Figure 2.1: Picture showing South Africa's Karoo region of Northern Cape and the SKA astronomy reserve. Inset: a picture of MeerKAT antenna design [16].

In 2006, progress involving site selection listing was done. In 2012, after a competitive bid two sites were selected. These are the Karoo region of South Africa and the Boolardy station in Western Australia. South Africa will host the dish receivers and medium frequency aperture arrays (AAs) while Western Australia will house the low frequency aperture arrays (AAs) and SKA survey [16]. The sites were chosen based on the radio frequency interference (RFI) level and population. Radio telescopes require RFI free environment which makes sparsely or low populated areas suitable for the instrument. SKA is a proposed large radio telescope, about 100 times more sensitive than the currently existing radio telescopes in the world. The name Square Kilometre Array is derived from the total effective collection area amounting to 1 km^2. The estimated cost of SKA is about €1.5 billion. A major component of the SKA telescope array will be an extensive array of approximately 3,000 dish antennas, which will be located in the Karoo region of the Northern Cape in South Africa. Approximately half of these dishes will be concentrated in a 5 km diameter central region, while the rest will be distributed out to 3,000 km from this central core. The site location and a MeerKAT dish picture is shown in figure 2.1. Some antennas (dishes) will be housed in Namibia, Botswana, Zambia, Mozambique, Kenya, Ghana, Madagascar and Mauritius. In addition to antenna array, the mid-frequency aperture arrays (AA) to be located in Karoo, South Africa and low frequency aperture arrays as well as survey elements in Western Australia collectively make SKA astronomical instrument of frequency range 70 MHz up to 20 GHz. An artiste's picture of AA low and medium is shown in figure 2.2 (a) and (b) respectively. The 911 low frequency aperture arrays and survey elements form the Australian Square Kilometre Array pathfinder (ASKAP) project.

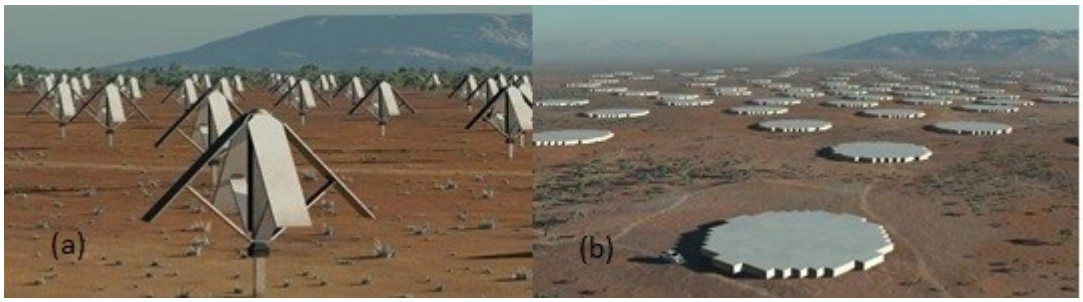

Figure 2.2: Picture of aperture arrays (a) AA-low and (b) AA-medium [16]

SKA construction is in different phases. KAT-7 array consisting of 7 functional dishes is situated at Karoo, South Africa. It is SKA prototype. The MeerKAT which is a precursor to SKA will consist of 64 dishes that are currently under construction as of 2014. The first phase of the MeerKAT comprising of 16 antennas is to be completed by end of 2015. Phase 2 consisting of the full array will be completed in 2016. Each MeerKAT antenna of an offset Gregorian type consists of a 13.5 m main reflector diameter and a sub-reflector of 3.8 m. On completion, MeerKAT will be the world's most sensitive radio interferometer in the L-Band

(1 to 2 GHz). Similarly, ASKAP and Murchison Widefield Array forms SKA precursor in Australia. MeerKAT and ASKAP through addition of receiver components will constitute SKA phase 1. For example, additional 190 dishes to the MeerKAT telescope array and establishment of medium AA antennas (SKA mid) will be part of the SKA phase 1 in South Africa. On the Australian side, 36 dish ASKAP (SKA survey) will be expanded out to 96 dishes while the low AA antennas (SKA low) increased in number. SKA phase 2 will constitute to about 3,000 dishes extending to over 1000 km. Together with medium AA antennas and additional antenna components in Australia will achieve the 1 km^2 of receiver area. The SKA timeline is provided in Appendix B of this thesis.

The SKA project will be completed in 2025 and a list of high priority science goals have been proposed. SKA is expected to transform our understanding about the physics of the universe. It will explain some fundamental issues concerning the evolution of the universe as well as prove theories of cosmic magnetism, investigate the nature of gravity, gravitational waves and predictions from Einstein's theory of general relativity. Gravitational physics will be examined through pulsar search and timing. SKA will also explain the history of star formation, galaxy existence and evolution. Moreover, it will elucidate on the dark energy and dark matter believed to be a possible cause of the mysterious acceleration and expansion of the universe. The origin and evolution of cosmic magnetism will be achieved through creation of maps of the cosmic magnets so as to infer their effect on the galaxy stabilization, influence on the star and planet formation and regulation of solar and stellar activity. SKA will probe the astrobiology and explain the origin, gradual development and apportionment of life in the universe. Through detection of very weak extraterrestrial signals, SKA will search for complex molecules and building blocks of life in space answering the possibility of life beyond the earth [16, 17].

2.2 SKA data transport requirement

Optical fibres will be used for data transfer, monitoring and control, timing and frequency reference (TFR) and external data connectivity to astronomers worldwide. A total of twenty four fibres [18] of two types (12 fibres G. 652 and 12 fibres G.655) from each antenna to the central station is planned for the MeerKAT fibre network. These fibres will be used for data transport, clock distribution, control and monitoring as well as spares. Upon completion, the dish array making use of wide field of view expansion technologies could lead to total data rates of approximately 120 $Tbps$ from the dishes for transmission and eventual processing. The total transfer of enormous amounts of information from individual dishes to a central processor after undergoing fast, high resolution sampling will produce 10 times the current global internet traffic. In the MeerKAT, each dish will stream data amounting to 40 $Gbps$ for transmission. The MeerKAT baseline is 8 km with the furthest dish about 12 km from

the Karoo processing station [19]. A baseline is defined as the longest distance between any two antennas in the array. In SKA 1 stage, each antenna will stream up to 160 *Gbps* of data pushing the data rates four times higher. Note that 120 *Tbps* is arrived at when each dish is streaming only 40 *Gbps* (MeerKAT antenna rate). Apart from the antennas, other receiver elements such as SKA 1 aperture array (AA)-low, SKA-survey and SKA 1 AA-mid are expected to stream data of ~ 9.2 *Tbps*, ~ 51.8 *Tbps* and ~ 17.1 *Tbps* respectively to the central signal processor [18]. The data rates presented may however change as these figures are only estimates, for instance 50 stations of AA-mid consisting of $11,200$ dipoles and of dual polarizations can stream up to 11 *Pbps* of data to central processor (data rate calculation given in Appendix B). For astronomer use, the data will be transported to science data processor. In South Africa, the data will be transported for 915 *km* from the correlator at Karoo to Cape Town while in Australia for 820 *km* from Murchison Radio-astronomy Observatory (MRO) to Geraldton (~ 315 *km*) and then to Perth [18].

2.3 SKA clock transport requirements

Distributing coherent and stable frequencies over an optical fibre is a vital tool in a variety of applications such as radio astronomy. Successful stable time and frequency signals sent over optical fibres have been reported. On a 4.6 *km* fibre, a fractional frequency stability of $1.7 \times 10^{-18}/\sqrt{Hz}$ for $5 - 20$ *Hz* of clock frequencies [20], 80 *MHz* of radio frequency signal achieved 6×10^{-17} over $10,000$ seconds (s) over 20 *km* of fibre [21] and a 10.03 *GHz* clock signal yielded a long term stability less than 1×10^{-16} over $10,000$ *s* over 100 *km* [22]. Timing and synchronization in the telescope networks is one of the most critical issues in the array. Time and frequency reference (TFR) signals will be distributed to each antenna using optical fibres. Clock transmission distances vary with antenna position from the processing building. SKA envisages use of intensity modulated distributed feedback (DFB) laser for its timing [18]. However, other possible options are currently under investigation by responsible consortium to provide a suitable and appropriate solution. DFB is suited for up to 80 *km* fibre links. At increased distances beyond 1000 *km* optical amplifiers or regenerators can be utilized. Other options are using intensity modulated laser with optical carrier stabilization or frequency comb transfer realized on a continuous wave laser that is externally modulated for cost reduction [18]. On each antenna, digitizers housing the analogue to digital converters (ADCs) among other components will be installed so as to convert the received electro-magnetic wave from radio frequency (RF) into a digital signal. A clock signal will be required for generation of a stable reference tone for phase coherence of the dishes, absolute time code for antenna controllers and beam formers, accurate timing ticks and counters for data stamping, operational monitoring and control and stable periodic synchronization [23]. The MeerKAT is considering the use of stable hydrogen maser, caesium or rubidium source to generate the stable clock signals. The

MeerKAT telescope clock frequencies will comprise of 1.712 GHz (L-band), 1.088 GHz (UHF band) and 14.5 GHz (X-band) in addition to 1 pulse per second (1 pps) for synchronization. If a maser is to be used in the MeerKAT telescope, a maximum phase drift less than 6 fs over 1000 s is provided for the temperature swings and Gauss magnetic field variations [23]. On the transmission path, maximum change in the fibre due to thermal effects and fi bre noise is required to be < 40 picoseconds (ps) from the exposed fibre and < 2 ps for the buried fibre. A 1 ps is also provided for factors relating to bending and twisting of the fibre [23]. The telescope array coherence over the measurement period depends on the clock stability. The RMS clock stability should not exceed phase error coinciding to the maximum allowable degradation of 2% in the telescope sensitivity over the measurement period [18, 24]. The RMS clock stability for the allowable degradation is 0.2 radians or 11^o. This phase error translates to 18.6 ps and 2.2 ps for MeerkAT's L and X bands respectively. In the MeerKAT TFR design, a laser source is modulated using a signal from a stable hydrogen maser and transmitted over fibre to the remote antennas. On the antenna, sits the digitizer which hosts the PIN photodiode which converts the optical signal to electrical. After the photodiode the signal is split to two to cater for the two polarizations (horizontal, H and vertical, V) with ADC requiring about 0 ± 4 dBm of electrical power. The transmitter for the clock is expected to introduce less than 130 fs of phase noise to the 1712 MHz clock signal over the frequency range 800 Hz-10 MHz. The frequency 800 Hz is set by half the narrowest channel resolution of the correlator while the 10 MHz is the 10 dB cut-off frequency of the filter used on the digitiser to limit the noise on the ADC.

2.4 Review of existing telescopes

There are a number of astronomical telescopes in the world. Few that portray similarities to the SKA in terms of design and magnitude are provided. The first one that forms part of the larger SKA is the Australian square kilometre array pathfinder (ASKAP) situated in Murchison region of Western Australia and funded by Australian government. ASKAP is a 36 antenna array, each 12 m in diameter. Its total collecting area is about 4000 m^2 with frequency range from 700 MHz to 1800 MHz. Each antenna streaming 2 $Tbps$ of data is connected to 216 fibre links of up to 8 km to the correlator. The correlated data is then transmitted to the science site centre about 400 km away. Non-zero dispersion shifted fibres (NZDSFs), G.655 and DWDM technologies with repeaters are employed. Control and monitoring uses one Gigabit Ethernet while the clock reference relies on a maser and the photonic system [25, 26]. Unlike the MeerKAT telescope, ASKAP transmits the radio frequency (RF) signals over fibre from the individual antennas to the processor building for digitization, beam forming and eventual correlation. The timing system is less stringent as digitization is done in the processor building. This however, poses a threat to astronomical data from possible RF interference

arising during the transmission. The MeerKAT telescope safeguards the astronomical data through the immediate digitization of the received signal upon detection on the antennas. It is because of this reason that the timing distribution issue arises.

The Expanded Very Large Array (EVLA) situated in San Augustin in Mexico comprises of 27 antennas, each of 25 m diameter with frequency coverage of 1-50 GHz. The 27 antennas are positioned to form an equiangular pattern with 9 antennas on each arm. It is funded by the US National Science Foundation (NSF), the Canadian National Research Council, and the CONACyT funding agency in Mexico. It was completed in 2012. EVLA is an upgrade of very large array (VLA) which has been operational since 1970 [27]. Data is transmitted at 10 *Gbps* using 1550 nm lasers over a maximum of 22 km of SMF in the array with an optical amplifier per antenna. The 3 links at different transponder wavelengths are independent but reproduce the sampled data. Four of the 3 channels are then coupled onto a single fibre using DWDM. EVLA relies on hydrogen maser, GPS-based with 512 MHz reference signals. Clock is transmitted on ZDW fibre (G. 652). It employs a round trip monitoring whereby the optical reference signal is split and part of it sent on a different SMF in the same cable. The signal phase change due to temperature and other mechanical effects is determined by comparing the 512 MHz transmitted with a 128 MHz offset to the master 512 MHz reference signal. Optical fibres are used for transfer to all antennas for the purpose of timing and frequency distribution [28, 29].

Atacama Large millimetre array (ALMA) comprises of 66, 12 m antennas located in Chile with the longest link of 25 km from the site centre. The data is then relayed to a central correlator housing up to 95 km from the site centre. The data flow is about 7.68 *Tbps*. Each of the antennas is connected to a fibre optic link carrying 12 wavelengths at 10 *Gbps* to the correlator. It uses wavelength division multiplexing to achieve the transmission. Each of the 12 wavelengths has a transmitter and receiver. The data signal is amplified using the EDFA so as to overcome the fibre losses [10]. A local oscillator (LO) is used to generate a lower frequency that is converted to the desired frequency using a suitable phase-locked source. The frequency range is 30 to 950 GHz with baselines up to 15 km [30, 31]. Two laser beams with frequency equal to that of local oscillator before multiplication are coupled into a single fibre from a technical building to the antenna. The two beams are combined in a photo mixer and the electrical signal fed into the front end receiver. The stable master laser to which the slave (second laser) is phase locked with LO frequency that is set by a tuneable microwave generator. Each antenna is connected by 8 single mode fibres; 1 for data transmission, one for photonics local oscillator, 2 for monitoring and control and 4 spares [32].

The e-MERLIN is a 7 antennas array situated in United Kingdom (UK). It is an upgrade of the former 5 dish Multi-Element Radio Linked Interferometer Network (MERLIN) with a maximum baseline of 220 km. Each telescope streams 30 *Gbps* at various bands; L band (1.2-1.8 GHz), C band (4.5-6 GHz) and K band (21-23 GHz). Distances from e-Merlin telescope

to the correlator is more than 100 km. The science centre is about 400 km away. For data transport, 3 lasers of 10 *Gbps* on a standard single mode fibre, G. 652 with amplification and dispersion compensation so as to overcome the losses over the distance. Previously MERLIN used the microwave links. The e-MERLIN forms part of the European Very large baseline interferometric Network (EVN). EVN links 14 other telescopes in Europe and China for better resolution [33, 34].

These described telescopes have utilized the optical fibre in their transmissions. SKA demands careful choice of technologies for signal and data transport so as to achieve the ultimate objective of being the world's biggest scientific instrument upon completion. The ultimate target in the data and clock reference transport in the SKA array is the improved quality of service, reliability and reasonable cost. The plan to deploy 24 fibres [18] (G.652 and G.655) is of great significance in future prove technologies and scalability at later stages. G.652 offers advantage on minimized nonlinearities while G.655 is suitable for DWDM application and low loss transmissions.

2.5 Analogy between astronomical telescope arrays and wavelength division multiplexed passive optical networks (WDM PONs)

In this section, we compare the telescope array to conventional telecommunication metro access networks. Conceptually, an astronomical arrays resembles an access optical network. Access network connects service provider central offices to individual subscribers. To increase the bandwidth in the access network, passive optical networks (PONs) have evolved. A PON is a point-to-point or a point-to-multipoint optical network where an optical line terminal (OLT) at the control office is connected to many optical network units (ONUs) through one or more optical splitters. The multiple splitter supports several ONUs ($1 : N$) commonly $1 : 64$, $1 : 128$ or even more over several tens of kilometres. PONs are bidirectional with a single wavelength dedicated to each directions. Upstream refers to the connection from the end users to the control office while downstream connects the control office to the users. More information about types of networks, standards, designs and access technologies are provided in [35, 36]. The available bandwidth is shared among users. The available bandwidth is sliced using the arrayed waveguide grating (AWG). To ensure scalability, increased reach, capacity and high user count, several architectures have been proposed [37-39].

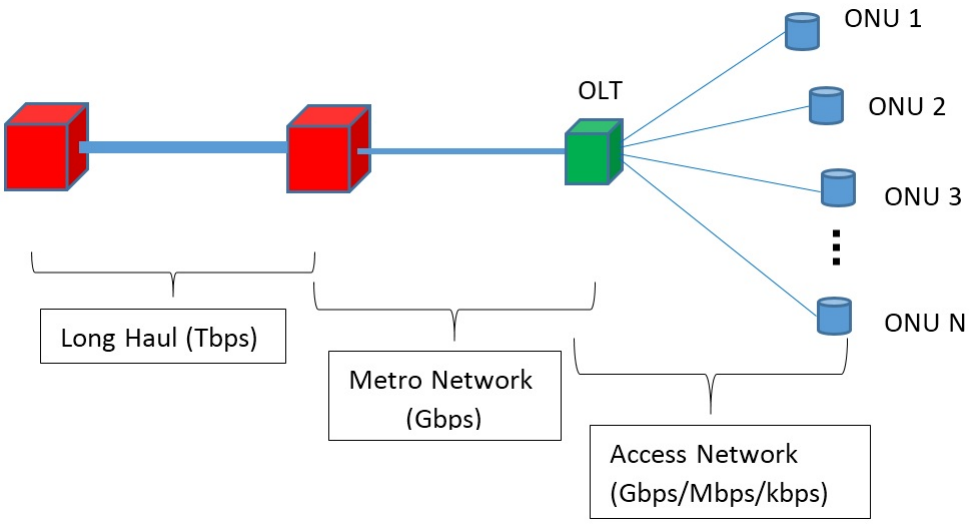

Figure 2.3: Diagram of a typical telecommunication network.

Figure 2.3 depicts an optical network scenario supporting N optical units. The ONUs represent homes/ businesses/ nodes/ buildings/ premises/ e.t.c. in a telecommunication network. If the ONUs are to be replaced by individual antenna in the MeerKAT telescope array and OLT as the Karoo array processing building (KAPB), then a telescope network supporting 64 antennas (ONUs) is created with the farthest transmission of about 12 km.

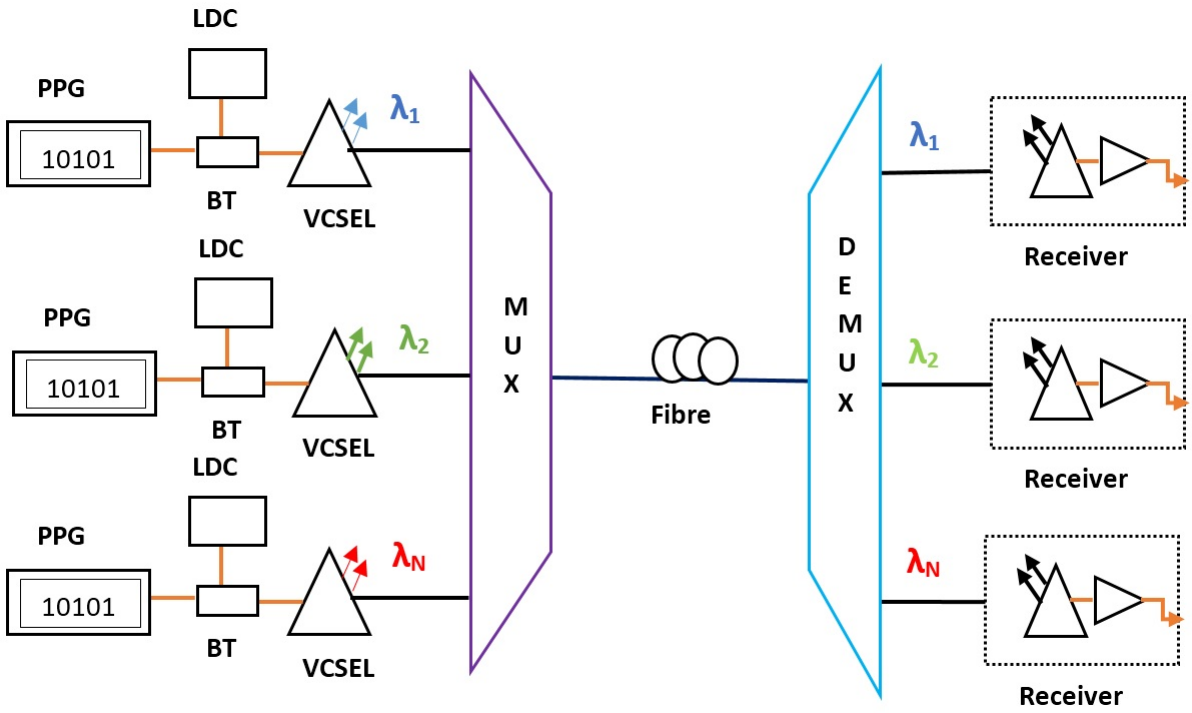

Figure 2.4: Illustration of a unidirectional wavelength division multiplexed optical link using VCSELs. PPG is programmable pattern generator, LDC is laser diode controller and BT is bias tee.

The transmission from the KAPB to the antennas represent the downstream while the vice versa is the upstream. The downstream is a typical case of time and frequency reference (TFR) distribution in the array while the upstream is the received astronomical data flow. The progression from MeerKAT (12 km) to SKA phase 1 (254 antennas) with distance of up to 100 km represent the metro network scenario in the illustration. SKA phase 2 with transmission distance beyond 1000 km with enormous data rates streaming from over 3000 antennas is a case of long haul system. The difference between a telecommunication network and a telescope network is the data flow in the upstream and downstream directions. Typically, the downstream in telecommunication network has a higher data rate than the upstream. Unlike telecommunication networks, the telescope networks experiences unidirectional data traffic with only point-to-point network topology practical. However, clock signal distribution and telescope manager signals for control and monitoring can be taken as a special case of downstream in the telescope network. The concept therefore relies on suitable choice of technology that meets the upstream and downstream requirements in the telescope array.

Point-to-point refers to communication connection between two nodes. The nodes for a telescope network is the antenna position in the array and the central processor building. The multiplexing is used to reduce the cost through fibre count reduction in a network. Due the enormous data rates in a telescope network, multiplexing technique provides a key solution. In multiplexing, several transmitters are coupled into a single fibre so as to increase transmission capacity. The use of a single fibre makes it economical. It can be time division multiplexing (TDM) or wavelength division multiplexing (WDM). In TDM, bandwidth sharing is in time-domain. Wavelength division multiplexing systems carry several number of optical signals each at its own wavelength. The WDM system has a number of transmitters (N) connected to one end of the transmission line and receivers at the other end as illustrated in figure 2.4. A single fibre is used for N optical signal channels. The WDM system can be considered as a number of parallel single wavelength optical systems [35, 36]. The wavelength division multiplexing depends on the channel spacing and the channel number, N. DWDM technology have channels with spacing ranging from 12.5 GHz to 100 GHz [40]. This requires stable transmitters to cater for the frequency stability. Depending on the fibre's bandwidth, several channels can be coupled resulting to increased transmission rate in the telescope array. The DWDM technique is suited for use in data transmissions from the central signal processor (CSP) to science data processor (SDP). As realized in the EVLA, ALMA and e-MERLIN projects in the preceding section, use of DWDM technologies in SKA is paramount so as to utilize the capacity of the fibre efficiently. As the transmission distances progress from 12 km (MeerKAT) to 100 km (SKA 1) and eventually to over 1000 km (SKA 2), some dispersion compensation mechanism and amplification is required. Intensity modulation is preferred due to its simplicity and cost.

2.6 Optical technologies used in wavelength division multiplexed passive optical networks

Transmission technologies involved in WDM PONs mainly comprise of transmitter-receiver pair and modulation techniques. Receivers can be positive intrinsic negative (PIN) or an avalanche photodiode (APD). Their structural designs render the difference in operating bandwidth range and sensitivity which translates to suitability in their application. PIN is used for relatively short distance but APD is used for long distances. APD uses more complex design and higher operating voltages to realize amplification. The detection can be done coherently or directly. Transmitters are light sources typically operating at various wavelengths commonly 850 nm, 980 nm, 1100 nm, 1310 nm and 1550 nm. These comprise of light emitting diodes (LEDs) and light amplification by stimulated emission of radiations (LASERs). LED emits light with large spectral width, typically 70-80 nm for 1550 nm sources with low modulation speeds of about 150-200 MHz.

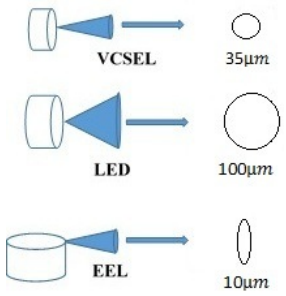

Figure 2.5: Schematic light emission profiles from different sources with corresponding beam spots

Lasers on the other hand have narrow spectral width which transform to different beam spot sizes. A sketch of spot sizes of emitted light from various optical sources is shown in figure 2.5. The lasers include vertical cavity surface emitting lasers (VCSELs), distributed feedback (DFB) lasers, Fabry-Perot (FP) lasers, electro-absorption modulated lasers (EMLs) and integrated laser Mach-Zehnder modulator. Most DFBs, FPs and EMLs are edge emitting lasers (EEL). Transmitters used in PONs are distributed-feedback (DFB) lasers [41, 42] and vertical cavity surface emitting lasers (VCSELs) [43-46], light emitting diodes (LEDs) [47] and the Fabry-Perot laser diodes [38, 48] among others [37].

Amplitude or intensity modulation commonly known as on-off keying (OOK) has been used extensively in telecommunication for several years because of the cost and its simplicity in terms of implementation and integration. It is an uncoded technique [49]. With capacity

demand, more advanced formats have been introduced. Binary phase shift keying (BPSK) has been developed for sensitivity applications in communication. Its modulation bandwidth can be improved using the M-ary orthogonal modulation or coding the information. To overcome the challenges of modulation bandwidths especially in WDM applications, narrow modulation is attained through two dimensional quadrature phase shift keying (QPSK). QPSK, M-PSK and M-quadrature amplitude modulation (M-QAM) with multiplexing and coherent detection have dominated the rise in 100 G technologies [50-53]. M is the number of symbols. The advantage of these coherent technologies is that they are able to overcome dispersion related effects. However, the cost and the complexity of these advanced formats limits their use in most telecommunication. Such advanced technologies may be appropriate more for CSP to SDP transmissions than use in data aggregation from individual receivers in telescope networks.

This chapter reviews the existing telescope networks, it describes SKA transport requirements and possible technologies. In the following chapter, we provide a detailed description of the VCSEL technology, optical link description and impairments.

Chapter 3

VCSEL technology and link description

This chapter starts by outlining the advantages of vertical cavity surface emitting lasers (VCSELs) over other sources then gives a detailed discussion on the state of the art of VCSELs tracing down from its birth nearly 4 decades ago. The photodiode receiver design, fibres types, optical fibre impairments in addition to link budgeting are also described.

3.1 Advantages of vertical cavity surface emitting lasers over other sources

In addition to the fact that the laser cavity is monolithically fabricated, VCSELs are attractive due to unique and vast advantages [54-59] which include;

a) Wavelength stability: the VCSEL diode lasers are stable and can operate in a single longitudinal mode within C-L bands [55].

b) Low power: low drive currents typically milli-ampere (mA) range and energy efficiency $> 50\%$ [54, 56-59].

c) Wavelength uniformity & spectral width: with improved growth technology, VCSEL wafers can be manufactured with less variance from the cavity wavelength. This enables the 2-D arrayed VCSEL diode lasers with little wavelength variation between the elements. In edge-emitters, bar-stacks bear significant wavelength variations from bar to bar due to lack of intrinsic mechanism for wavelength stabilization, resulting to wide spectral width. Full-width at half maximum spectral $< 1\ nm$ [55].

d) High bandwidth: high data rates (>10 Gbps) compared to LEDs [54, 57, 59].

e) Wavelength tuneability: ideal for wavelength division multiplexing (WDM) [54].

f) The convenience of direct modulation: do not need external modulator [59].

g) Temperature sensitivity of wavelength: the wavelength of emission in VCSEL diode lasers is less sensitive to temperature changes than in edge-emitters. This is because the lasing wavelength in VCSELs is defined by the optical thickness of the single-longitudinal-mode-cavity. The optical thickness minimizes the temperature dependence. Concisely, the cavity's refractive index and physical thickness have a little dependence on the temperature. On the other hand, the emission wavelength of the edge emitters is defined by the peak-gain wavelength. The peak gain wavelength has a much stronger dependence on temperature. Consequently, high power arrayed VCSELs have narrower spectral line-width than in edge-emitter-arrays [55, 57].

h) High temperature operation: VCSEL diode laser devices can be operated up to temperatures of 80^oC without cooling [55].

i) Higher power per unit area: VCSELs may deliver a higher power per unit area than edge emitters. The gap between the bars in edge emitters has to be maintained for the flow of the coolant [55].

j) Beam quality: VCSELs emit a circular beam. VCSEL diode lasers emission can be achieved in a single transverse mode (circular Gaussian) with a small divergence angle through proper cavity design. The simple beam structure greatly reduces the complexity and cost of coupling/beam-shaping optics and increases the coupling efficiency to the fibre or pumped medium [55].

k) Reliability: VCSELs do not have the failure modes such as the dark line defects observed in traditional laser structures. Since they can be implemented in arrays and have very long wear-out life, they are not prone to problematic optical damage [55, 56].

l) Manufacturability and yield: fabrication cost of VCSELs is low because of planar or all vertical construction [56].

m) Scalability: for high-power applications, VCSEL diode lasers can be directly processed into monolithic 2-D arrays, whereas for edge-emitters only 1-D monolithic arrays are possible. Moreover, a complex and thermally inefficient mounting scheme is required to mount edge-emitter bars in stacks [55, 56].

n) Packaging and heat-sinking: high-power 2-D arrayed VCSELs mounted in a junction-down configuration is straightforward, making the heat-removal process very efficient. This can easily enable LED replacement with VCSELs in existing applica-

tions. Chip-on-board technology and custom packaging are available to simplify system integration [54].

o) Cost: with the ease of production and heat-sinking technology, packaging of 2-D VCSEL arrays is easier than an equivalent edge-emitter bar-stack. The heat removal significantly reduces the cost of the high-power module. Generally the cost of a VCSEL is cheap compared to DFB lasers [54].

p) Testability: VCSELS can be tested and burned-in while still in wafer form. This increases manufacturing yield and lowers cost of production [56].

q) Integrability: semiconductor production and wafer integration of VCSELs is compatible with photodiode receivers and other circuitry for various applications [56].

3.2 Development of VCSELs

The first idea and demonstration of VCSEL was started by Prof. Kenichi Iga and colleagues at the Tokyo Institute of Technology in the year 1977. The first VCSEL device emitting at 1300 nm was developed in 1979 using GaInAsP–InP as the active-region gain material [60]. A GaAlAs/GaAs surface was designed in 1986 [61] and the first room-temperature continuous wave (CW) GaAs VCSEL consequently produced in 1988 [62]. In 1989, a GaInAs VCSEL exhibiting a 1–2 mA threshold current was demonstrated by Jewell [63]. Reduction of threshold current and improved efficiencies [64] accelerated development. The oxide-confinement enhanced significant performance of the VCSEL device. These oxide-confined VCSELs gave a significant threshold reduction [65-67] and high power-conversion efficiencies [68, 69]. High output powers of up to 1.8 mW at 80 $^{\circ}C$ temperature with efficiencies up to 56% on InP has been reported [70].

In the recent years, research has shown constant progress and growth on the long wavelength and high speed data transmission using VCSELs as light sources. High data rates of 25 *Gbps* up to 64 *Gbps* at different operating conditions have been demonstrated successfully. Among the highest data speeds reported on different transmission wavelengths are; 40 *Gbps* at 1550 nm [71], 12.5 *Gbps* at 1310 nm [72], 25 *Gbps* at 1060 nm [73], 49 *Gbps* at 980 nm [74] and 55 *Gbps* with equalization at 850 nm. Without equalization, 44 *Gbps* at 850 nm was achieved [75]. Most recently, IBM recorded the highest speed of 64 *Gbps* on an 850 nm VCSEL over a 57 m multimode fibre (MMF) by use of conventional non-return-to-zero (NRZ) modulation. On the same VCSEL, IBM transmitted over 107 m MMF at 60 *Gbps* [76]. The different VCSELs demonstrated, show that effective high speed transmission has been achieved on all the transmission windows. The transmission windows are illustrated in the attenuation graph shown in figure 3.1.

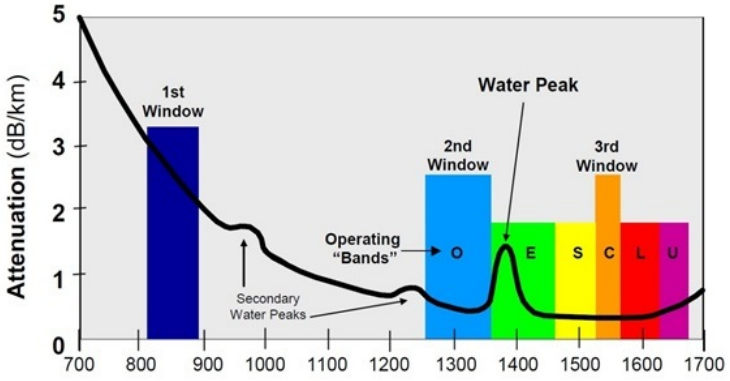

Figure 3.1: Attenuation of optical signal at different transmission windows [77].

In order to meet the 100 G and beyond technologies, VCSEL arrays [78] and advanced modulation formats for serial optical transmission [79] have become an option. These advanced modulation formats have seen the VCSEL achieve higher transmission rates on single mode operation. For example, 100 *Gbps* on 1550 *nm* VCSELs has been achieved using 4-level pulse amplitude modulation (4-PAM) [80] and the combined 4-PAM with polarization division multiplexing (PDM) coherently detected [81]. Using a 3-PAM and coherent detection, [82] transmitted 105.7 *Gbps* over 960 *km*. VCSEL arrays are also used in high power [83-85] and high bandwidths applications [45, 86].

Short wavelength VCSELs mainly 850 *nm* have been applied in data centres, storage area networks, local area networks and high computing optical interconnects. Due to continuous size expansion in data centres, the demand for longer reach optical links is dealt with by the use of small spectral width single-mode VCSELs that give the potential of reduced chromatic dispersion along optical fibres of few hundreds of metres. The suitability of the short wavelength on these applications is mainly due to high attenuation on the window as depicted in figure 3.1. Exploring applications, long-wavelength VCSELs (1300–1550 *nm*) have consistently become widely used.

Progress on long wavelength VCSELs in terms of output power, tuneability, operating temperature and modulation bandwidth has continuously grown as research on different semiconductors and designs dominate the developments. This long wavelength production has been achieved by either use of different mirror material, active region material, substrate material or wafer bonding. InPGaAs VCSELs grown on GaAs substrate perform better than that of InP substrate. The InP substrate is characterized by high threshold current, poor temperature performance and low output [87]. This is due to small conduction band offset between InGaAsP and InP that enables electrons with sufficient thermal energy to escape from the quantum well. Auger recombination and limited carrier confinement is responsible for low power lasers. In Auger recombination process the electron-hole pair recombine but instead of emitting a photon, the energy is given to another electron carrier in the conduction band

moving it to the edge of the band limiting the lifetime and efficiency of the system. GaAs on the other hand is a good thermal conductor thus helps with cooling. High reflectivity of DBR grown on GaAs/AlAs is as a result of large refractive index contrast. The electrical resistance and optical losses are reduced due to decreased mirror thickness as well as growth time. The effective thermal conduction, better electron confinement and high reflectivity yield better temperature performance, efficiency and output power [87]. Using a high contrast gratings as the top output mirror, about 25 nm mechanical tuning range and 2 mW of output power was shown on a 1550 nm VCSEL [88]. InP semiconductor VCSEL with power of 6.7 mW [89], 102 nm tuneability at 1.55 μm [90] and 18 GHz modulation bandwidth [91] have been reported. The 18 GHz modulation bandwidth is however small as compared to 28 GHz on 850 nm wavelength VCSEL reported in [92]. Similarly, GaSb lasers operating at high temperatures of 55-90°C with tunings of 0.5-1.03 nm/mA at 2.3 and 2.6 μm have been reported [93]. Structural designs have improved VCSEL performance in terms of modulation, efficiency and operation conditions. Analysis of the temperature-dependence with modulation performance at elevated temperatures up to 80°C on 1.55 μm high-speed VCSELs is given [94, 95]. These developments have seen the VCSEL applications expand from not only data centres, chip to chip and optical interconnects but also to access, metro networks and even long haul transmissions [96]. The rise of fibre to the home/ building/ premise/curb/node (FTTX) in Europe, US and Asia propelled the wide use of long wavelength VCSELs. Most recently fibre to the hut, a FTTH solution tailored for African perspective and making use of VCSELs has been proposed by our group [97]. Demonstration of VCSELs for wavelength division multiplexing (WDM) passive optical networks (PONs) has been given in [43, 45, 46, 98-101].

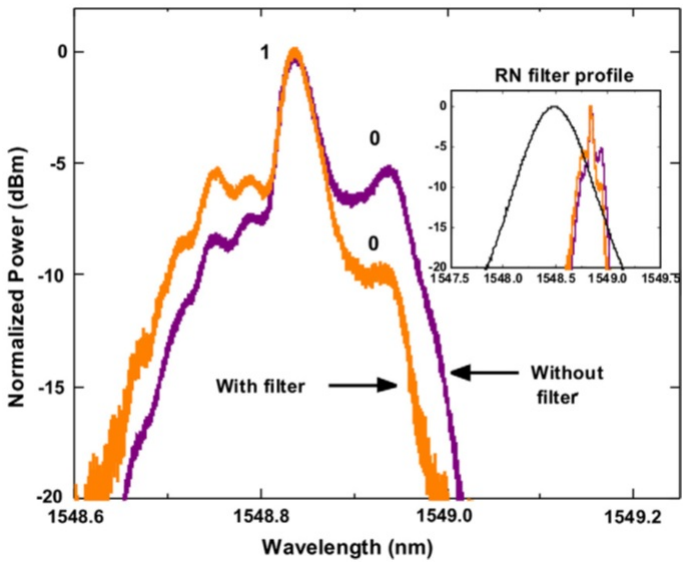

Figure 3.2: Signal spectra showing normalized power versus wavelength with and without filter [43].

With several structural designs to enhance the device performance, VCSELs still suffer the chromatic dispersion and chirp related effects. This chirp is the change of wavelength or optical frequency in response to variations in optical power. Some techniques of minimizing chirp have been suggested. These include wavelength offsetting [43, 98], adjustable optical spectrum reshaper filter [102] and tuneable approach reported in optical injection locked VCSELs [103]. With filter off-setting, [43] effectively eliminated the chirp effects in the VCSEL as shown in figure 3.2. This reduce dispersion penalties thus improving the reach. With injection locking, the spectrum is greatly narrowed because of the reduced chirp as evident on figure 3.3. This was obtained on an 8.58 dB injection ratio. The asymmetric free-running spectrum is broad indicating the dominance of adiabatic chirp and the unbalanced transient chirp [103]. Dynamic chirp is a wavelength shift associated with on-off modulation while adiabatic chirp refers to a steady state emission frequency difference between on and off states.

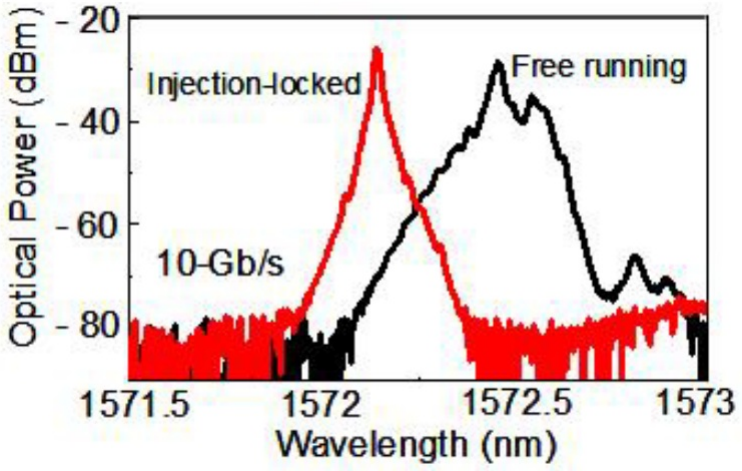

Figure 3.3: Signal spectra showing injection locked and free running VCSEL [103].

3.3 VCSEL structure and confinement schemes

A gain medium of a VCSEL is an active region that is vertically stacked between two distributed Bragg reflectors (DBRs). The illustration of a VCSEL structure by Raycan Company is shown on figure 3.4. VCSELs emit light in the direction perpendicular to the plane of the active region layers, therefore amplification takes place during a limited part of the cavity round trip. The length of the active region is minimized ($\sim 10's\ nm$) so as to achieve a single mode operation at the desired lasing wavelength. The generation of longitudinal modes associated to Fabry-Pérot cavities is eliminated by the short cavity [104].

In order to provide enough gain, the active region typically consisting of multiple quantum wells (QWs) sandwiched between higher band gap barriers and placed in an antinode of the optical field to achieve optimal gain. The finite width of the central antinode of the optical

field and the optimal number balances the increase in gain length and the reduction in confinement factor with increased number of QWs thus limiting the number of QWs [105]. The DBR mirrors are highly reflective and oppositely doped i.e. n-DBR and p-DBR. Through a current-guiding structure, the active region of the VCSEL receives current by either proton-injected surroundings or through an oxide aperture. There are different confinement schemes in VCSELs. These are the etched air-post, the regrown buried mesa, the ion-implanted, the oxide confined, and the buried tunnel junction VCSEL structure [106, 107]. Early VCSELs employed the simple etched air-post structure but suffered diffraction loss, surface recombination and thermal management issues. The development of the regrown buried mesa reduced the semiconductor/air interface issue. This regrown buried mesa scheme however suffered the layer exposure in AlGaAs based short wavelength systems. The ion-implanted structure was used in the first commercial VCSELs due to its relatively simple fabrication and excellent device life-time and reliability [108]. Currently, the most common confinement method in GaAs based systems is an oxide aperture formation. The oxide confinement technique is preferred to ion-implantation because it offers better optical mode and gain overlap, which give VCSELs with lower threshold currents, higher differential efficiency, and more linear current-power relationship. A demerit of this oxide confinement design however is the difficulty to produce predetermined aperture sizes. For electrical and optical confinement, a buried tunnel junction (BTJ) is used. It has an effective confinement of the current to the BTJ area and to the active region just next to it. The BTJ has wider bandgap than the QWs to avoid band-to-band absorption. The refractive index step from the BTJ and the surrounding cladding material propagates through the VCSEL structure and gives rise to index guiding of the optical field. The drawback of BTJ scheme is the fabrication process for a BTJ VCSEL that is rather complex, therefore not much successful in application [109].

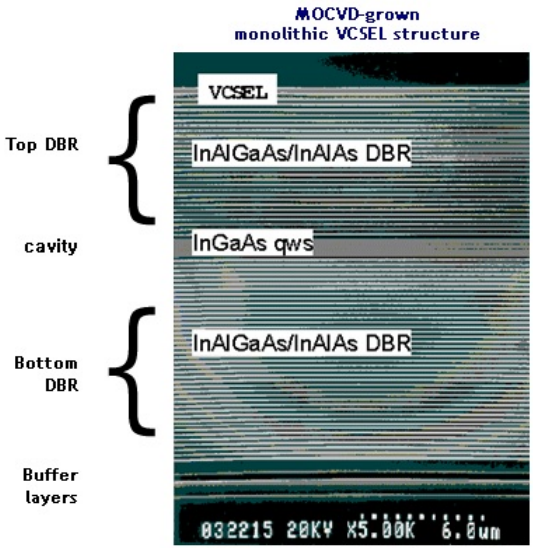

Figure 3.4: Schematic Raycan VCSEL structure [110].

The Raycan VCSEL used in this study utilizes InAlGaAs for the DBRs, InGaAs for its quantum well on the InP substrate as illustrated in figure 3.4. It also relies on the air gap confinement scheme. The combination of different semiconductor materials provides it with desirable qualities that are key for long wavelength VCSELs for various applications.

3.4 VCSEL assembly

VCSELs used in this study are of class IIIb from Raycan, South Korea [111]. The bias tee and the boards comprising of Transmit Optical Sub-Assemblies (TOSA) and Receive Optical Sub-Assemblies (ROSA) are from Finisar Company, United States [112]. The Raycan VCSEL was mounted on a Finisar evaluation board shown on figure 3.5. The VCSEL with the flexible printed circuit board (FPCB) was attached to its position on the Finisar board using a holder. The assembled VCSEL is as shown in figure 3.6.

The bias tee has two electrical inputs and one output, the two inputs are basically a direct current (DC) which powers the device while the other input is the alternating current (AC) couple which feeds the data / pattern into it. Laser diode controller supplies DC to the VCSEL.

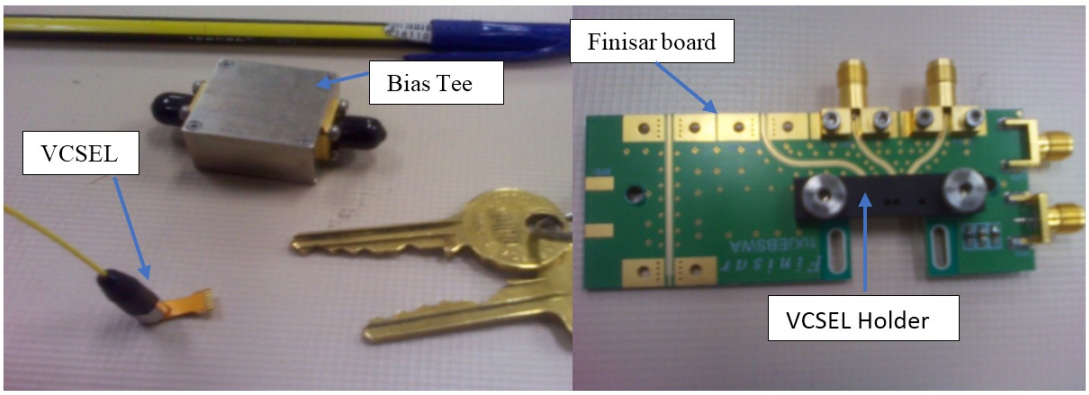

Figure 3.5: Photos of Raycan VCSEL and Finisar Board

Its operating range is adjustable and the limit can be tuned so as to protect the device by giving recommended current / power range. In the single drive mode, a VCSEL uses one bias tee on either the anode or cathode feed of the board depending on the configuration while the remaining arm is terminated using a 50Ω load during operation. The 50 Ω load matches the series resistance of the device. By terminating the unused driver, the available modulation current is halved. In the differential driven mode, two bias tees are used. The DC connections on both the bias tees are connected which in turn automatically locks the two laser diode controllers to a similar current level. Any of the LDCs is used to control the bias current of the VCSEL. Both the arms of the two bias tees were driven by RF in different polarities (data-P and data-N) from the pattern generator. In the differential drive, the VCSEL modulation

current is not halved as in a single-ended drive. This is turn improve the swing levels between '1' level and '0' level hence the overall performance.

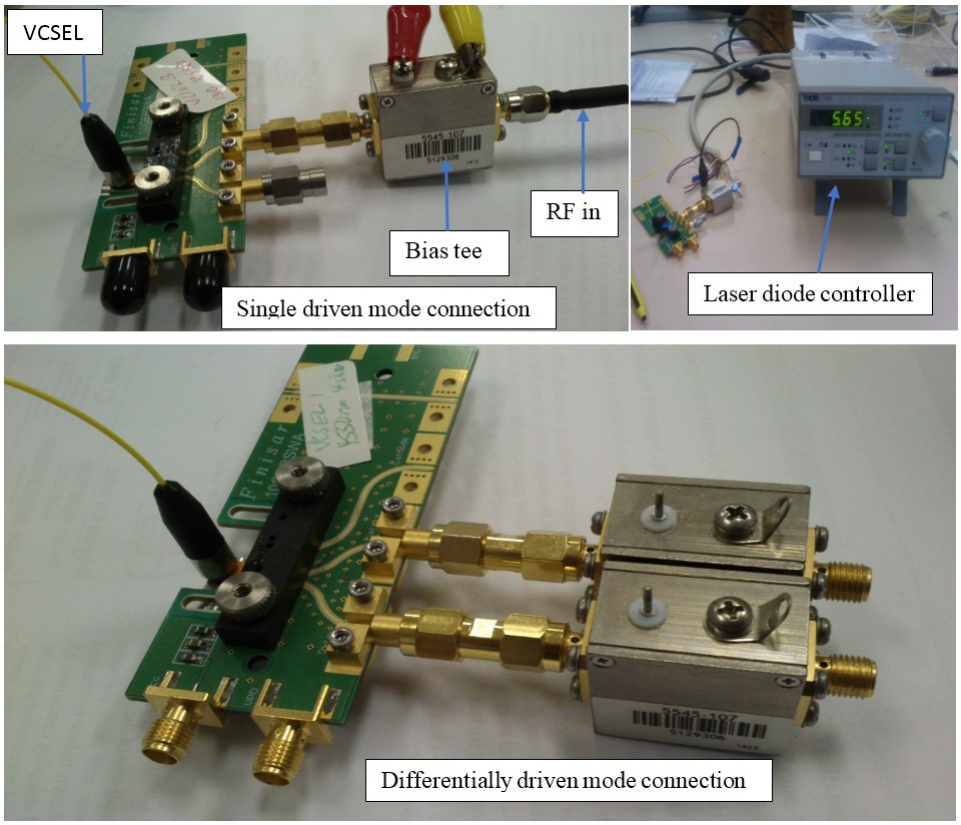

Figure 3.6: Assembled VCSEL in a single driven and differential mode connection. Inset: A picture of a laser diode controller.

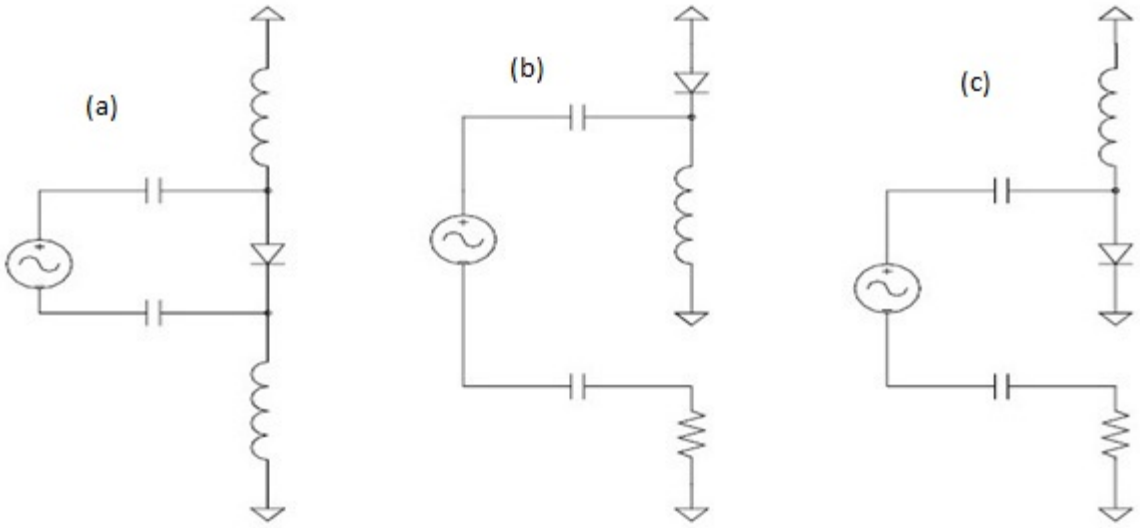

Figure 3.7: Schematic illustration of the circuits showing the (a) anode, (b) cathode and (c) differential configuration respectively [112].

Figure 3.6 shows a picture of the two configurations. In a single drive, a bias tee is connected either to an anode or a cathode arm of the board and the other arm terminated to a 50 Ω load. In this case, only one data feed is used. On the other hand, differential drive makes use of both arms of the board therefore, two bias tees are used with the P and N data feed onto each of the bias tees. The electronic equivalent circuits for the anode, cathode and differential configuration are as shown in figure 3.7. The inductor, L, capacitor, C and resistor, R circuits presented result to different effective impedances in the circuit. The packaging parasitics for these configurations too affect the VCSEL operation [112].

3.5 Modulation

A modulator is a device that is used to systematically inscribe digital signal/data onto the light. The modulated light is then carried in a medium. When the propagated light is received on the other node, it is decoded to the original signal. Modulation types depend on the adjustable parameter. The common modulations in optical systems are amplitude or intensity modulation (IM), frequency and phase modulations.

Direct intensity modulation of lasers avoids the additional complexity and the additional power loss introduced by external modulators. Direct modulation is also convenient and easy to implement. It does not require careful selection of optical power like external modulation. It reduces power consumption as no additional components are needed. Direct modulation is also possible at high data rates > 10 *Gbps*. On the other hand, external modulators allow for a higher modulation speed, large extinction ratios, and a low chirp [113]. Direct modulation leads to an undesirable wavelength chirp, which causes additional chromatic dispersion penalties at high speeds. Moreover, lasers develop undesirable relaxation oscillations at few GHz - frequencies, which hinder the maximum frequency for direct modulation. The data rate, average output power and the extinction ratio are all limited in direct modulation. External modulation is achieved by biasing the optical source using an external device. The optical modulator is put between the optical carrier (a laser source) and the communication channel (a fibre optic cable). It is expensive but it has a number of advantages. The most common optical modulators at 1550 nm transmission window are electro-absorption modulator (EAM) and the Mach-Zehnder modulator (MZM). MZM is an interferometer. To modulate the intensity, MZM splits its input light equally between a two parallel arms (paths). The phase changes on the two arms result in constructive and destructive interferences, therefore achieving the desired light power variation at the output [1, 114].

Lithium niobate ($LiNbO_3$) is mostly utilized in electro optic modulators. The wave-guides are designed by diffusing titanium or hydrogen into the lithium niobate, increasing the refractive index of the wave-guide. $LiNbO_3$ MZM require high drive voltage ($6 - 10$ V_{pp}) and are used for reaches above 100 km. For transmission distances < 40 km, EAM are commonly

used. EAM require about $2-3\ V$ voltage drive. Voltage control is able to absorb the lasing wavelength that generates a shift in the semiconductor band gap. EAM are smaller and allow high level of integration. In Tbps capacity optical communication systems, chromatic and polarization mode dispersions in standard single mode fibres (SMF) hinder the system performance by limiting higher transmission bit rates and distances. Pre-chirp involving the use negative chirp devices, is employed to compensate for the chromatic dispersion in the SMF [115]. Pre-chirp refers to re-shaping the modulated signal before transmission. Negative frequency chirp is used so as to reduce the signal distortion in a standard single mode fibre. Lithium niobate external modulators give the required bandwidth for high bit rate and the fibre dispersion effects can be minimized using the adjustable – chirp operation [116]. Making use of the electro optic effect, an electric field is applied across the wave guide so as to create a phase shift. It is because of this electro optic effect that the light modulates its phase and not its intensity. Zero-chirp silicon Mach–Zehnder modulator has also been reported in [117]. Direct modulation commonly used in VCSELs, Fabri-Perot and DFB are modulated by current with about 50 ohm termination corresponding to a peak to peak voltage of $1.5-2\ V$.

Direct modulation of semiconductor lasers introduces chirp to the optical signal, which broadens the spectrum. A VCSEL, just like other directly modulated lasers is limited by chirp. Chirp can be defined as the instantaneous change of the central wavelength or optical frequency, ν in response to variations in optical power i.e. residual frequency modulation of an amplitude modulated optical wave. The instantaneous frequency chirp can be expressed [118, 119] as

$$\Delta\nu\left(t\right)=\frac{\alpha}{4\pi}\left(\frac{1}{P\left(t\right)}\frac{dP\left(t\right)\varepsilon}{dt}+\frac{P\left(t\right)\varepsilon}{\tau_{p}}\right)=-\frac{\alpha}{4\pi}\left(\frac{d}{dt}lnP\left(t\right)+\kappa P\left(t\right)\right) \tag{3.1}$$

The first term describes transient chirp. Transient chirp relates to the time derivative of the instantaneous change in the ln of optical power with the rising and falling edges of the pulse. The second term describes adiabatic chirp which is the instantaneous optical power itself. $P(t)$ is the instantaneous optical power τ_p is the photon lifetime and α is the linewidth enhancement factor given by the expression

$$\alpha=-\frac{{}^{dn}/_{dN}}{{}^{dg}/_{dN}}=-\frac{4\pi}{\lambda}\frac{dn}{dg} \tag{3.2}$$

where n is the refractive index, g is the gain per unit length, λ is the wavelength and N is the carrier density. The linewidth enhancement factor quantifies the effect of the change of refractive index with carrier density on the dynamic properties of lasers [120]. The adiabatic coefficient, k parameter is a constant related to the non-linear gain and depends on the geometry of the device. The k parameter is expressed as

$$k = \frac{2\Gamma\varepsilon}{V\eta h\nu} \tag{3.3}$$

where Γ is the confinement factor, $h\nu$ is the photon energy, ν is the optical frequency, η is the laser quantum efficiency V is the cavity volume and ε is the gain compression factor. In a modulated VCSEL, transient chirp is characterized by the presence of large data signals that leads to a phase shift during the transitions of the data while adiabatic chirp due to long-term shift in the laser frequency. Chirp results from refractive index changes associated with changes of the carrier density, which leads to time dependence of the instantaneous frequency.

3.6 Receivers

Photodetectors absorb photons and generate an electrical current. A photodiode is used almost exclusively for photo detection in fibre optic communication systems [121, 122]. To meet high transmission capacity, high performing photo receivers with high bandwith and high sensitivity must be employed. The evolution of 1300 - 1550 nm transmission wavelengths utilize the optimum windows for low attenuation and reduced dispersion, this has led to advanced structural developments of photodetectors for high-bit rate fibre optical communication [123]. When a photon with energy greater than the bandgap is incident on a semiconductor material, the photon energy is absorbed and an electron-hole pair is generated in the material. The electron-hole pair will carry the electric current in an optical receiver when a voltage is applied. Different designs have different structures hence varied performance. A positive-intrinsic-negative and an avalanche photodiode receivers have different structural designs in addition to elemental composition of the semiconductors; these give different optical properties hence unique characteristics and performance of the devices [124].

3.6.1 Positive intrinsic negative photodiode

A positive-intrinsic-negative (PIN) photodiode has an intrinsic semiconductor layer between the p-n junction. On a reverse bias, a depletion layer is created across the intrinsic layer. The depletion layer has a low carrier density and high impedance hence a large built-in electric field is established. The electric field leads to current flowing across the p-i-n junction.The current generated when light is incident to a photodiode is called photocurrent, I_{ph} and is proportional to optical power, P_{in} as

$$I_{ph} = R_{PIN}P_{in} \tag{3.4}$$

where is R_{PIN} is responsivity of the photodiode. For PIN, the responsivity is related to quantum efficiency as

$$R_{PIN} = \frac{q\eta}{h\nu} \tag{3.5}$$

Where q is electron charge, $h\nu$ is photon energy and η is quantum efficiency. Quantum efficiency is the ratio of the number of photogenerated electrons to the number of incident photons. The photodiode response is limited by carrier transit time which is related directly to bandwidth of the photodiode [125].

3.6.2 Avalanche photodiode

An avalanche photodiode (APD) has an intrinsic layer and p layer between the $p^+ - n^+$ junction. The p layer between intrinsic layer and the n^+ region creates an avalanche effect.

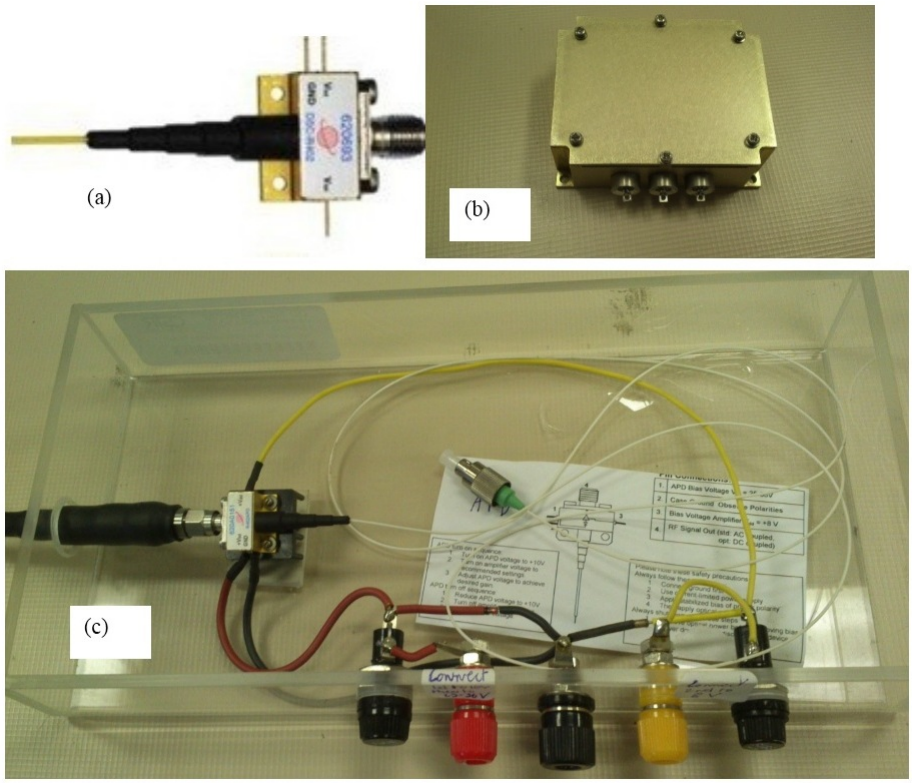

Figure 3.8: (a) DSC-R402PIN - 10 GHz Linear PIN + TIA without connection. (b) Special casing with RF shield for a photo receiver (c) connected DSC-R402APD - 10 Gbps APD + TIA

Unlike PIN, APD has an internal current gain hence higher responsivity. The internal current gain is achieved through impact ionization resulting from p layer. The responsivity of APD is given by

$$R_{APD} = \frac{q\eta M}{h\nu} \tag{3.6}$$

where q is the electron charge, $h\nu$ is photon energy, η is quantum efficiency and M is the current amplification given by the ratio of total current, I_{APD} to photocurrent, I_{ph} [126-128].

In this study, a positive intrinsic negative (PIN); DSC-R402PIN - 10 GHz receiver is compared with an avalanche photo detector (APD); DSC-R402APD - 10 Gbps receiver using vertical cavity surface emitting laser (VCSEL) as a light source. Both the receivers are from Discovery semiconductors. Figure 3.8 shows the pictures of the receivers. Both receivers under study are high speed with sensitivities of -19 dBm and -26 dBm for PIN and APD respectively. The 10 GHz PIN has photodiode bias of 7 -12 V and an amplifier bias range of 7.5-8.4 V. APD on the other hand has an amplifier bias of 8 -8.5 V and a high APD voltage of 25-36 V. The responsivities of PIN and APD are 0.8 A/W and 0.7 A/W respectively [129].

3.7 Optical fibres

Optical fibres used in optical transmission are can be categorized into two, namely, single mode fibre (SMF) and multimode fibre (MMF). SMF supports one mode of propagation while MMF supports several modes. The typical core diameter range of a single mode fibre (SMF) is 8-12 µm whereas multimode fibre (MMF) has about 50-100 µm for graded index and 50-200 µm for step index. The cladding are 125 µm, 125-140 µm and 125-400 µm respectively [126]. MMF suffers more dispersion related effects because of additional intermodal dispersion [126, 130]. Most single mode fibres (SMFs) operate at 1310 nm and 1550 nm windows where attenuation is minimum thus their suitability in long distance transmission. Multimode fibres are designed for short transmission and operate mainly at 850 nm and some at 1310 nm. The core-cladding structure among other factors, define the fibre characteristics which include: attenuation, light collection ability, pulse and transmission capacity, splicing tolerances, wavelength of operation, environmental tolerances, strength, flexibility and cost. For instance, in the step index structure, the acceptance angle is about 24^o [130]. The two categories provide different advantages; larger core in multimode enable easy light coupling into the fibre and at connection points. A relatively large core results in high numerical aperture and high coupling efficiency. For larger diameter, light emitting diodes (LEDs) can also be used as transmitters. Because of small diameter typically about 12 µm, SMF require for special light sources such as lasers.

The characteristics of these fibres are defined in different standards, mainly International Telecommunications Union (ITU-T) and International Electrotechnical Commission (IEC). The two standards are however closely similar especially description regarding fibre characteristics. For instance, IEC 60793-2-50 Ed2 category B is comparable to ITU-T G 652-655 description [131, 132]. In this particular work, we base on international telecommunications union (ITU-T) standard.

The difference in SMFs is as a result of their properties in terms of attenuation and dispersion values at different wavelengths. The shifting of dispersion at different wavelengths is

realized through tailoring of the waveguide dispersion [133]. Through tailoring, fibres have been shifted from the conventional zero dispersion wavelength, 1310 nm (G.652) to 1550 nm (G.653 and G.655). G.653 is a zero dispersion shifted fibre (ZDSF). This G.653 is however not common because of fibre nonlinearities at zero dispersion at 1550 nm. G. 651.1 are the multimode fibres (MMFs). The characteristics of a 50/125 µm multimode graded index optical fibre cable for the optical access network is given in detail. This standard was formerly ITU-T G.651 characteristics of a 50/125 µm multimode graded index optical fibre cable [134]. These fibres are ideal for short reach up to distances of 2 km. This is suited for short wavelength VCSELs used in short reach applications. The ability to support two or more modes makes it susceptible to both intermodal and intramodal dispersions. It is because of this intermodal dispersion that led to the development of graded index fibres [130]. G.652 is the conventional single mode fibre (SMF) that has been in use in most telecommunication networks. It operates on the second window of optical communication. It is optimized for use in the 1310 nm wavelength region (zero dispersion wavelength, ZDW) but can be used at 1550 nm too [135]. Different categories differ in water peak attenuation at 1383 nm window. G.655 is a SMF optimized for 1550 nm window. It has low dispersion values at 1550 nm and 1625 nm. The low chromatic dispersion is used to suppress the growth of four-wave mixing, which is a non-linear effect that can be a problematic in dense wavelength division multiplexing (DWDM) systems [136]. This fibre is suited for long haul and backbone applications. It has different categories with different polarization mode dispersion (PMD) values. G.657 is the latest standard that came with emergence of fibre to the home (FTTH). It is a SMF that is meant to support the existing ITU-T G.652 single-mode fibre through improved bending performance. It is designed to bend at small radii of 10 mm and 7.5 mm. It is ideal for technologies in broadband access networks [137]. It can be considered for use in the processor building.

3.8 Fibre impairments

These are mainly factors that degrade the optical transmission limiting the performance of optical communication systems. They include fibre losses (attenuation), linear and nonlinear effects [1, 138]. Linear effects comprise of chromatic dispersion (CD), polarization mode dispersion (PMD) and modal dispersion realized in multimode fibres. Nonlinear effects include stimulated Raman scattering (SRS), stimulated Brillouin scattering (SBS), self-phase modulation (SPM), cross-phase modulation (XPM) and four-wave mixing (FWM). Regarding fibre nonlinearities, this study is confined to SRS due to its application in Raman amplification used to extend the VCSEL reach. The fibre impairments can further be categorized based on data or time and frequency reference (TFR) requirement in the array. Generally, all the impairments influence the data transfer, but of particular importance to TFR optical transport is PMD due to clock polarization stability in the telescope array.

3.8.1 Attenuation

Attenuation limits the optical power in the transmission path. The power transmitted in the fibre is given by the expression

$$P_T = P_0 exp\left(-\alpha L\right) \tag{3.7}$$

where P_T is the transmitted power, P_o is the launched power, α is the attenuation coefficient and L is the fibre length. The attenuation coefficient is expressed in dB/km using the relation

$$\alpha\left({}^{dB}/_{km}\right) = -\frac{10}{L} Log_{10}\left(\frac{P_T}{P_0}\right) \approx 4.343\alpha \tag{3.8}$$

The fibre losses consist of intrinsic and extrinsic losses. Intrinsic can be further characterized by material absorption and Raleigh scattering. Extrinsic factors are mainly waveguide related issues. These are micro-bending, micro-bending losses, joint or splice loss and core and cladding losses [126]. Intrinsic absorption loss in optical fibres is a function of wavelength (λ^{-6}) and depends on the material transparency. For example in silica fibres, this is due to ultra-violet and infra-red absorptions occurring at $\lambda < 0.4$ µm and $\lambda > 7$ µm respectively. Transitional metal ions and water ions are impurities that cause extrinsic absorption. However, modern fibres have reduced attenuation at 1400 nm. The water absorption peaks have been minimized through impurity removal.

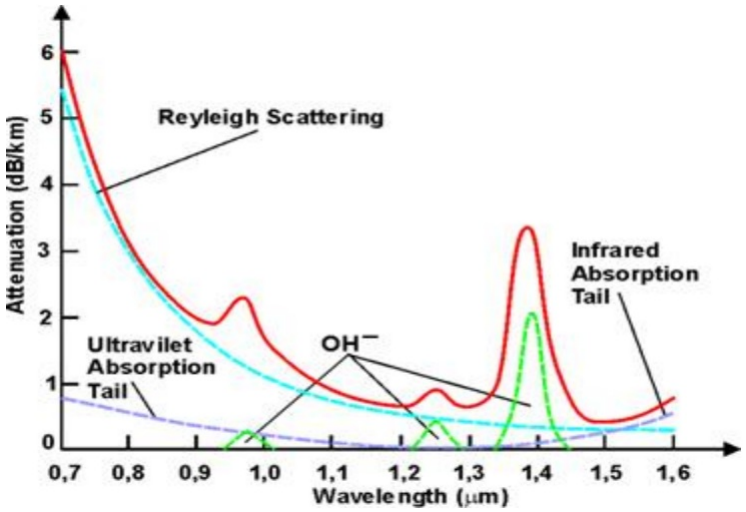

Figure 3.9: Attenuation versus wavelength in silica fibre [139].

Raleigh scattering is due to inhomogeneities of the fibre material. When a fibre is bent beyond the critical curvature, radiation occurs because phase velocity exceeds that of the plane wave in the cladding. Bending in small radius (cm) is known as microbending. Macrobending on the other hand arise because of power coupling from the fundamental mode to a radiation

mode. It causes imperfections in the cylindrical geometry during manufacturing. During fibre permanent or temporary joining, axial misalignment of the core lead to losses [138, 140]. Core and cladding losses arise because of different compositions hence different attenuation constants. Figure 3.9 shows various attenuation factors at different wavelengths. The fibre losses have consistently reduced from 100 dB/km at 1310 nm in 1970 to about 0.25 dB/km and 0.15 dB/km for 1310 nm and 1550 nm respectively in 1980 [140]. The first window of transmission with wavelength range between 800-900 nm suffers high attenuation losses above 2 dB/km. The second window (O band) of the spectrum that covers 1250-1350 nm range has reduced attenuation of about 0.4 dB/km while that of the third window (C band) covering 1530-1550 nm has least attenuation value of about 0.2 dB/km as shown in figure 3.1.

3.8.2 Polarization effects

To understand birefringence in a fibre, it is important to know the polarization behaviour of a light wave. We consider a wave propagating in the z direction, the electric fields are confined in the x-y planes due to the transverse nature. The components of the field are expressed as

$$E_x = A_x cos\,(kz - \omega t + \delta_x) \tag{3.9}$$

$$E_y = A_y cos\,(kz - \omega t + \delta_y) \tag{3.10}$$

where A_i is the amplitude $(i = x, y)$, k is the wave number and ω is the angular frequency.

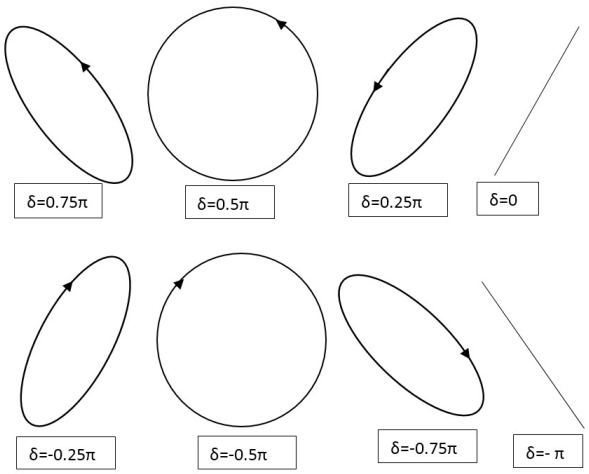

Figure 3.10: Illustration of polarization ellipses of different phase angles as seen in $-z$ axis position with $A_x = A_y$.

The overall amplitude is given by $\sqrt{A_x^2 + A_y^2}$. To eliminate the explicit space and time dependence in equations (3.9) and (3.10), we rewrite cosine terms using trigonometric identities

and by squaring and adding the resulting equations, the expression for a curve traced by the tip of the E-vector is given by,

$$\left(\frac{E_x}{A_x}\right)^2 + \left(\frac{E_y}{A_y}\right)^2 - 2\frac{E_x E_y}{A_x A_y} cos\delta = sin^2\delta \tag{3.11}$$

in which $\delta = \delta_y - \delta_x$ $(-\pi \leq \phi \leq \pi)$.

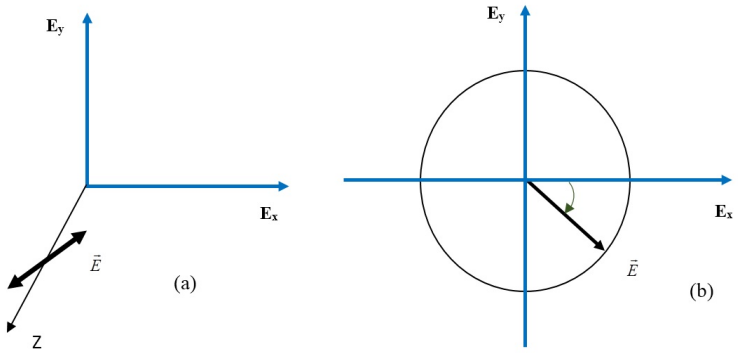

Figure 3.11: (a) Linearly and (b) left circularly polarized light propagating along the z direction.

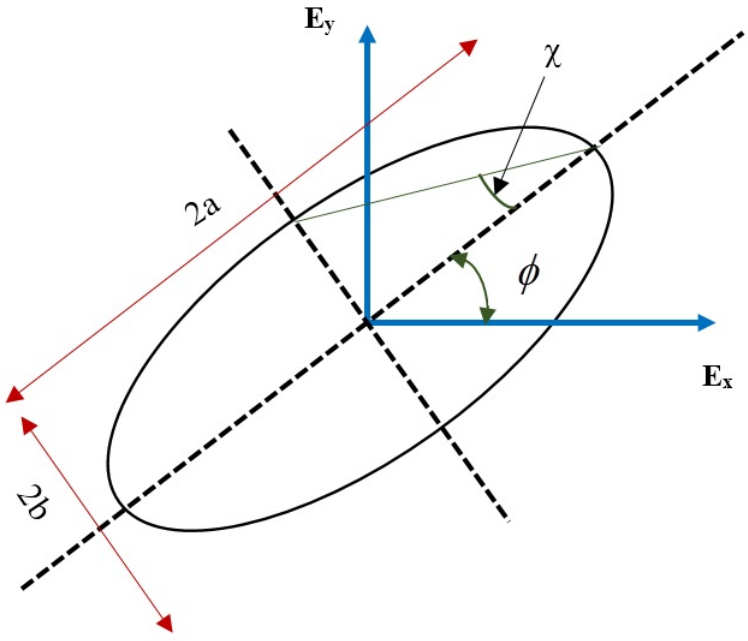

Figure 3.12: Polarization ellipse described by equation (3.11).

Equation (3.11) represents equation of an ellipse in the $E_x - E_y$ plane. This is the state of an elliptically polarized electromagnetic wave. With $A_x = A_y$, different degrees of ellipticity will describe different polarization states (see figure 3.10). For example, when $\delta = \pm\frac{\pi}{2}$ and $A_x = A_y$, equation 3 represents circular polarization. Linear polarization state of electromagnetic

field is represented when (m=0, 1, 2 .....) and $\frac{E_y}{E_x} = (-)^m \left(\frac{A_y}{A_x}\right)$(see figure 3.11). Rewriting equation (3.11) in terms of a new coordinate system x' and y'

$$\left(\frac{E_{x'}}{a}\right)^2 + \left(\frac{E_{y'}}{b}\right)^2 = 1 \tag{3.12}$$

From the illustration in figure 3.12, the lengths of principal axes is 2a and 2b. Thus the new coordinate system is rotated with respect to the original by an angle ϕ, given by,

$$tan2\phi = \frac{2A_xA_y}{A_x^2 - A_y^2} cos\delta \tag{3.13}$$

The ellipticity is defined using the lengths of principal axes as

$$\xi = \pm\frac{b}{a} \tag{3.14}$$

We take $b \leq a$ implying that ellipticity satisfies $0 \leq \xi \leq 1$. The "+" denotes the right elliptical polarization while the "-" is left. One can distinguish the right and left elliptical polarization using the phase. When the vertical component lags in phase, the E-field vector rotates in a clockwise direction which is right elliptical polarization. If it leads in phase, the E-field vector rotates in a clockwise direction resulting to left elliptical polarization [141]. For a linear polarized light, the ellipticity parameter $\mid \xi \mid = 0$ and the phase shift defined by $\delta = \pm m\pi$.

3.8.2.1 Jones vector representation

Light propagation in an optical fibre may be complex, however, simplified mathematical fomalisms describe the light in the medium. Light polarization can be represented by a 2x1 matrix commonly referred to as Jones matrix. This vector expresses the relative amplitude and the phase of orthogonal components of the E-vector. The complex amplitude is represented as

$$\vec{\varepsilon} = \hat{x}\varepsilon_x + \hat{y}\varepsilon_y \tag{3.15}$$

where $\varepsilon_x = A_x e^{i\delta_x}$and $\varepsilon_y = A_y e^{i\delta_y}$. The matrix is expressed as

$$\bar{J} = \begin{pmatrix} A_x e^{i\delta_x} \\ A_y e^{i\delta_y} \end{pmatrix} \tag{3.16}$$

A linear polarized electric field oriented at angle ϕ can be expressed as $\bar{J} = \begin{pmatrix} cos\phi \\ sin\phi \end{pmatrix}$and so forth. Generally, the y axis is the vertical component of the E-vector while the x axis component is the horizontal component. This Jones vector approach is restricted to fully polarized light [141].

3.8.2.2 Stoke's vector representation

To describe both the partially and fully polarized light, Stoke's formalism is used. In Stoke's formalism, two angles are used to describe the polarization ellipse. The two angles are orientation, ϕ and ellipticity, χ as illustrated in figure 3.12 where $0 \leq \phi \leq \pi$ and $-\frac{\pi}{4} \leq \chi \leq \frac{\pi}{4}$. Polarization state of a light signal with intensity E^2 and orthogonal components E_{0x} and E_{0y} of relative phase δ can be rewritten in terms of Stoke's vectors as

$$s_0 = \frac{E^2}{E_0^2} \tag{3.17}$$

$$s_1 = \frac{E_{0x}^2 - E_{0y}^2}{E_0^2} = cos2\chi cos2\phi \tag{3.18}$$

$$s_2 = \frac{2E_{0x}E_{0y}cos\delta}{E_0^2} = cos2\chi sin2\phi \tag{3.19}$$

$$s_3 = \frac{2E_{0x}E_{0y}sin\delta}{E_0^2} = sin2\chi \tag{3.20}$$

where the intensity of the polarized component is given by $E_0^2 = E_{0x}^2 + E_{0y}^2$. The degree of polarization, DOP is a ratio of polarized to the launched intensity given by

$$DOP = \frac{I_{polarised}}{I_{polarised} + I_{unpolarised}} \tag{3.21}$$

In terms of Stoke's vectors,

$$DOP = \frac{\sqrt{S_1^2 + S_2^2 + S_3^2}}{S_0} \tag{3.22}$$

The DOP =1 for a fully polarized light and 0 when it is depolarized. These Stoke's vectors represents coordinates which allows convenient description of polarized light in the three-dimensional (3-D) graphical tool called Poincaré sphere [142, 143]. Fully polarized light is represented by a point on the surface of the Poincaré sphere while partially polarized is represented within the volume of the Poincaré sphere.

When light is coupled into an optical fibre, it propagates as two orthogonal polarization states as described in the preceding section. Due to fibre geometry asymmetry, bends and environmental conditions, it leads to variation in refractive index causing a delay between two orthogonal states. This dependence of refractive index on polarization is referred to as birefringence. The time delay between the two orthogonal modes implies that the signal energy reaches the fibre end at different point in time causing a delay between the fast and the slow axes. This delay is called differential group delay (DGD) [114, 138]. DGD is a measure of polarization mode dispersion (PMD). PMD leads to pulse broadening and system impair-

ment thus limiting the transmission capacity of the fibre [144]. PMD has its origin in optical birefringence and complicated by the mode coupling in the fibre link. This birefringence is caused by intrinsic and extrinsic perturbations in the fibre. Intrinsic perturbations result from the manufacturing process mainly core's ellipticity or eccentricity while extrinsic perturbations are due to stress induced during the cabling and deployment process and environmental changes such as temperature and wind [145, 146]. Mode coupling is due to randomly concatenated birefringent sections in the fibre length [114]. In unstressed glass fibre, the medium is isotropic as the physical properties of the fibre material are uniformly distributed. When a form of stress is introduced, regions of anisotropy within the glass in the form of a non-circular core or asymmetrical stress fields in the cladding is created. As the polarization of the light-wave drifts between the birefringent axes, the phase of the clock will be altered by an amount corresponding to the DGD. The birefringence difference between fast and slow axes can be expressed as

$$\triangle\beta = \frac{\omega n_s}{c} - \frac{\omega n_f}{c} = \frac{\omega \triangle n}{c} \tag{3.23}$$

where ω is the angular optical frequency, c is the speed of light and $\triangle n = n_s - n_f$ is the differential refractive index between the slow and fast modes [147].

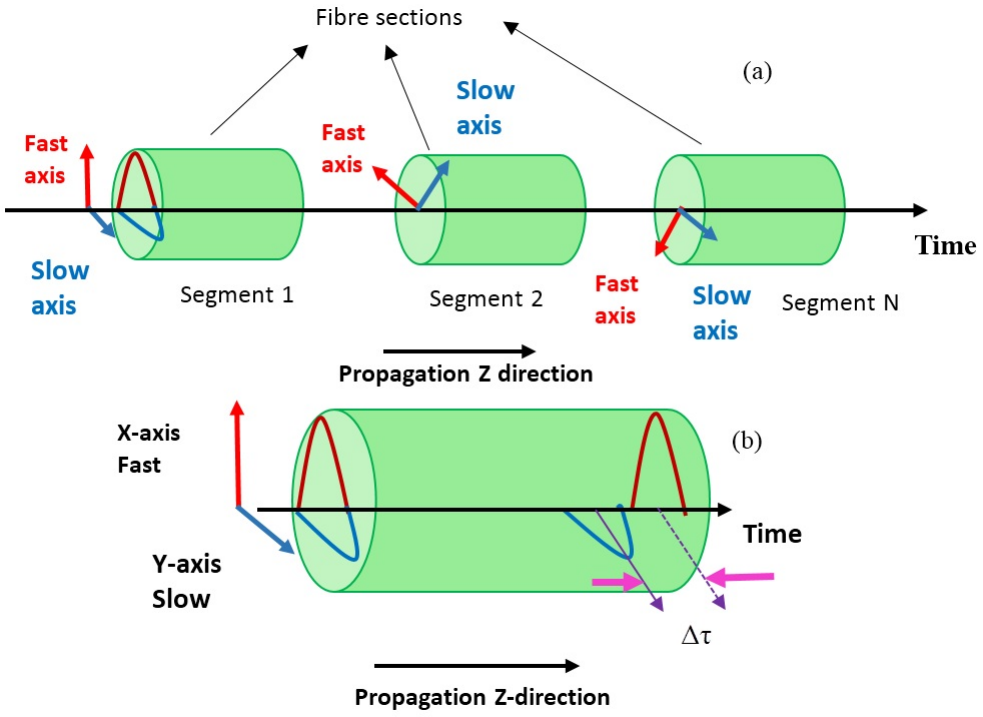

Figure 3.13: Diagram illustrating the effect of PMD in an optical fibre (a) the birefringent axes at different fibre sections, (b) launched pulses at the output separated by the DGD, $\triangle\tau$

In long fibre lengths composed of large number of segments as shown in figure 3.13 (a),

each segment has its own slow and fast modes and a portion of the signal propagates on each of them. At the boundary between these sections, the polarization vectors will be resolved into new pairs of local modes belonging to the next segment. The process of rotating the polarization vector into the new modes of the following segment is known as mode coupling [148]. The two polarization components of a pulse travel with different group velocities such that the pulse disperses in time as in equation (3.24). Figure 3.13 (b) illustrates the overall PMD effect in an optical fibre. The time delay is expressed as,

$$\triangle\tau = \mid \frac{L}{V_{gx}} - \frac{L}{V_{gy}} \mid = L \mid \beta_{1x} - \beta_{1y} \mid = L(\triangle\beta_1) \tag{3.24}$$

where L is fibre length, V_{gi} is group velocity along particular axis, β_{1i} is modal birefringence $(i = x, y)$. The mode coupling process allows the DGD to increase proportionally to the square root of the length of the fibre as given in equation (3.25).

$$PMD = \sqrt{\langle\triangle\tau^2\rangle} \equiv \tau_{RMS} = D_{PMD}\sqrt{L} \tag{3.25}$$

where $\triangle\tau$ is DGD, $\Delta\tau_{RMS}$ is root mean square of the DGD, L is fibre length and D_{PMD} is the PMD coefficient. Mode coupling makes the DGD and the fibre modes to be frequency dependent [149].

3.8.2.3 Polarization stabilization in optical fibres

Generally, the polarization-based measurements are important as a fundamental tool for scientific research and other applications such as engineering, optical fibre sensing among others [150, 151]. Polarization of an optical signal in a fibre changes randomly over time, in an unpredictable way [138, 152]. Some active polarization stabilization techniques may be needed in order to keep a correlation between the light polarization at the input and output of a fibre. To control and monitor polarizations in fibres, a clear understanding of the light signal and the fibre material is critical [153-158]. Some proposed stabilization techniques have been put forward. Dynamic polarization control using a fibre squeezer or arranged waveplates with fixed orientations and variable retarders have been found to control polarization fluctuation [159]. An algorithm which makes use of symmetries of optical polarization to decouple the varying SOP has also been suggested [160]. A control system involving two multiplexed reference signals which are looped back so as to create compensation for quantum communication has been demonstrated [161]. Polarization stabilization can also be done using special type of fibre known as polarization maintaining fibre (PMF) [162]. PMF is designed to maintain a particular state of polarization throughout the fibre section. The structural make-up is achieved by introducing some high birefringence commonly stress rods on the opposite sections of the fibre core. The condition for PMF is that light must be highly polarized so as to

prevent unpredictable output polarization state resulting from launching of both the fast and slow modes [163]. For clock transmission, frequency mixing to cancel phase fluctuations over the fibre length [164] can also be invoked as a stabilization mechanism.

3.8.3 Chromatic dispersion

Chromatic dispersion is a characteristic of an optical fibre causing different wavelengths of light to propagate at various speeds. This is because the optical transmitters do not emit an output of a single wavelength. Instead, they emit a narrow range of wavelengths or a band of spectral width. On propagation through an optical fibre, the received signal is broadened. These effects accumulate with distance and result in intersymbol interference and power fading causing increased bit error rate. In SMFs, CD comprises of material and waveguide contributions while in multi-mode fibres, additional modal dispersion is realized. CD phenomenon is also referred to as group velocity dispersion (GVD) because dispersion result from group velocity being dependent on wavelength [126].

3.8.3.1 Theory of chromatic dispersion

The inherent property of the fibre is responsible for the dispersion. Speed of light is dependent on the refractive index of the fibre. The refractive index therefore varies with wavelength [130]. The different wavelengths in a light pulse will propagate with different group velocities, ν_g in the fibre due to finite spectral widths of the signal thus resulting in group delay being dependent on the optical frequency, ω. The group velocity is given by

$$v_g = \left(\frac{\partial \beta}{\partial \omega}\right)^{-1} \tag{3.26}$$

where ν_g is the group velocity and β is the propagation constant. Propagation constant is given by fibre's length per unit group velocity i.e. $\beta = L/\nu_g$. Note that $k = 2\pi/\lambda = \omega/\nu$.Different group velocities lead to group delay, T_G is given by

$$T_G = \frac{\partial \varphi}{\partial \omega} \tag{3.27}$$

where φ is the optical phase and ω is the optical frequency. Differentiating T_G with respect to ω, we obtain

$$D = \frac{\partial^2 \varphi}{\partial \omega^2} \tag{3.28}$$

where D is the fibre dispersion. Mathematically, D is the second order derivative of the optical phase with respect to the optical frequency as shown in equation (3.28). Second order dispersion parameter, β_2 describes the group-velocity dispersion (GVD), and is related to the

dispersion parameter at the reference wavelength, λ as

$$\beta_2 = -\frac{\lambda^2}{2\pi c} D \tag{3.29}$$

The dispersion, D in equation (3.29) can be rewritten as

$$D = \frac{\partial}{\partial \lambda}\left(\frac{1}{v_g}\right) = -\frac{2\pi c}{\lambda}\beta_2 \tag{3.30}$$

where ν_g is group velocity, c is speed of light, β_2 is the group-velocity dispersion and λ is reference wavelength. Differentiating equation (3.30) with respect to wavelength, it yields the dispersion slope, S given by

$$S = \frac{\partial D}{\partial \lambda} = \frac{2\pi c}{\lambda^3}\beta_2 + \left(\frac{2\pi c}{\lambda^2}\right)^2 \beta_3 \tag{3.31}$$

where S is the dispersion slope, β_2 is the group-velocity dispersion and β_3 is the third order dispersion parameter. At zero dispersion wavelength, β_2=0. So the dispersion slope is proportional to β_3 [128]. In SMFs, the total chromatic dispersion is given by the sum of material and waveguide contribution.

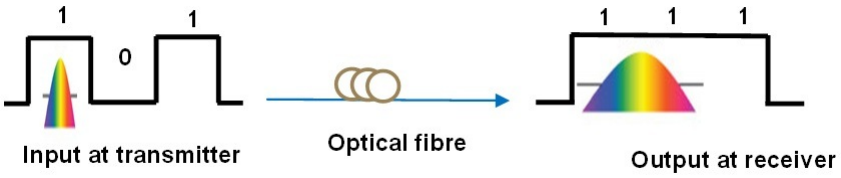

Figure 3.14: Illustration of dispersion effects in an optical fibre.

Figure 3.14 shows how errors are introduced because of pulse broadening in an optical fibre. The broadening of the pulse limits the available bandwidth and transmission distance especially as the bit rates increase. Therefore to increase the transmission distance at increased bit rates some compensation may be needed. Owing to the property of the fibre, the broadening arises because of the line width of a laser. If a laser has a very small line width, then there are few spectral components thus reduced broadening. Raycan VCSEL has a line width of about 0.2 nm at -20 dB full width. Together with the chirp arising from direct modulation of the VCSEL, dispersion penalty affects limits the transmission distance especially at higher data rates.

3.8.3.2 Chromatic dispersion measurement

Different CD measurement techniques employed in optical fibre communication can be classified into phase shift technique [126, 165], pulse delay method [166, 167] and interferometric technique [168-173]. The dispersion coefficient, D in a fibre can determined using,

$$D = \frac{\triangle\tau}{(\triangle\lambda)\, L} \tag{3.32}$$

Similarly, D can be expressed in terms of phase as,

$$D = \frac{\triangle\phi}{360^0 f_m L\, (\triangle\lambda)} \tag{3.33}$$

where $\triangle\tau$ is time delay (see equation (32)), $\triangle\phi$ is the phase change, f_m if the modulation frequency, $\triangle\lambda$ is the average between the two wavelengths and L is the length of the fibre. In the phase shift method, sinusoidally modulated signals at different wavelengths are propagated in a fibre and the phase change determined. The pulse delay also known as time of flight technique, measures the propagation time between pulses simultaneously launched into a fibre. The third technique uses two paths created using a Mach-Zehnder or Sagnac interferometers to measure the delay in a fibre. One is the reference path while the other is the path under test. Interferometric technique has a higher resolution of 0.1 ps but suited for distance below five metres of fibre. The phase shift and pulse delay methods are used for fibre lengths greater than 0.5 km and have resolutions of 10-20 ps and 50-100 ps respectively [174].

3.8.3.3 Chromatic dispersion compensation

Chromatic dispersion compensation approaches have been implemented in optical networks. The three main categories employed in telecommunication are precompensation, in-line and postcompensation schemes [1, 175].

The precompensation schemes are prechirp, novel coding and nonlinear prechirp techniques. The prechirp technique was introduced to reduce chirping in lasers that are directly modulated [102, 103] though it can be employed in externally modulated lasers [176]. Novel coding also known as dispersion supported transmission [177] involves the use of frequency shift keying (FSK) or duo binary coding [176] as opposed to conventional amplitude and frequency modulations. Nonlinear prechirp technique on the other hand helps limit the chirp effects related to carrier induced variations in the fibre's refractive index leading to self-phase modulation, cross phase and four-wave mixing in WDM systems [178].

Postcompensation techniques involves electronic correction and equalization of the signal at the receiver [75]. Advanced techniques make use of forward error correction to recover the correct information at the receiver [179]. Forward error correction improves the sensitivity and expands scalability while mitigating dispersion as well as nonlinearities in the transmission [47, 176, 180, 181]. In the digital domain, offline dispersion compensation can be done using the digital signal processing (DSP) [38, 182-185]. DSP in practice has a drawback because of data accumulation during processing especially if the program and hardware are not fast enough. It can be costly when large bandwidth signals are involved.

The in-line compensation techniques comprise of optical filters, optical phase conjugation [186], fibre Bragg grating (FBG) and use of dispersion compensating fibres (DCFs) [1]. Each of the compensation techniques mentioned has pros and cons. DCF is widely used because of cost, ease of implementation and its effectiveness. Dispersion compensating fibre (DCF) is a fibre with large negative dispersion coefficient (up to -100 $ps/nm.km$) at 1550 nm. It is achieved by tailoring the fibre properties making use of the anomalous dispersion regimes. Different designs of DCF optimized for different fibres and applications are provided [187-189]. DCF is used in optimizing 1550 nm transmission in conventional single mode fibres [190] and non-zero dispersion shifted fibres (NZDSFs) [191]. The DCF is added to an existing SMF to cancel the dispersion. When the dispersion is cancelled the transmission reach is improved. For instance, 10 $Gbps$ over 1000 km of transmission aided by Erbium doped fibre amplifiers (EDFAs) over L band has been achieved using conventional DCF [192]. The length of the DCF required for compensation can be reduced by using fibres with very large negative dispersion coefficients [190]. Therefore, the higher the dispersion coefficient of the compensating fibre, the shorter the length. The relationship is given as

$$L_{DCF} \times D_{DCF} = -L_{SMF} \times D_{SMF} \tag{3.34}$$

where L_{DCF} is the length of the DCF, L_{SMF} is the length of the SMF, D_{DCF} is the dispersion value of the DCF and D_{SMF} is dispersion value of the SMF.

New designs of DCF for cabled applications called inverse dispersion fibre (IDF) have been introduced [193]. The typical dispersion coefficients for various fibre designs reported are -20.8 $ps/nm.km$, -39.9 $ps/nm.km$, -54.2 $ps/nm.km$ and -100 $ps/nm.km$ for IDFx1, IDFx2, IDFx3 and conventional DCF respectively. The attenuation for IDFx1, IDFx2, IDFx3 and DCF are 0.233 dB/km, 0.258 dB/km, 0.293 dB/km and 0.5 dB/km respectively. The nonlinear coefficients are 3.51 $W^{-1}km^{-1}$, 4.25 $W^{-1}km^{-1}$, 5.22 $W^{-1}km^{-1}$ and 7.87 $W^{-1}km^{-1}$ respectively. IDFx2 and IDFx3 offer better compensation performance than IDFx1 because of reduced nonlinear signal degradation due to high attenuation and dispersion [193, 194]. It has high negative dispersion values depending on SMF to DCF length ratios and negative dispersion slope enabling both dispersion and dispersion slope compensation [190]. The negative dispersion and dispersion slopes are achieved by doping the core of the compensating fibre. Tailoring the core makes it possible for the accumulated dispersion in the transmission fibre to be cancelled over a wide range of wavelength [195]. The dispersion and dispersion slope of the DCF and transmitting fibre should be matched in order to compensate the accumulated dispersion effectively over all the wavelengths [187]. The condition for both dispersion and dispersion slope compensation is that the relative dispersion slope (RDS) of the compensating and compensated fibre must be equal [191, 196]. RDS is given by

$$RDS = \frac{Dispersion\_slope}{Dispersion} = \frac{S}{D} \tag{3.35}$$

RDS values of 0.00904 nm^{-1} and 0.0064 $nm^{-1}$are reported to give total dispersion and dispersion slope compensation for RZ-NZDSF in the C- and L bands respectively [191].

3.8.4 Stimulated Raman scattering

Nonlinear effects in an optical fibre arise because of high intensity leading to refractive index change with power. This power-dependent phenomenon is referred to as Kerr effect. This relation is given by the expression

$$n = n_0 + n_2 \frac{P}{A_{eff}} \tag{3.36}$$

where, $n_2 \alpha \frac{\chi^3}{2n_0}$, n - refractive index, n_0 - refractive index at low optical power, n_2-nonlinear refractive index, P - power and A_{eff} - effective area. This change in the refractive index with power causes self-phase modulation (SPM), cross-phase modulation (XPM) and four-wave mixing (FWM). The other nonlinear effect arises because of scattering phenomenon where energy exchange between electromagnetic field and dielectric takes place. This causes stimulated Raman scattering (SRS) and stimulated Brillouin scattering (SBS) [138].

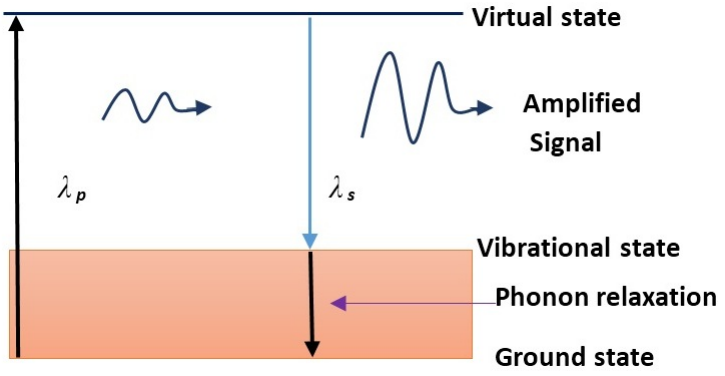

Figure 3.15: Illustration of stimulated Raman scattering.

Extensive research has been done since the observation of SRS in 1962 [197]. Stimulated Raman scattering (SRS) limits the performance of multichannel lightwave systems by transferring energy from one channel to another. It involves transfer of electromagnetic energy from lower frequency to higher frequency state [138]. This deleterious effect has been made useful in optical communication through Raman amplification. In Raman amplification, a high power pump ($> 15\, dBm$) is used to generate frequency-shifted radiation called the Stokes wave which then transfers energy to the signal [198]. SRS process is as shown by the quantum representation in figure 3.15. When a high power pump of wavelength, λ_p interacts with a signal of

wavelength, λ_s in a fibre, a pump photon is converted to a signal photon replica of the first as the residual energy forms an optical phonon [138]. For silica fibres, the condition for Raman amplification to occur is that the wavelength spacing between the signal wavelength and pump wavelength should be 100 nm (13.2 THz). Figure 3.16 shows the gain profile variation with Stokes shift. The shift exhibit maximum gain at 13.2 THz which corresponds to 100 nm - wavelength difference between the pump and the signal. Raman amplification occurs at C - band implying the pump wavelength should be about 1450 nm [199]. Advantages of Raman amplification over erbium doped fibre amplifiers and semiconductor optical amplifiers include improved noise figures and reduced nonlinear penalties which allow longer amplifier spans, higher bit rates, closer channel spacing, and operation near the zero-dispersion wavelength. Unlike erbium doped fibre amplifiers (EDFAs) which are slow and require special fibre, Raman gain processes are fast and SRS can occur in any optical fibre (does not need a special fibre). Semiconductor optical amplifiers (SOAs) gain is polarization dependent due to short lifetime of charge carriers leading to large crosstalk and inter-modulation distortion. SOAs and EDFAs have limited bandwidths [138, 200, 201]. Raman gain can be tailored to provide amplification over a wide range of wavelengths through the use of multiple pumps. Raman amplification can be either distributed or lumped. In distributed Raman amplification (DRA) the entire transmission fibre is the gain medium for the signal propagating. In lumped amplifiers, the amplification takes place on a small section preferably in a module. So the signal undergoes amplification periodically. DRA has advantage in the sense that the signal is amplified before getting attenuated to very low powers thus improved optical signal to noise ratio (OSNR) [202]. The nonlinear interaction between the signal and the pump is given mathematically. The pump power (P_p) and signal power (P_s) along the propagation direction, z of the fibre can be expressed [199] as

$$\frac{dP_s}{dz} = -\alpha_s P_s + \left(\frac{g_R}{A_{eff}}\right) P_p P_s \tag{3.37}$$

$\backslash/$

The polarization dependent expression is

$$\xi \frac{dP_p}{dz} = -\alpha_p P_p - \left(\frac{\nu_p}{\nu_s}\right)\left(\frac{g_R}{A_{eff}}\right) P_s P_p \tag{3.38}$$

where g_R is the gain, P_p and P_s are the pump and signal powers, ν_p and ν_s are pump and signal frequencies respectively. ξ indicates the polarization dependency and A_{eff} is the effective area.Equations show that the pump power provides the energy for amplification and the pump is depleted as the signal power increases. Attenuation in the fibre reduces the optical power as the fibre length increases.

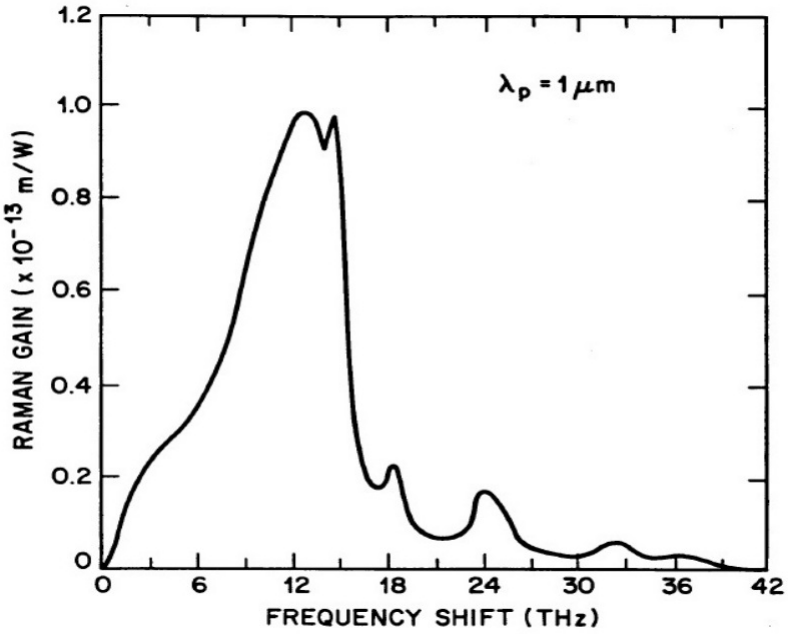

Figure 3.16: Raman gain spectrum for silica at pump wavelength = 1μm [203].

With amplification, the signal power transmitted for forward pumping can be expressed as

$$P_s(L) = P_s(0)exp\left(\frac{g_R P_0 L_{eff}}{A_{eff}} - \alpha_s L\right) \tag{3.39}$$

The effective length, L_{eff} is the length over which SRS occurs [204], and is given as

$$L_{eff} = \frac{1 - exp(-\alpha_p L)}{\alpha_p} \tag{3.40}$$

where α_p and α_s are pump and signal attenuation coefficients respectively.

The on-off amplification gain, G_A can be defined as the ratio of the signal with and without Raman amplification. This is given by

$$G_A = \frac{P_s(L)}{P_s(0)exp(-\alpha_s L)} = exp(g_R P_0 L_{eff}) \tag{3.41}$$

High on-off gains have been achieved in silica fibres. Since the SRS process is polarization dependent, the PMD due to fibre birefringence can lead to Raman gain fluctuations. To overcome the polarization which is unpredictable in a fibre, we make use of orthogonally polarized pumps [199, 205].

3.8.4.1 Raman pumping techniques

There are three pumping schemes of Raman amplification in fibre optic communication. These are forward, backward and bidirectional. In the forward pumping scheme, the pump and the signal co-propagate in the same direction in an optical fibre. Forward pumping has a

higher optical signal to noise ratio (OSNR). In the backward or counter pumping scheme, the signal and pump propagate in opposite direction, the walk-off effect between the signal and the pump leads to lower polarization dependent gain as compared to the forward pumping. This scheme also has a low OSNR as the signal is weakest when the pump is strongest as they traverse each other. However, the intensity noise transfer from pump to signal is lower compared to co-pumping scheme. Bidirectional pumping involves the use of two pumps. This pumping scheme balances the noise figures between the co- and counter pumping schemes, thus flat and wide bandwidth is achieved. Pump noise transfer largely affects the signal [205]. This is because the Raman amplification uses virtual excited states. There is no smoothening of pump fluctuations due to lack of population inversion. Noise transfer is a problem in most amplified optical signals. Distributed Raman amplification suffer relative intensity noise (RIN), Raleigh backscattering and pump polarization fluctuations which limit the gain. Similarly pump depletion as a result of interaction between pump-to-pump, pump-to-signal, signal-to signal limit optimum performance [206].

3.9 Link budgeting

To account for the gains and losses in a link, system design budget is necessary. It accounts for the attenuation in the medium with respect to the available power. The important aspects are the transmitter power, receiver sensitivity at acceptable bit error rate and additional components contributing to the path loss and gain. Modulation technique is a key consideration as it defines the sensitivity. Amplification brings about the gain. Mathematically, the available power for budgeting is given by

$$P_A =\mid R_s - P_0 \mid \tag{3.42}$$

where P_A is the available power (dBm), R_S is the receiver sensitivity (dBm), P_0 is the transmitter output Power (dBm). The range budget, R_B is given by

$$R_B = \frac{P_A - S_{IL} - CS_L - M_s}{O_L} \tag{3.43}$$

where S_{IL} is the splitter insertion loss, C_{SL} is the connector and splice losses, M_S is system margin and O_L is the optical loss given by the attenuation coefficient of the fibre. Therefore the power budget is expressed as

$$P_0 = R_s + C_L + M_s \tag{3.44}$$

where C_L is the channel loss taking into account the fibre loss, splitter insertion losses, connector and splice losses while M_S is system margin. System margin allocates power penalties

and other additional sources in the link that may develop because of component degradation. Power penalties arise due to several factors which include dispersion (CD and PMD), polarization dependent losses, crosstalk and nonlinear effects.

In chapters 4, 5, 6 and 7 to follow, we present our findings performed through experiments and simulations. Chapter 4 discusses the field measurements performed at Karoo telescope site while chapters 5, 6 and 7 describes VCSEL transmissions over typical SKA distances performed in a laboratory testbed.

Chapter 4

Polarization effects in KAT-7 telescope and its relevance to MeerKAT time and frequency reference

Polarization related impairments affect the accuracy and stability of the time and frequency reference signal in the array. Optical fibres are expected to maintain the same of state of polarization throughout its length but due to birefringence and mode coupling arising from the factors explained in section 3.9.2 of chapter 3, the polarization stability is changed. The dependence of refractive index of the fibre on the polarization and direction of light affect the transmitted signal. The stability of a clock signal sent over fibre therefore is subjected to the birefringence in the fibre. Clock accuracy and stability in the array is required for proper functioning of the telescope. The telescope monitoring and control as well as analogue to digital conversion of streaming astronomical data relies on a clock. In this section, we study the polarization effects arising from the antenna dynamics in the KAT-7 array. KAT-7 array comprising of 7 antennas has a single mode fibre network linking the individual dishes in the array to the processing station in Karoo. The KAT-7 study is relevant to the MeerKAT telescope network because of similar dish dynamics in addition to the environmental conditions arising from the same geographical area. We also consider similar fibre type of typical distance expected in the MeerKAT telescope.

4.1 Experimental set-up to investigate polarization

Figure 4.1 shows a picture of KAT-7 antennas. This picture displays the pedestal and the focus of an antenna. It also points the antenna service container (ASC) building which lays some few metres (up to 200 m) from the individual antenna.

Figure 4.1: A picture of KAT-7 antenna [16].

Figure 4.2 gives the fibre layout and illustration of the antenna angular displacements and degrees of freedom. Computing container (CC) building refers to the control point adjacent to the processing office in Karoo. ASC refers to a point at the antenna site where the fibres from the individual antenna in the KAT-7 array are connected to the buried fibre.

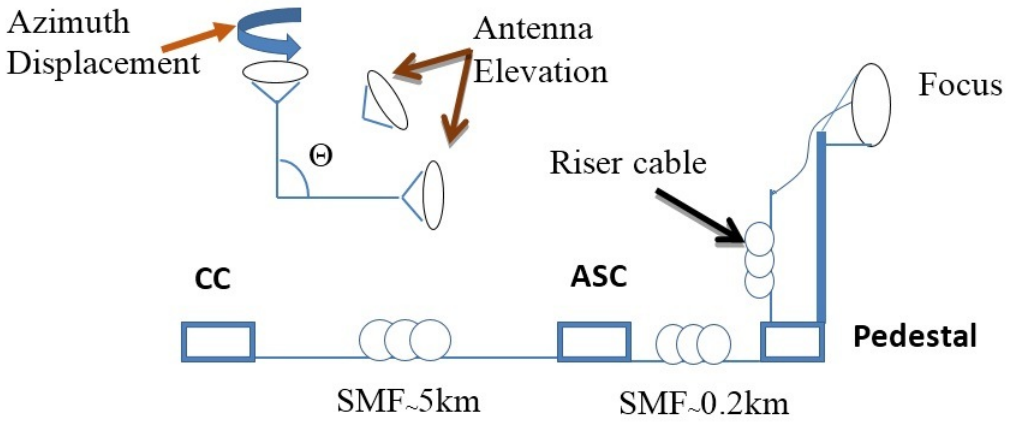

Figure 4.2: Schematic fibre layout in KAT-7 telescope with antenna degrees of freedom i. e. Azimuthal angular displacement (shown by arrow) and elevation angular displacement (Θ). Single mode fibre (SMF), computing container (CC) to Antenna service container (ASC).

Pedestal refers to the base of the antenna while focus refers to radiation convergence point (dish feeder) at the top of the antenna. The exposed section of the fibre from the pedestal to the focus is referred to as riser cable and is $< 25\ m$. Using optical time domain reflectometer (OTDR) measurements, the fibre lengths were determined where the return trip from CC to ASC is 9.76 km, return trip from CC to pedestal is 10.17 km and return trip from CC to focus is 10.25 km. The SMF is buried $1m$ below the surface of the ground.

Figure 4.3: (a) Picture of a Femtosecond PMD analyzer (EXFO FPMD 5600) used in the measurement (b) Research set-up used to study the polarization effects. CW is continuous wave and FUT is fibre under test.

Femtosecond PMD system displayed on figure 4.3 (a) uses the polametric technique to establish the differential group delay (DGD) in a fibre. It is one of the PMD measuring methods that has advantage of ability to measure DGD to the femto second range over a wide range of wavelength. Its wavelength range is 1250 nm to 1700 nm. It can be used to characterize the DGD in broadband and narrowband. Figure 4.3 (b) depicts experimental design set at the CC unit in KAT-7 telescope. Polarimeter, Adaptif A1000 and a 1450 nm continuous wave (CW) laser module was used. We considered one antenna in the KAT-7 array. Three sections of the fibre network were studied. The first section is the buried fibre section between the CC and ASC. Secondly, a loop back at the pedestal was used to study the fibre section excluding riser cable. Lastly, the entire fibre section from the CC to the focus (including riser cable) was analysed. The dish positions in terms of azimuth and elevation angles were varied as the antennae scanned the sky, and the measured polarization and DGD data recorded.

4.2 State of polarization fluctuation due to antenna dynamics

In this study, we present our findings under two different conditions over 14-hour period. As the state of polarization (SOP) change between the fast and slow axes in a fibre, the phase of the clock changes by an amount equal to the differential group delay (DGD) of the fibre section after the point of SOP change.

4.2.1 Fibre buried section (CC to ASC)

Figure 4.4 shows the overnight SOP monitoring on the buried single mode fibre. From the path traced on the Poincaré sphere in figure 4.4 (a), it is clear that the SOP of the buried fibre is very stable with a very slow drift of 15^o over 14 hours as shown in figure 4.4 (b).

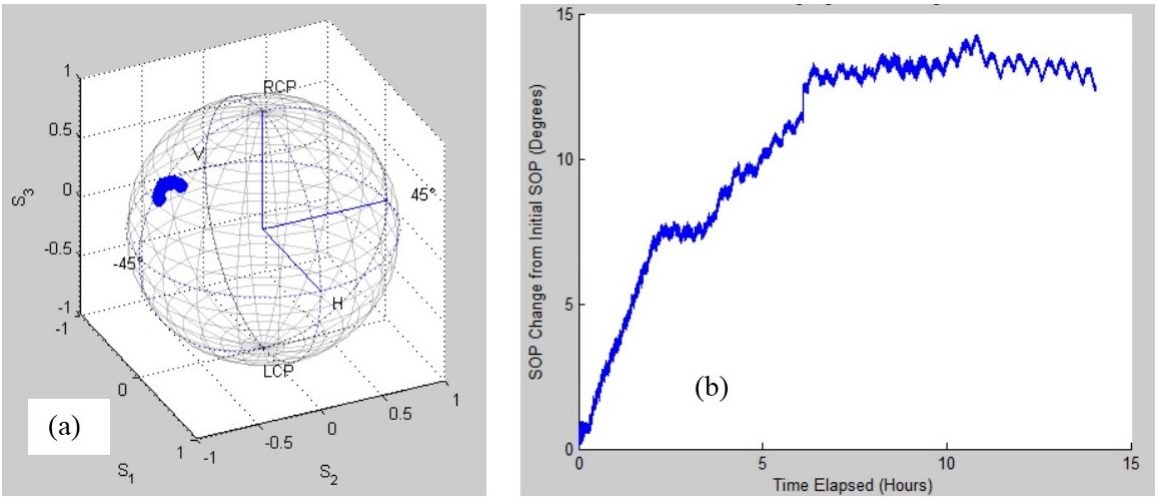

Figure 4.4: SOP monitoring from the processing office to the base of the dish (a) Total path traced out by the SOP on the Poincaré sphere as the polarization changes with time. (b) Angular deviation of the SOP from its original starting SOP as a function of time.

The ripples could be attributed to the vibrations from running machines in the CC unit probably air conditioner used to control the temperature in the CC. However, correlation between the magnitude of vibrations and vibrational frequency must be established to ascertain this.

4.2.2 Entire fibre (buried and riser cable sections)

In this section, we subject the polarization measurement to two conditions.

4.2.2.1 Case 1: Real time astronomer use of the telescope

The first case presented in figure 4.5 provides real time measurement during astronomer use of the telescope. The polarization was monitored from 6 pm to 9 am (overnight). Figure 4.5 (a) shows the total path traced by SOP on the Poincaré sphere as the dish describes all the possible degrees of freedom as it scans the sky. Figure 4.5 (b) shows there is random and high SOP change (up to $\sim 180^o$) due to dynamics of the dish. Clearly, the SOP randomness is relative as not all the Poincaré sphere is populated by the polarization states or light orientations. The SOP path can be related to the dish motion but the complexity arises due to other birefringent factors and multiple scans described by the dish while tracking over the 14 hour period. From the stability of the buried fibre as inferred from figure 4.4, it is found that the SOP change is contributed by riser cable section as the antenna scans the target astronomical object in the sky. The exposed section of the cable is subjected to extrinsic perturbations contributing to the overall birefringence.

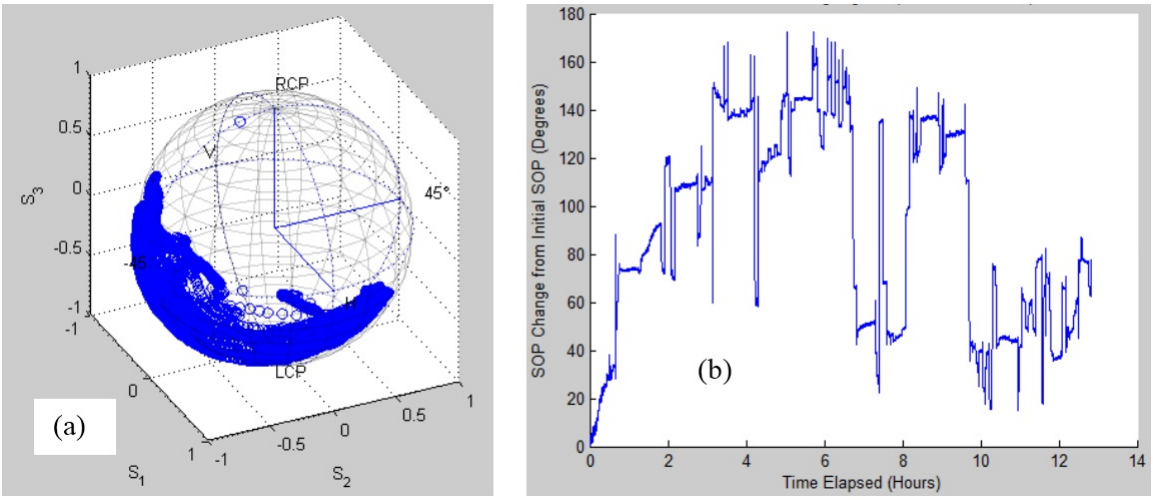

Figure 4.5: SOP monitoring from the processing office to the focus of the dish a) Total path traced out by the SOP on the Poincaré sphere as the polarization changes with time. b) Angular deviation of the SOP from its original starting SOP as a function of time.

Basically, the riser cable is a special case of a deployed aerial fibre but with small or minimized galloping. Galloping is the sagging of aerial fibres between the poles because of strong or moderate winds. The two other aerial fibre displacements are vortex induced and wake induced vibrations. The categories are based on frequency range, peak to peak amplitude, the wind velocity and the nature cable surface [207]. All these wind oscillations eventually cause some resonance which affects the signal in the fibre. Vortex induced vibrations are small in amplitude compared to wake induced vibrations. The stress and strain from the dish dynamics describes similar case to the wind blowing in random varying directions at varied velocities. Also the wind effect on the fibre is not completely isolated from temperature variation as in a dish environment. The exposed fibre section is prone to temperature changes which has pronounced influence on aerial fibres [145]. On the contrary, the dish scanning is continuous unlike winds which can sometimes be calm. The additional factors evident in the telescope environment are the twists and bends whose effects on the fibre are elaborated in [155]. Birefringence mechanism is introduced by fibre asymmetry leading to an anisotropic refractive index distribution in the core region. The change in the ellipticity and orientation of the light signal in the fibre leads to change in the Stoke's vectors thus varying the polarization. The asymmetry can arise because of geometric deformation or material anisotropy through elasto-optic, magneto-optic and/or electro-optic index changes [155]. The geometrical asymmetry and stress induced material birefringence is used in the description of polarization fluctuation with relation to fibre parameters. The non-circular core induce a linear birefringence. This makes the light component on the smaller diameter of the core propagate faster than the longer diameter in a fibre. Similarly, a linear birefringence is caused by asymmetrical lateral stresses through elasto optic index changes. When there is a bent on a fibre, one side is

subjected to tension while the other is compressed, this effect is translated to the lateral stress in core leading to linear birefringence. When a fibre is twisted, the stress induced leads to circular birefringence because of the coupling of the modes [155]. It is due to all these factors that polarization changes in a fibre. The overall effect of polarization is that the phase of the clock signal can drift by the magnitude of the birefringent difference in the fast and slow axis affecting the accuracy [208].

4.2.2.2 Case 2: Controlled mode of telescope

Figures 4.6, 4.7 and 4.8 give a controlled state of the antenna (dish) where the instrument is restricted to describe defined degrees of movement over a short time ($\sim$ 15 minutes). The antenna degrees of movement is elevation or/and azimuth displacements.

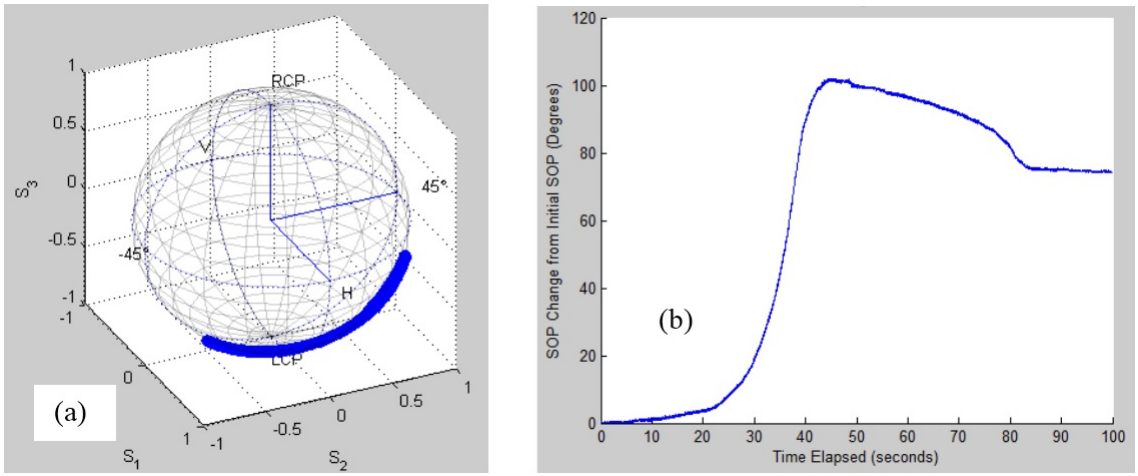

Figure 4.6: (a) SOP fluctuations over 10° to 90° elevation scan for constant azimuth angle of -30° (b) corresponding SOP angular change with time.

Figure 4.6 (a) shows the SOP on the Poincaré as the dish makes the 80^o elevation angular displacement, the corresponding SOP change with time is shown in figure 4.6 (b). The dish motion as it rises subjects the fibre cable to a bent which leads to a compressional and tensional force on the different transversal sides of the fibre. This however depends on the neutral position (stress free). If in a neutral position the dish focus is facing parallel to the ground, then the elevation displacement induces lateral stress on the fibre. If the fibre is at neutral position when the dish focus is perpendicular to the ground, then the 80^o angular displacement relaxes the fibre from a possible lateral stress. In the latter case, environmental factors contribute to the birefringence while the fibre movement changes the SOP. The drop at 40 seconds (s) on figure 4.6 (b), suggest that the fibre that was bent is regaining by shifting to low lateral stress position thus changing the polarization of light. Linear birefringence prevails in this condition [155].

Figure 4.7 (a) presents the Poincaré representation of SOP dynamics as the elevation is maintained while azimuth angle is varied. The dish describes 390^o about the vertical axis while maintaining the elevation angle at 90^o. The azimuthal displacement induce a twisting or a torsional force causing circular birefringence on the fibre. A maximum SOP change of about 80^o over the measurement period is as shown in figure 4.7 (b). Compared to the case in figure 4.6 (b), we can conclude that the fibre movement is responsible for the SOP change. As expected, an elevation change is expected to make more displacement than in a twisted case.

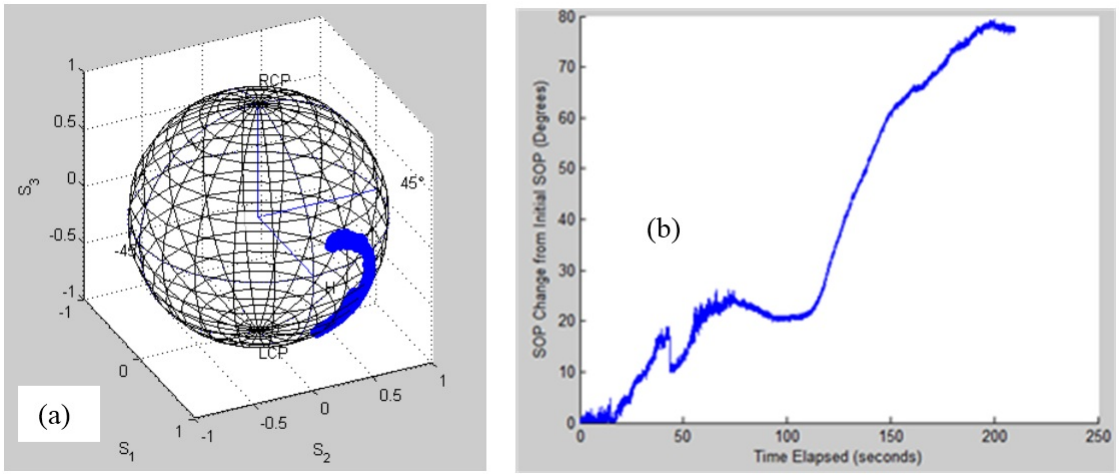

Figure 4.7: (a) SOP fluctuations over -180^o to 210^o azimuth scan for constant elevation angle of 90^o (b) corresponding SOP angular change with time.

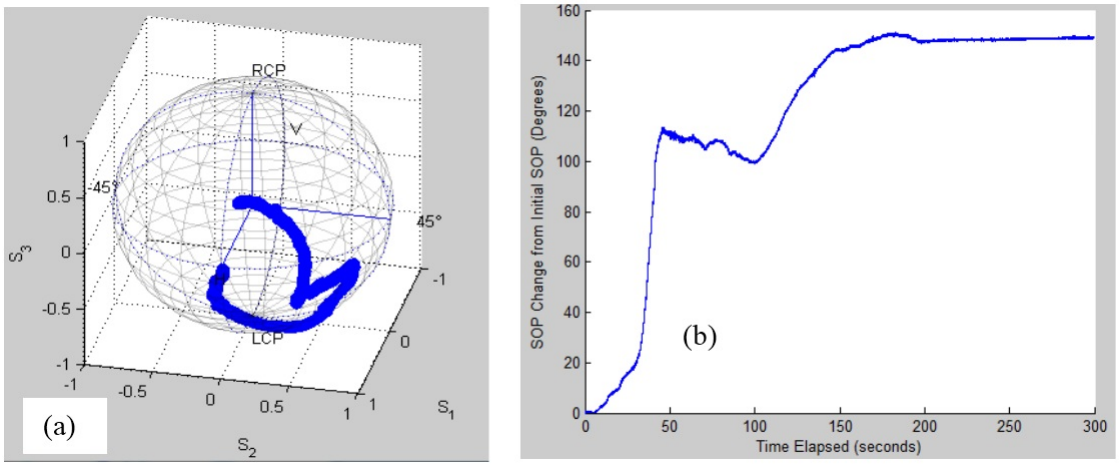

Figure 4.8: (a) SOP deviation as elevation angle is tuned from 10^o to 90^o, whilst azimuth angle is simultaneously tuned from -180^o to 210^o (b) corresponding SOP angular change with time.

Figure 4.8 (a) shows the Poincaré representation of SOP as the dish makes both the elevation and azimuthal displacements. The dish described 80^o on elevation while making

390^o of azimuth. This is a complex case combining the effects in figure 4.6 and figure 4.7. It is characterized by both lateral and torsional forces in the fibre [155]. Figure 4.8 (b), shows the SOP change for the simultaneous angular displacements. In this case, both the aspect of bending and twisting contribute to the birefringence change in the fibre. The simultaneous elevation and azimuthal angular displacements caused a high SOP fluctuation of up to 150^o due to fibre movement. The drop at 50 s could be as a result of the fibre relaxation, the SOP change is found to stabilize at 150^o from t =200 s to 300 s suggesting a stationary dish after the scan. In this case, the combined effects of linear and circular birefringence in the fibre contribute to SOP change. Figure 4.8 is a similar situation as in figure 4.5 but over a shorter time.

In this study, we have assumed the environmental conditions due to the short time of measurement. However, over a length of time, changes in temperature and wind may significantly alter the SOP. The exposed riser cable is susceptible to environmental conditions such as temperature and wind. Temperature change leads to thermal variation which greatly affects the SOP in a fibre. During spring season (end August- December) in Karoo, the daily temperatures may vary from 9 to 18 degrees Celsius (^oC), but on winter and summer seasons it may go low below freezing point and high above 40^oC respectively. This may further alter the stability of the SOP of the signal. Essentially, environmental conditions together with fibre disturbance (on the riser cable) cause the geometry of the fibre core to change causing a variation in the ellipticity and orientation of the light. The resulting change in ellipticity and orientation can be observed as defined by Stoke's vectors on a Poincaré sphere. The polarization fluctuations may have serious impact on optical fibre transmission where accuracy depends on the phase stability and therefore may need some polarization stabilization so as to minimize DGD in the network. The rate of clock drifts is related to the rate of polarization fluctuation.

4.3 Polarization stabilization using polarization maintaining fibre

In this section, we show the effect of polarization maintaining fibre (PMF) on a disturbance prone environment. The laboratory environment however does not bring a typical antenna movement as illustrated in the preceding section. In figure 4.9, a WDM DFB laser was used to generate a signal which was then scrambled before monitoring the polarization using a polarimeter over a short period of time. We used a fan to create some disturbance on the wound fibre under test (FUT). The fan is used as a mini -antenna to investigate movement or tracking of the dish. The fan describes only azimuthal displacement but less than 360^o as expected in a real telescope environment. Note that the FUT is not cabled. The SMF fibre

under test was then replaced with a PMF and the polarization monitored. In each case, the SOP was monitored for 15 minutes.

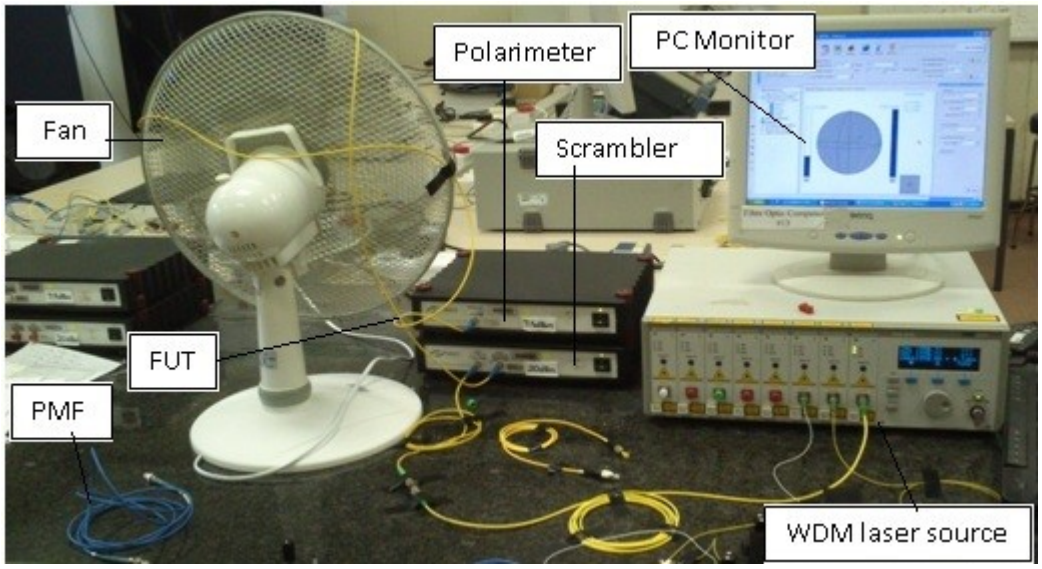

Figure 4.9: Experimental laboratory set up to demonstrate SOP stabilization using PMF.

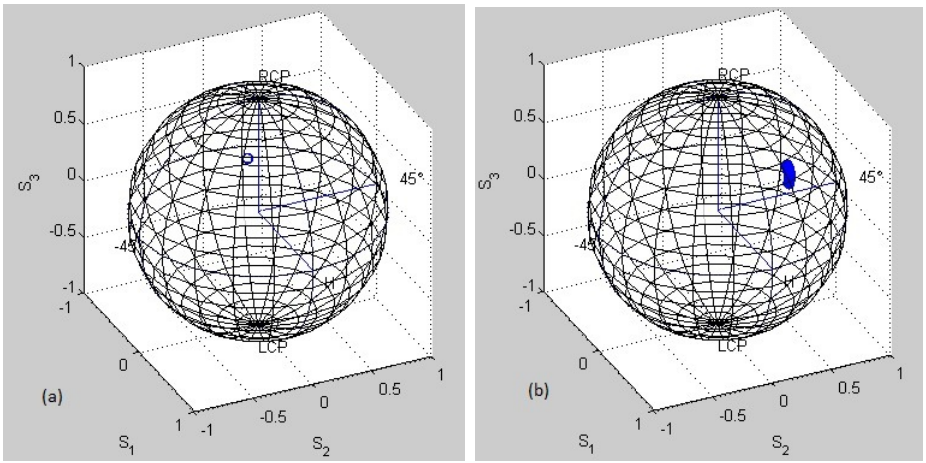

Figure 4.10: Polarization states of an undisturbed fibre (a) SMF (b) PMF monitored over 15 minutes.

The Poincaré representation in figure 4.10 shows comparative analysis of the polarization of the two fibres in a still environment. It is clear that SMF performance is marginally more stable and suitable in such environment. The two wound fibres were then separately subjected to a disturbance created by the running fan and the polarization monitored for 15 minutes. The disturbance illustrates the dish movement during a possible scan. The paths described in figure 4.11 shows performance of the SMF and PMF in a disturbed condition. It can be clearly noted that the magnitude of SOP change is reduced in PMF as compared to SMF. The PMF is seen to stabilize the polarization. Therefore to achieve stability, we recommend that

PMF fibre could possibly be used on the riser cable (from the pedestal to the focus). In this case, we minimize the effects of lateral and torsional stresses induced by the antenna dynamics during a possible scan of the sky. The reduced SOP will stabilize the clock signal transmitted in the fibre. The minimized SOP change is important in reducing polarization fluctuation of a clock signal transmitted in the fibre. For improved stability, thermal proof cabling for the exposed fibre section (riser cable) can be used to minimize temperature variation which affect fibre's birefringence during the different seasons of the year.

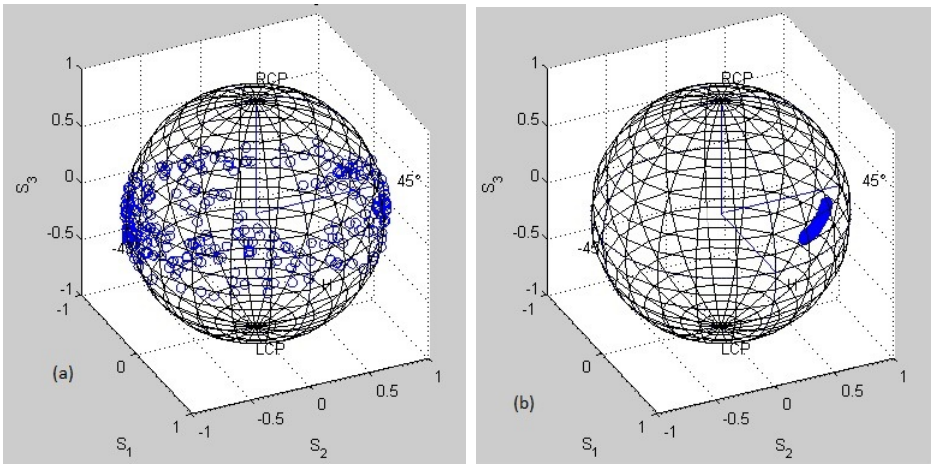

Figure 4.11: SOP representation of a disturbed fibre (a) SMF (b) PMF monitored over 15 minutes.

4.4 Differential group delay of the single mode fibre in KAT-7 telescope

Polarization mode dispersion (PMD) measured in KAT-7 telescope network is presented in this section. As mentioned at the beginning of this chapter, the aim of the measurement is to estimate fibre effects on the clock signal distribution in the MeerKAT telescope network. The fibre stretch from CC to focus and back to CC closely coincides with the MeerKAT's furthest antenna about 12 km from Karoo array processor building.Figure 4.12 shows a typical DGD variation with wavelength over the range $1530 - 1570$ nm as measured using a femtosecond PMD analyser. The fibre under test is labelled fibre 41-42 for identity purpose. This is one of the fibre links considered during the DGD measurements in KAT-7 network. The variability of the DGD is caused by the combined effects of birefringence and mode coupling in a fibre. The maximum and minimum DGDs are 0.277 ps and 0.0000779 ps respectively. The mean DGD for this measurement is 0.0861 ps. This is the average obtained over the range of wavelengths.

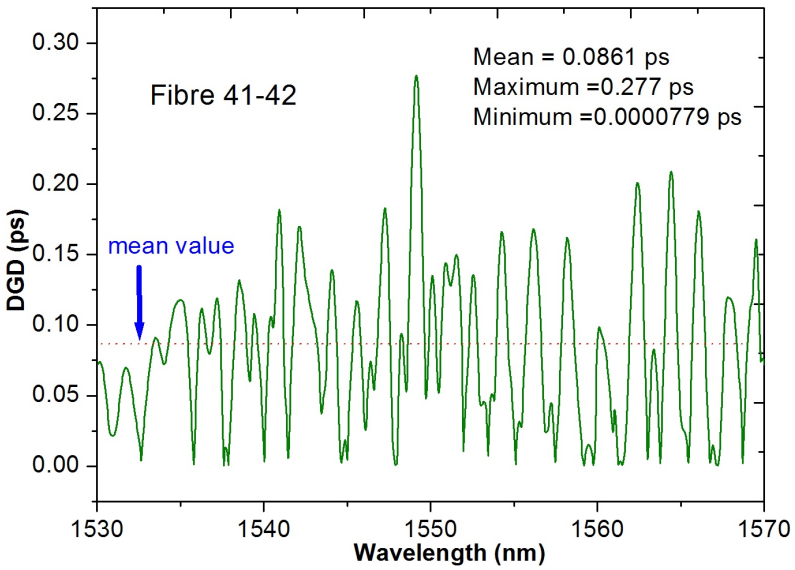

Figure 4.12: Typical relation between DGD and wavelength as measured on fibre 41-42.

Ideally the DGD should be measured over a long period of time under varying environmental conditions to obtain a statistically sound average result. For the rest of the measurements in this section, the DGD of all fibre links were measured over $1530 - 1570$ *nm* wavelength range. The DGD of the deployed and the undeployed fibres were measured so as to study the contribution of the deployment process.

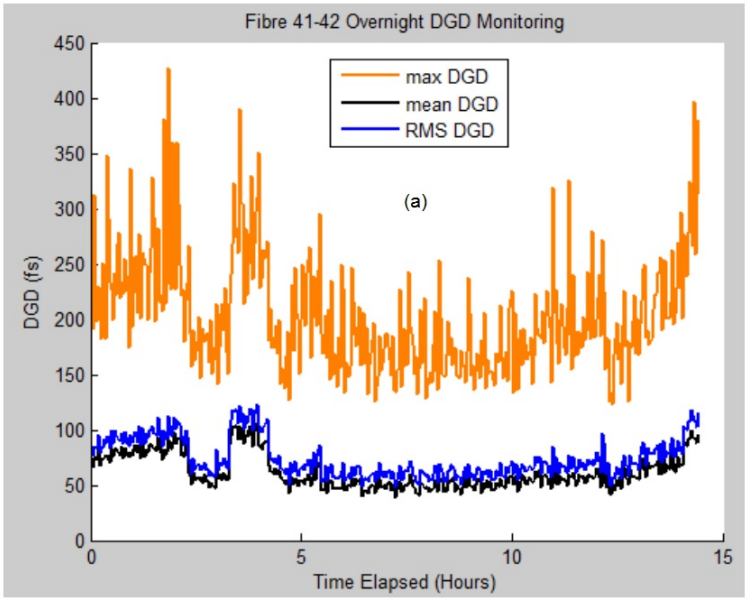

Figure 4.13: Maximum, mean and RMS DGD for as measured over the wavelength range 1530-1570 nm for the 15 hour overnight period.

Figure 4.13 gives the maximum, mean and root mean square (RMS) DGDs obtained from fibre 41-42 over the 15 hour period of measurement. The DGD versus wavelength measure-

ments were taken approximately every two and half minutes for the 15 hour period. These were then used to determine the maximum, mean and RMS DGDs. RMS DGD value is approximately equal to the mean DGD. The obtained values for the maximum and mean are 427 fs and 62.1 fs respectively. Figure 4.14 is a histogram for the measurement presented in figure 4.13 over the 15 hour period. The long term monitoring is to provide a statistical PMD value resulting from the particular environment.

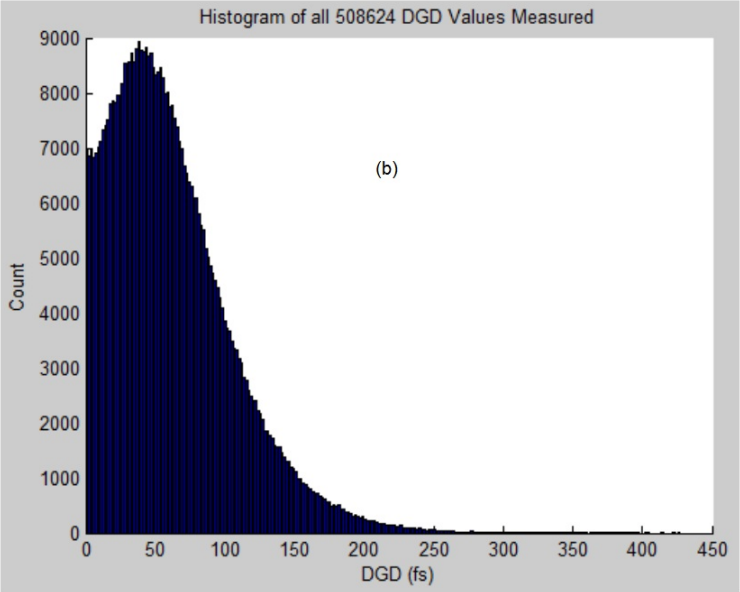

Figure 4.14: A histogram summarizing the DGD results over the 15 hour period.

Table 4.1 presents the DGD values of the deployed fibres. The fibres 13-14 and 15-16 were found to have a slightly higher DGD than other fibres and may be attributed to the stress induced on the particular fibres at the patch panel inside the antenna pedestal. he maximum mean DGD coefficient is 47.0 $fs/km^{1/2}$ and 30.48 $fs/km^{1/2}$ respectively. All the fibres from CC to ASC gave approximately same value of mean DGD and hence mean DGD coefficients of about 19 $fs/km^{1/2}$.

Table 4.1: Measured DGD values for the deployed SMF.

Fibre	Description	Mean DGD (fs)	Max. DGD (fs)	Mean DGD coefficients (fs/sqrtkm)
Fibre 3-4	CC to ASC	60.1	205.8	19.24
Fibre 9-10	CC to ASC	62.5	239.7	20.01
Fibre 11-12	CC to ASC	59.4	241.7	19.01
Fibre 13-14	CC to pedestal	149.9	378.5	47.00
Fibre 15-16	CC to Pedestal	97.2	306.9	30.48
Fibre 41-42	CC to Focus	84.8	217.7	26.49

The maximum and mean DGD for the 10.25 km (Fibre 41-42) deployed link is found to

be 217.7 fs and 84.8 fs respectively. From the DGD stability on fibres from CC to the ASC, the additional DGD on fibre 41-42 may have been contributed by the fibre from ASC to the focus; probably during deployment and also the exposed section comprising the riser cable [209]. The riser cable acts as a polarization hinge between two looped back fibre sections. The obtained DGD values are however low signifying high quality fibre and increased reliability in transmission.

Table 4.2: Measured DGD values for the concatenated undeployed SMF.

Fibre Id	Length (km)	Mean DGD (fs)	Max DGD (fs)	Mean DGD coefficients (fs/sqrtkm)
Fibre 1	1	8.3	16.3	8.30
Fibre 2	2	15.4	21.9	10.89
Fibre 3	3	19.3	34.8	11.14
Fibre 4	4	25.5	34.2	12.75
Fibre 5	5	32.3	43.0	14.44
Fibre 6	6	52.3	69.9	21.35
Fibre 7	7	44.1	56.8	16.67
Fibre 8	8	26.6	46.3	9.40
Fibre 9	9	29.7	54.5	9.90
Fibre 10	10	36.3	58.6	11.48
Fibre 11	11	43.6	69.7	13.15
Fibre 12	12	35.2	58.0	10.16

Table 4.2 presents the DGD values for the undeployed fibre. The undeployed cabled fibres were wound on a drum of diameter about 1 m in a store on the site. The cable consisted of 6 tubes, each with 8 fibres, for a total fibre count of 48. Each of the fibre was 1 km long. The 1 km fibres were spliced giving the various fibre lengths as shown in Table 4.2. The mean DGD values in Table 4.2 vary nonlinearly with the fibre length increase. This is because of the complexity introduced by the random mode coupling between adjacent fibre sections. For significantly long sections of fibre; such behaviour is known to introduce square root length dependence as in equation (3.25). Figure 4.15 presents the DGD values of the individual fibres in the undeployed cable. The variance in the DGD between the individual fibres is quite large. It ranges from 10 fs - 32 fs for the maximum DGDs and 4 fs - 25 fs for the mean DGDs. The general trend of the maximum values is seen to follow the mean values. The maximum and mean DGD of the 10 km undeployed fibre obtained is 58.6 fs and 36.3 fs respectively as shown in Table 4.2. Compared to the DGD of the deployed links with approximately the same length (see Table 1), there is seen to be a significant increase in the level of DGD in the deployed fibre. This could be explained by stress related perturbations during deployment, as well as environmental conditions such as temperature.

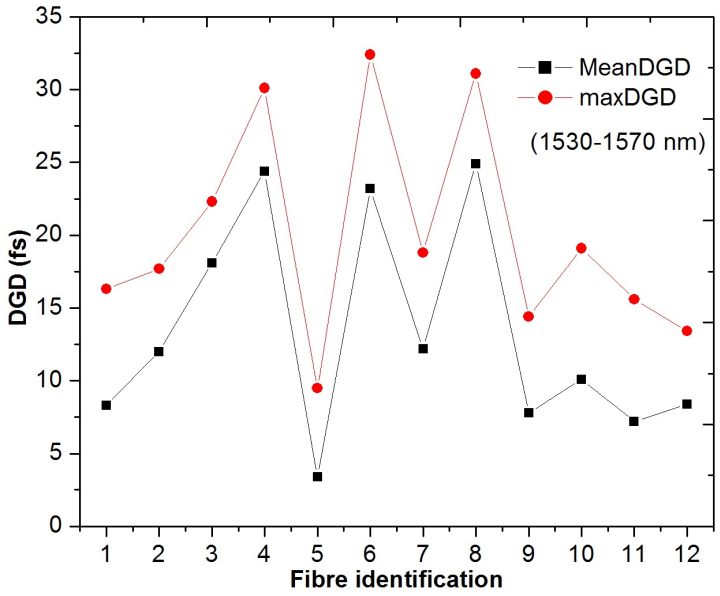

Figure 4.15: DGD values for individual 1 km undeployed links.

It should be noted that obtained PMD values for the deployed fibres are still low compared to levels that would be problematic for telecommunication applications. However, such PMD levels still need to be taken into consideration for the distribution of a highly stable clock reference tones over the fibre in the telescope array network. Clock stability depends on the fibre's DGD and polarization stability of the lightwave carrier. The magnitude of the clock drifts corresponds to the fibre's DGD after the point of polarization change. In the MeerKAT telescope array, clock signals of frequency 1712 MHz (L band), 1088 MHz (UHF band) and 14.5 GHz (X-band) will be distributed to remote dishes over fibre. In the L band of the MeerkAT, the measured DGD value of about 62.1 fs results to 0.01% of the clock period while the X-band frequency translates to 0.09%. The telescope proper functioning demands a clock stability as stipulated in section 2.3 of chapter 2. The stability is derived from the maximum allowable degradation which is about 2% in the instrument sensitivity. The 2% degradation translates to 0.2 radians or 11 degrees. The clock stability budget corresponds to 18.6 ps and 2.2 ps for L and X bands respectively in the MeerKAT telescope. The mean DGD of 62.1 fs is therefore within the allocated budget in the MeerKAT telescope. PMD however is not deterministic and higher values may be realized at later phases of SKA.

4.5 Summary

We have presented the polarization effects that result from fibre disturbance during dish movement as it scans. This fibre disturbance leads to SOP fluctuation that may result to changes in optical phase of the signal. The riser cable is subjected to environmental and physical conditions that may induce birefringence to the fibre core altering the polarization of the

clock signal. Fibre disturbance contributes to the birefringence and hence DGD of the optical network. This may affect the accuracy of time and frequency reference in MeerKAT and the later SKA fibre network. We have also demonstrated that polarization can be stabilized using polarization maintaining fibre. We have presented the PMD characterization for the SMF in the KAT-7 optical fibre network[1]. It is found that the PMD is relatively low, in the femto second range. It is also found that the PMD may change during deployment. This work of this chapter is valuable in providing SKA with relevant information pertaining the polarization and its management on clock signal distribution in the MeerKAT and SKA network.

The next chapter presents VCSEL performance on various transmissions mainly MeerKAT distances. It starts by characterization of the VCSEL device; the different VCSEL configurations, the transmitter-receiver optimization through modulation, performance comparison of PIN and APD photodiode and then performing transmissions on different fibres so as to establish the dispersion penalties. We then derive a link budget for the MeerKAT telescope fibre network from achieved VCSEL transmissions.

[1]The author is grateful to Eng. Renier Siebrits and Eng. Roufurd Julie, both of SKA, SA for the help in the organization of the site field measurements.

Chapter 5

High speed VCSEL transmission

The two paramount factors in an optical network are power consumption and quality of service. We start by explaining the VCSEL characteristics before dealing with the transmissions. VCSEL technology has become popular because of vast advantages over other sources as listed in chapter 3. MeerKAT telescope will have the furthest dish housed 12 km from the Karoo array processor building. In fact, even if the round trip monitoring is to be employed the farthest transmission distance is expected to be about 24 km.

5.1 VCSEL characteristics

The static and dynamic characteristic of Raycan VCSELs used in this study are provided. The characterization of the dynamic behaviour of the VCSELs is necessary for optimum performance if they are considered for direct modulation. The other interest is to show some of the advantages listed in chapter 3.

VCSELs used in the experimental work were manufactured by the Raycan Company. Both 4.25 *Gbps* 1550 nm and 10 *Gbps* 1310 nm VCSELs were considered in the study. Both showed similar characteristics in terms of power output as depicted in figure 5.1 (a) i and (b) i. The output power, P, variation with bias current, I_b, of the device is at room temperature. They have low threshold currents between $1 - 2$ mA. Both VCSELs operate in the mA range showing the energy efficiency of the device. The low power device is suitable for relatively short distances. Tuneability of about 3 nm and 5 nm for 1310 nm and 1550 nm respectively obtained as shown in figure 5.1 (a) ii and (b) ii. The threshold currents were found to be 2 mA and 1 mA for 4.25 *Gbps* and 10 *Gbps* VCSELs respectively. The device availability at 1310 nm and 1550 nm wavelengths with high data rates of more than 10 *Gbps* is an important feature for various applications in the telescope network. This implies that one of the wavelengths can possibly be dedicated to the control and monitoring while the other be used in the data transmission. Ease of direct modulation in VCSELs is cost effective as opposed to using

external modulators.

Figure 5.2 (a) shows the VCSEL wavelength tuneability and power change as bias current is varied. This shows that a VCSEL can be tuned to different channels using the bias current. Therefore, if VCSELs with similar characteristics are to be used, then each wavelength within the tuneability range could be dedicated to each device. The wavelength stability and tuneability allows for wavelength multiplexing which is used to increase the data rate over a single fibre in the array.

Simulation results on temperature relation with power output are also provided in figure 5.2 (b). The simulations in this work done were done using VPI [210]. VPI is a photonic simulation software supporting requirements of active and passive integrated photonics, fibre optic applications, optical transmission systems as well as network applications. Generally, simulation is a powerful tool in science and engineering for exploring the features and properties of systems which one may not be able to experimentally test due to the limitation of equipment as well as the risk of damaging a device. It allows the investigation of new ideas, trends and verification of some systems when build in an environment. The temperature behaviour is simulated due to lack of a heating chamber to experimentally investigate the performance in the expected typical environment.

To simulate the VCSEL temperature characteristics, the thermal effect parameters on the VCSEL model were set on. The current and power values were adjusted on the VPI tool so as to reproduce the $I_b - P$ characteristic curve as measured experimentally at room temperature. The parameters adjusted were the threshold current, I_{th}, thermal roll over current and thermal roll-over power. The thermal rollover current refers to the bias current corresponding to the maximum output power at specified temperature. The thermal roll-over power is the maximum possible power from the continuous wave laser at a particular ambient temperature. The model allowed the reproduction of the original characteristics of the device which in turn was used to investigate its performance at different temperatures. The ambient temperature was then increased as the $I_b - P$ behaviour was obtained. The experimental and the simulated VCSEL behaviour at room temperature agree as depicted in figure 5.2 (b). In the experimental curve, the bias current is restricted to 10 mA so as to avoid the damage of the device. The VCSEL performance is seen to reduce with increase in temperature. This is because temperature changes affect semiconductor band gap and change the carrier concentration. Temperature increase lead to performance degradation, therefore heat sources need to be minimized and efficient heat transport from the active region to a heat-sink is essential. The performance degradation is not only the power output as seen on figure 5.2 (b) but also the emission frequency is affected. Detailed device design measures to curb temperature related issues are given in [107]] [211, 212]. The issue of the VCSEL behaviour is critical because of the possible subjection of the device to a variation of temperatures in the telescope environment.

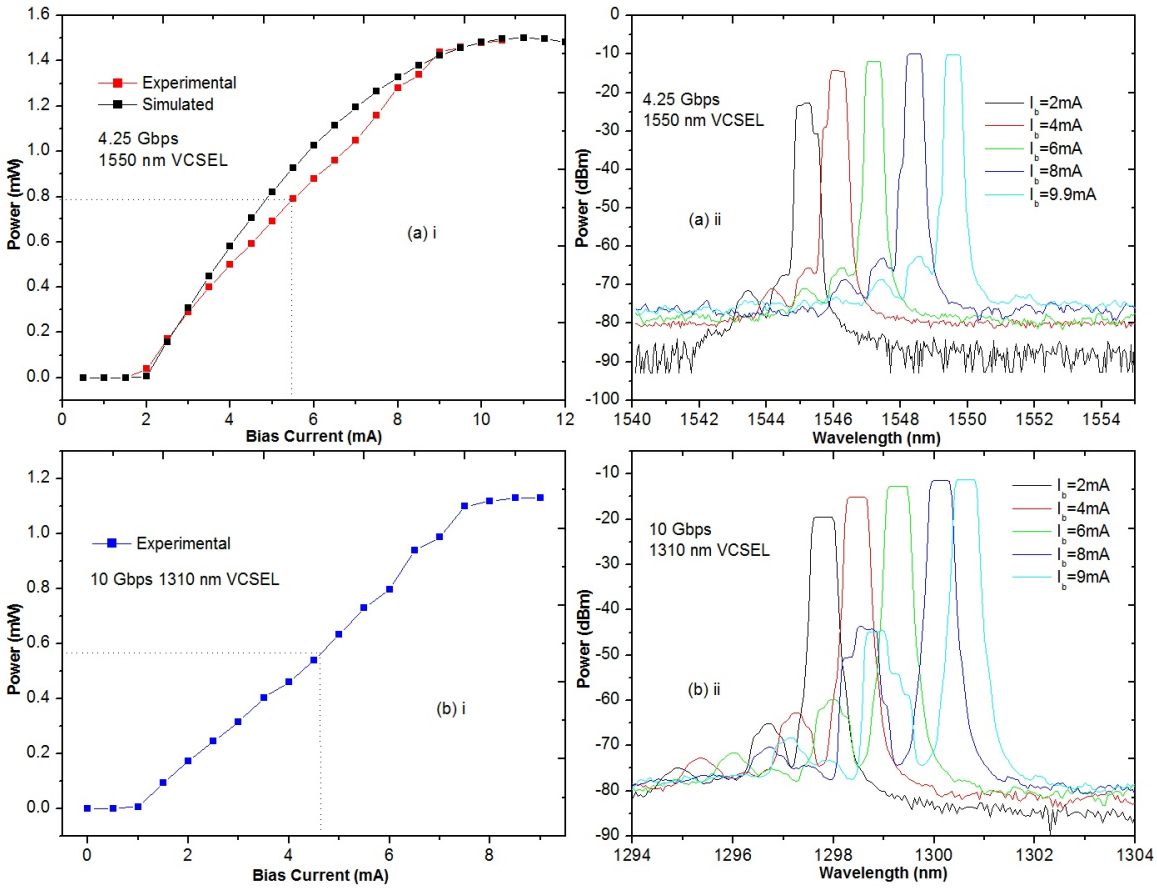

Figure 5.1: Unmodulated VCSEL output power as a function of bias current and corresponding wavelength response (a) i and ii refer to a 4.25 Gbps 1550 nm VCSEL while (b) i and ii is a 10 Gbps 1310 nm VCSEL.

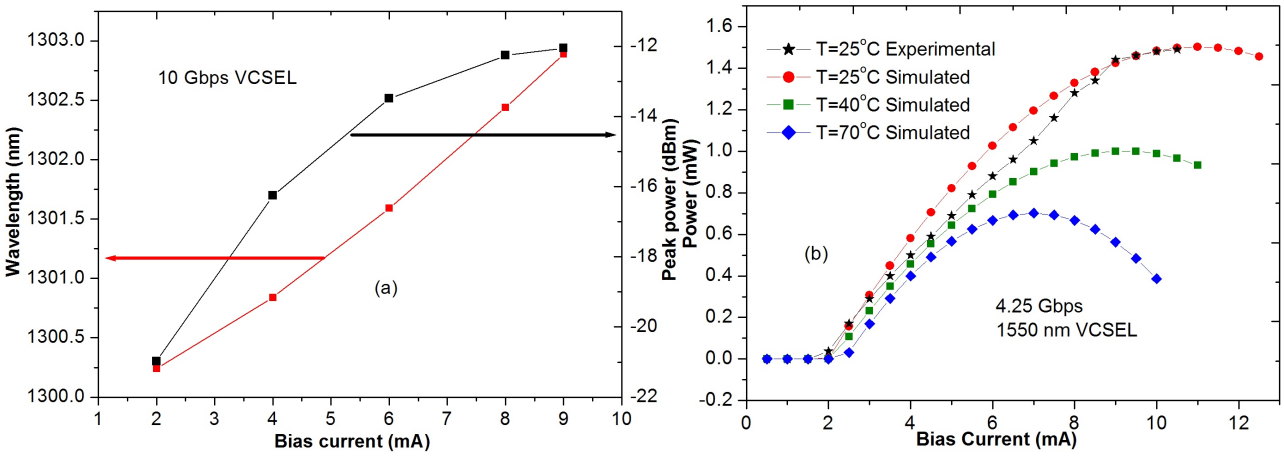

Figure 5.2: (a) Wavelength and power change with input current for 1310 nm VCSEL (b) Simulated temperature response of the 1550 nm VCSEL.

The VCSELs will be mounted on the dish for data transmission after digitization. Karoo telescope site is a desert environment with harsh conditions. The temperatures rise up to 40^oC

during summer and decrease to about freezing point at winter. The behaviour illustrated in figure 5.2 (b) shows that the device will be slightly affected in performance at 40^oC, implying the device can be used in the uncooled mode. However, at extreme temperatures rising above 70^oC as provided in the manufacturer's data sheet, some cooling may be needed. For instance, air conditioning in addition to heat sinking or use of temperature controllers may be used for cooling.

5.2 Simulation and experimental set up to demonstrate VCSEL transmission

In the subsequent sections of this chapter, both experimental and simulation results on the 1310 *nm* and the 1550 *nm* VCSELs are presented. The experimental set-up was as shown in figure 5.3. A VCSEL is a directly modulated laser, therefore data is coupled directly into the device using a bias tee (BT). The LDC is used to adjust the VCSEL bias current. A VCSEL is modulated at different bit rates by a non-return-to-zero (NRZ) pseudo-random binary sequence (PRBS, 2^7-1) signal and transmitted over a standard single mode fibre (SMF). The VOA varies the optical power at the receiver. The optical power is varied so as to establish bit errors at different power levels. The EA is used to amplify the received signal so as to satisfy BERT operation voltage. BERT determines the number of bit errors in the transmission. Both the 1310 *nm* and the 1550 *nm* VCSELs are investigated for different fibre types of varied lengths.

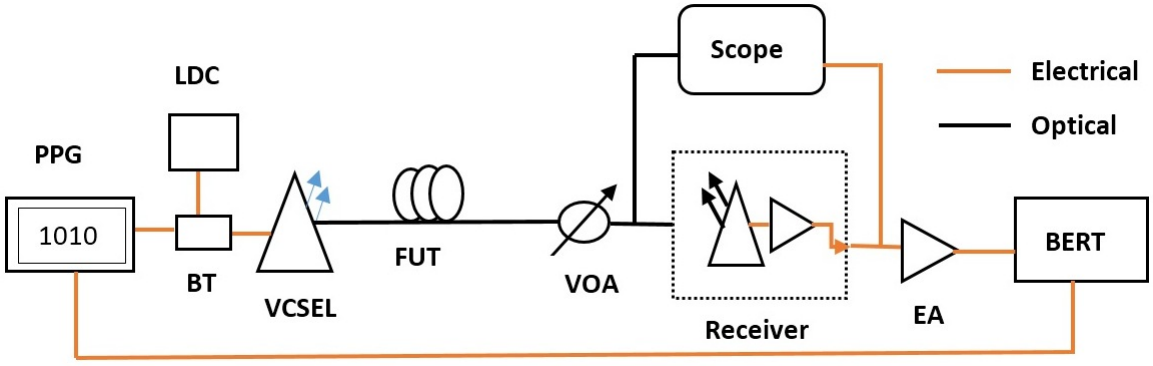

Figure 5.3: Simulation and experimental set-up used to study the VCSEL transmission. PPG is the programmable pattern generator, LDC is the laser diode controller, BT is the bias tee, FUT is fibre under test, VOA is the variable optical attenuator, EA is the electrical amplifier and BERT is the bit error rate tester.

Due to the need to verify different VCSEL performance on different fibres and investigate the trends, VPI simulation was used. For example, a10 *Gbps* 1550 *nm* VCSEL which was not available for experimental demonstration, was simulated. The modelled VCSEL presented in the preceding section was used in the transmission. VPI software has different modules

emulating the different components in a real experimental setting. These include pseudo-random bit sequence (PRBS) module that generates a pseudo-random data sequence, VCSEL driver with adjustable parameters such as modulation type (non-return-to-zero or return-to-zero), bit rates and output levels for '0' and '1' states for on off keying (OOK). The specified output levels were used to determine the modulation depths. The frequency of emission can be specified on the modelled VCSEL. Universal fibre module with parameters such as attenuation coefficient, dispersion coefficient, effective area, nonlinear effect constants and length enabled the modelling of different fibre types. Other modules are optical attenuators, signal analysers and optical receivers with bit error rate (BER) estimation. Positive intrinsic negative (PIN) or avalanche photodiode (APD) detector type can also be selected from the receiver modules. A similar set-up was built on VPI and used to characterize the 1550 *nm* VCSELs.

5.3 Transmission performance of a 1310 nm VCSEL

Optoelectronic lasers emitting at 1310 *nm* wavelength are suited for conventional/standard single mode fibres, G. 652 which are optimized for zero dispersion wavelength (ZDW).

5.3.1 Transmitter-receiver pair optimization

A 1310 *nm* VCSEL was modulated at a bit rate of 10 *Gbps* NRZ-PRBS and the back to back transmission performed so as to optimize the transmitter- receiver pair [213].

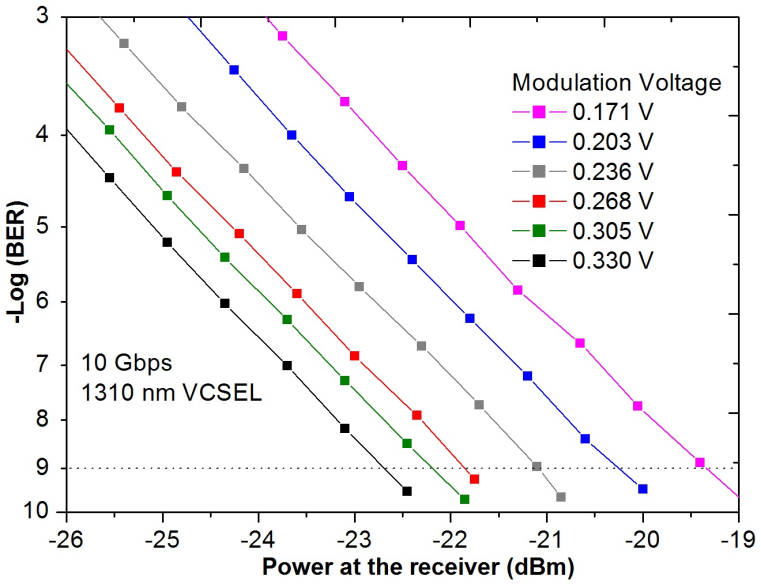

Figure 5.4: Experimental BER measurements for back to back with varying modulation voltage, V_{rms}.

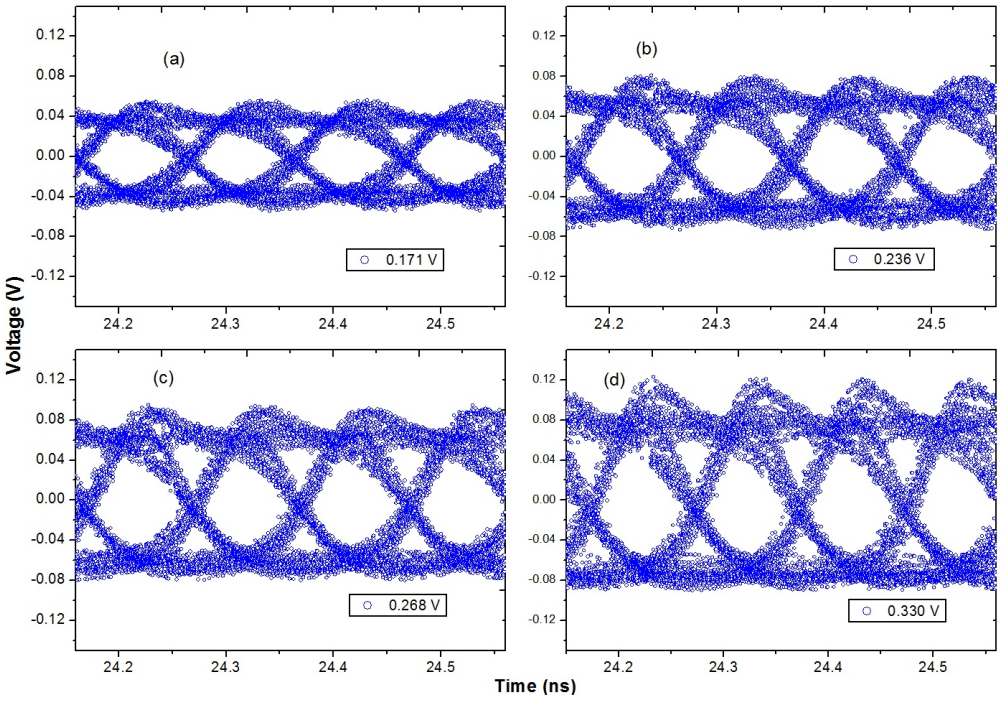

Figure 5.5: Corresponding eye diagrams for the 10 Gbps transmission at (a) 0.171 V, (b) 0.236 V, (c) 0.268 V and (d) 0.33 V modulation voltages, V_{rms}.

The characteristics of the VCSEL used are given in section 5.1. A bias current, I_b of 5.5 mA was set on the laser diode controller and the bit error rate measurements on the transmissions were performed in order to establish the sensitivity. The proper bias current is set above the current threshold, I_{th} value preferably mid of the linear region in the $I - P$ curve so as to enable optimum performance. When the I_{th} is below or very close to I_b of VCSEL, it leads to pulse width distortion that in turn causes jitter [214]. The modulation voltage is carefully varied as the BER of the transmission output is measured. The modulation voltages herein refer to the root mean square (RMS) voltage, V_{rms} values. The corresponding eye diagrams at telecommunication BER threshold of 10^{-9} were captured on the scope. BER threshold is the acceptable error level i.e. one error on a billion bits sent (10^{-9}). Eye diagram refer to the pattern obtained by superposition of digital signal i.e. stream of '1's and '0's. From figure 5.4, it is found that the sensitivity is improved from -19.3 dBm to -22.6 dBm when the modulation voltage, V_{rms} is increased from 0.171 V to 0.33 V. The improved sensitivity is because of increase in the extinction ratio (ER). Sensitivity is improved by 3.3 dB. Figure 5.5 shows that as the modulation voltage is increased, the chirp is increased. Chirp is characterised by overshoots [215] on the eye (Also see figure 5.8). It is clear that high modulation voltage gives high extinction ratio (ER) but increases chirp. This is contributed by the change of refractive index which in turn changes the wavelength of the light source. The refractive index of a material increases with increase in temperature thus increasing the optical length of the laser cavity. The refractive index and laser cavity determines the laser mode frequency.

Moreover, temperature increase causes the semiconductor bandgap to decrease [124] thus affecting the gain.

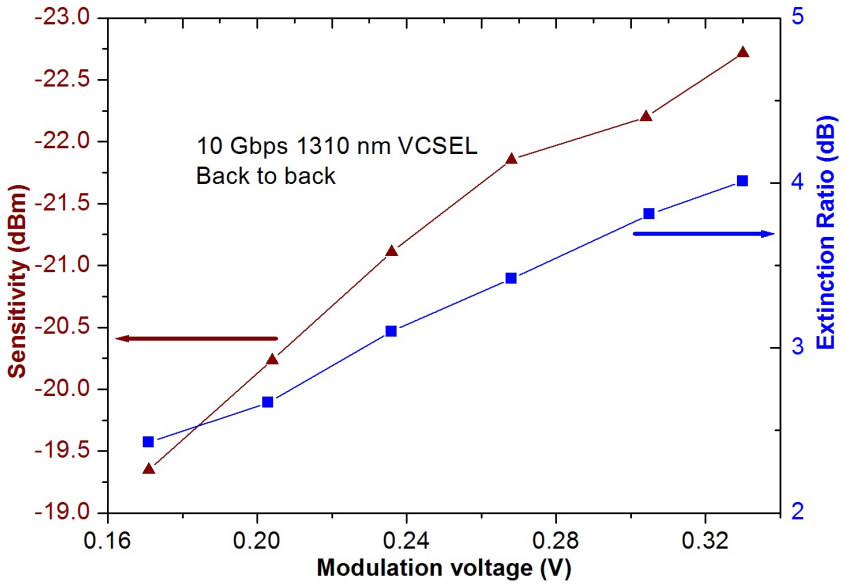

Figure 5.6: Varying modulation voltage with sensitivity and extinction ratio.

Temperature affects the carrier concentration. Refractive index decreases with increase in carrier concentration [216]. These are the two effects that contribute to frequency chirp. The chirp can be expressed as in equation (3.1). The transient chirp which is the dynamic effect relates to the laser power change with time while the adiabatic chirp arise from the wavelength difference between '0' and '1' levels. Adiabatic chirp is mostly related to thermal effects in the semiconductor. Mitigation of the chirp using injection locking [103] and filtering [43] has improved the VCSEL performance through reduced penalties resulting from fluctuations. Similarly, shaping of the injection current [215] have been proposed to reduce the chirp on an intensity modulated laser. Shaping the injection current involves the use of bias and modulation voltage inputs that suppress the relaxation oscillations in the laser device. This electrical approach is not cost effective, it is expensive and increases complexity. Chirp related issues makes direct modulation a demerit over the external modulation. Sensitivity is noted to increase with increase in modulation voltage as shown in figure 5.6. The extinction ratio (ER) also increases with increase in modulation depth. Generally, ER describes the efficiency with which the transmitted optical power (digital signal) is modulated. When the ratio between the '1' and '0' levels is improved, the chances of errors are reduced in the transmission. When the ER is low, chances of receiver mistakenly detecting a '1' for a '0' is high thereby introducing errors. We can infer that chirp and ER is a trade off when choosing the optimal modulation.

5.3.2 VCSEL drive configurations

This section compares the single and differential driven VCSEL configurations as depicted on figure 3.7 in chapter three. The BER measurements were performed on an 11.5 km G.652 fibre link using a 1310 nm 10 $Gbps$ VCSEL. The BER measurements of the two configuration were then compared. In both cases, a positive intrinsic negative (PIN) receiver was used. Figure 5.7 shows the BER of the two configurations. It is found that the differential driven has a better performance than the single drive by a factor of 1.32 dB as established at 10^{-9} threshold. As described in section 3.4 of chapter 3, the difference is attributed to the modulation drive current that is halved in the case of single ended configuration when 50 Ω termination is used.

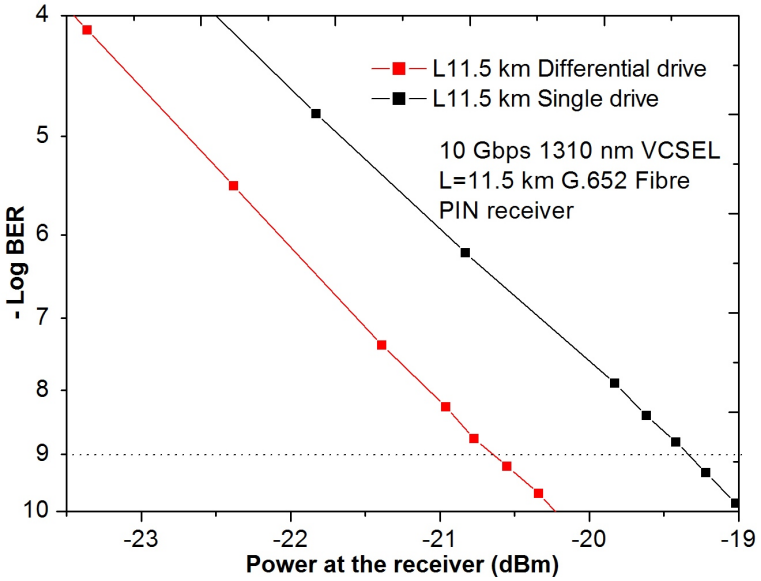

Figure 5.7: Experimental BER measurement for the 11.5 km transmission for different drive configurations.

5.3.3 PIN versus APD receivers

The performance of the PIN and APD receivers on VCSEL transmission is experimentally investigated. This work relies on the intensity modulation direct detection of the optical data. PIN and APD receivers used are high speed InGaAs photodiodes with 10 GHz bandwidth. An NRZ PRBS was used to modulate a 10 Gbps 1310 nm VCSEL and sent over an 11.5 km G.652 fibre. After the fibre, equal optical power of -6.8 dBm was coupled into the different receivers. It is noted that the bits are clear and distinct in both the PIN and APD receivers. However, the magnitude in voltage is different, with APD receiver giving higher voltage levels compared to PIN as shown in figure 5.8. Note that the bit synchronization was not done and that the shown bits is a short portion of the streaming PRBS as captured on the wide bandwidth oscilloscope, model 86105C from Agilent company. The overshoots on the individual bits is chirp arising from high modulation voltage as expected in a directly modulated laser.

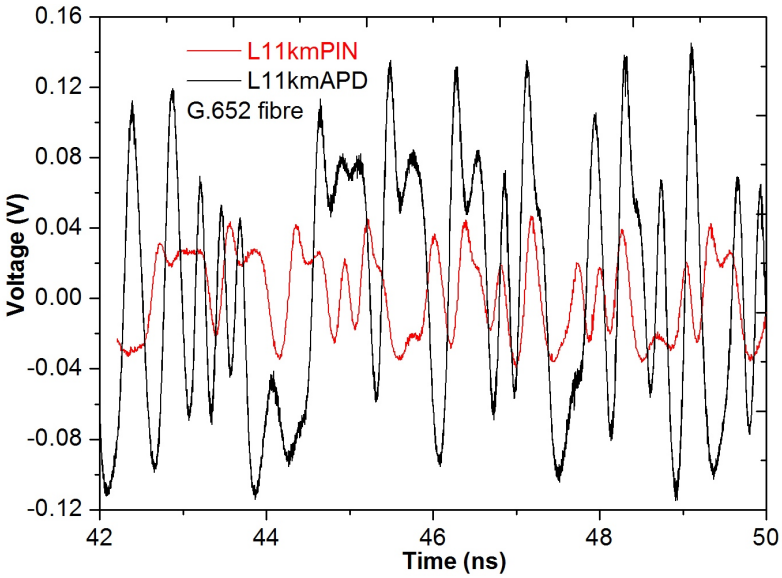

Figure 5.8: Experimental graph showing individual bits as detected by different receivers on the 11.5 km transmission.

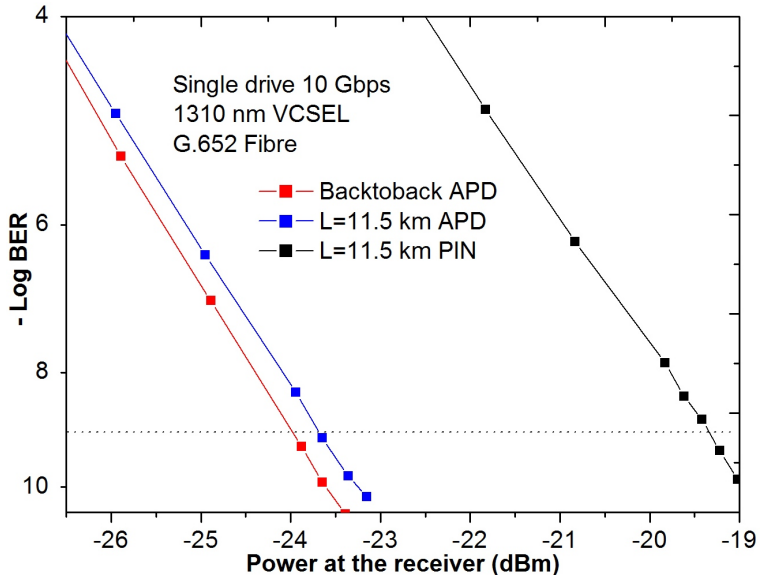

Figure 5.9: Experimental BER measurement for 11.5 km with different receivers.

The BER performance of the two receivers is then compared on the 11.5 km G.652 fibre transmission. A 10 $Gbps$ VCSEL in the single drive configuration was used. BER measurement depicted in figure 5.9 complement the magnitude of received voltages in figure 5.8. The APD receiver performed better than PIN receiver by 4.39 dB in the 11.5 km transmission. This is because of the different sensitivities, APD has a sensitivity of -26 dBm while PIN has a sensitivity of -19 dBm. Also current amplification in the avalanche stage of the APD played a role. The APD bias voltage range was $25 - 36$ V while that of the PIN was $7 - 12$ V. The sensitivity of APD makes it ideal for longer transmissions.

5.3.4 Dispersion penalties at different transmission lengths

CD and chirp in VCSELs lead to power penalties in the transmission. Figure 5.10 shows the BER measurements over different transmission distances on a differentially driven 10 *Gbps* 1310 *nm* VCSEL over a G.652 fibre. A PIN receiver was used in this particular measurement.

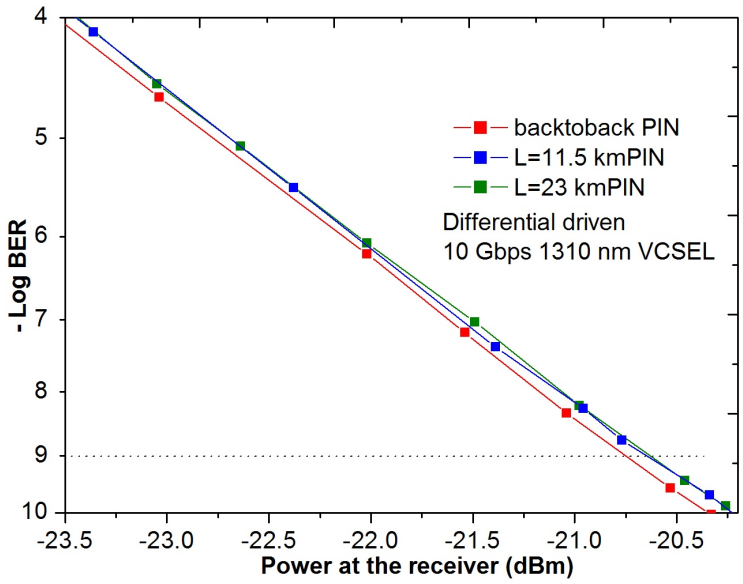

Figure 5.10: Experimental BER measurement of a 10 Gbps 1310 nm VCSEL over a G.652 SMF.

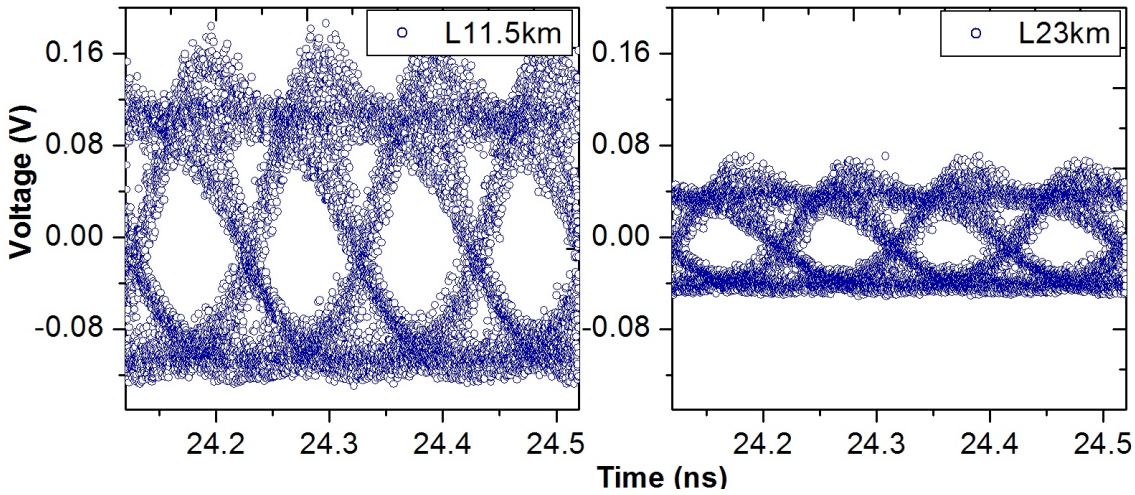

Figure 5.11: Eye diagrams for 10 Gbps 1310 nm VCSEL transmission on G. 652 fibre over 11.5 km and 23 km respectively.

A receiver sensitivity of $-20.7\ dBm$ is attained. A small dispersion penalty of about 0.1 dB is obtained for up to 23 km G.652 fibre. The open eye in figure 5.11 signifies the signal clarity. The trivial penalty over 23 km G.652 fibre is expected at this zero wavelength dispersion. The

optical powers were $-17.5\ dBm$ and $-20.6\ dBm$ for 11.5 km and 23 km respectively. The eye size for the 23 km G.652 fibre transmission is smaller than that of 11.5 km G.652 fibre due to attenuation which exponentially increases with length.

5.4 Demonstration of a 1550 nm VCSEL transmission

This section discusses the VCSEL transmission at 4.25 *Gbps* and 10 *Gbps*. Transmission at 1550 nm window are currently favoured as it makes use of the minimum attenuation and its application in wavelength division multiplexing (WDM). A 10 *Gbps* and 4.25 *Gbps* VCSELs are investigated over different type of fibres and transmission penalties established. Generally, optical sources emitting at1550 nm are suited for use on a G.655 fibre but can be used on a G.652 fibre with a dispersion penalty.

5.4.1 10 Gbps 1550 nm VCSEL

Simulations of a 10 *Gbps* 1550 nm VCSEL on G.652 fibres were performed. Simulation enables analysis of different transmission lengths which may not be available in the lab for experimental investigation. At 10 *Gbps* transmission, dispersion penalties of 0.37 dB, 1.47 dB, 2.52 dB and 5.17 dB for 1.4 km, 5 km, 7.5 km and 10 km respectively over G.652 were obtained as shown in figure 5.12.

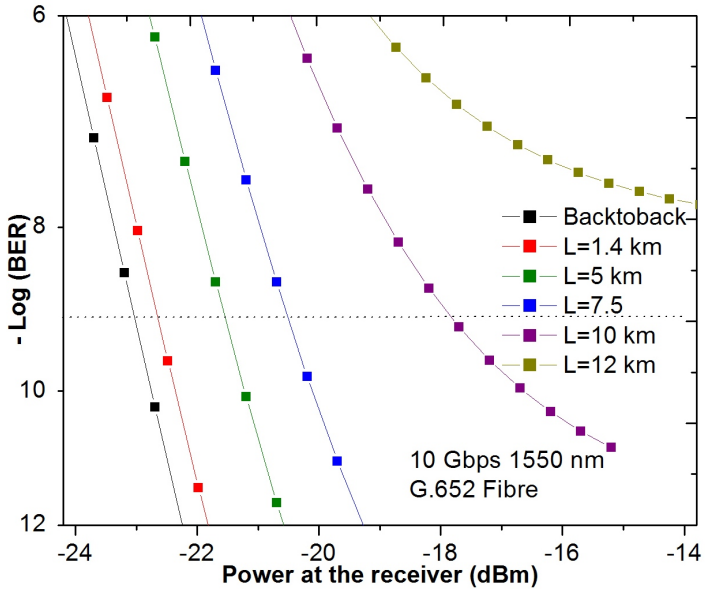

Figure 5.12: Simulated BER for 10 Gbps 1550 nm VCSEL over ITU-T G.652.

Transmission penalty increases with increase in fibre length. The error floor for this transmission is at 12 km G.652 fibre length. Error floor refers to the point at which the BER flattens without crossing the telecommunication threshold. This is due to distortions that

cause irreducible errors. In other words, it is the point at which the receiver fails to distinguish between the two levels, no matter what power is given to it. Comparing the performance to 10 *Gbps* 1310 *nm* VCSEL in figure 5.10, it is noted that fibre choice is vital in matching transmission wavelength. With 1550 *nm* VCSEL, high dispersion of about 17 *ps/nm.km* on a G.652 give rise to power penalties. Unlike 1550 *nm* VCSEL, 1310 *nm* VCSEL experience minimal dispersion values at zero dispersion wavelength making the VCSEL transmit longer distance.

5.4.2 4.25 Gbps 1550nm VCSEL

Figure 5.13 (a) and (b) compares the 4.25 *Gbps* 1550 *nm* VCSELs over two types of fibres; G.652 and G.655.

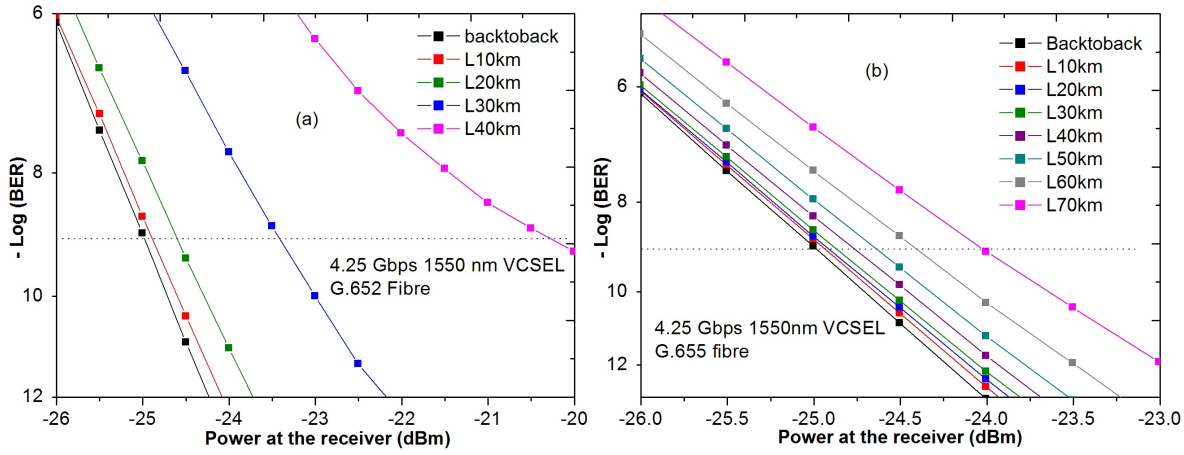

Figure 5.13: Simulated BER for 4.25 Gbps 1550 nm VCSEL transmission on a (a) G.652 (b) G.655 fibre.

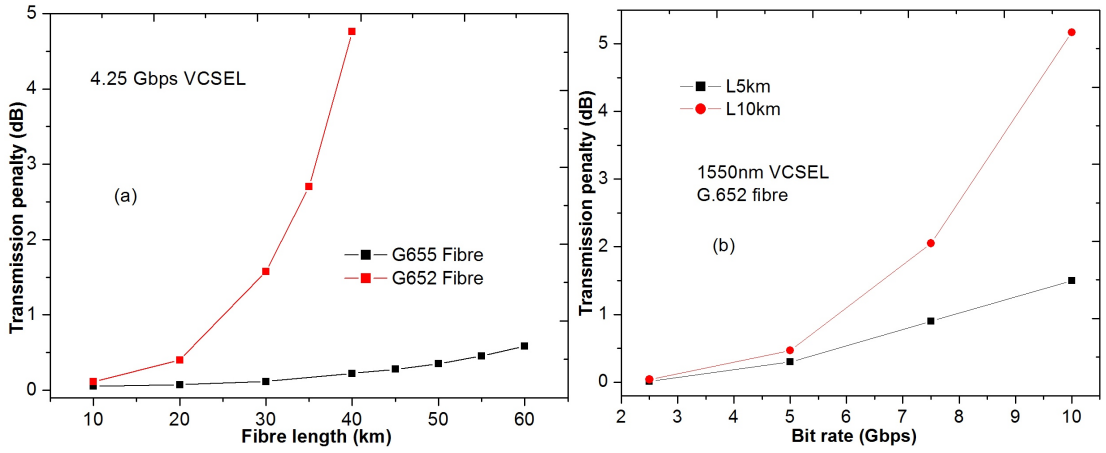

Figure 5.14: (a) Summarized transmission penalties on different fibres on a 4.25 Gbps 1550 nm VCSEL (b) summarized transmission penalties with varying transmission rates at different fibre lengths

For a transmission over a G.652 fibre, error floor occur at about 42 km. The G. 655 fibre on the other hand can transmit up to 70 km as shown in figure 5.13 (b). G.655 fibre has low dispersion value of about $2-6$ $ps/nm.km$ while G.652 fibre has a dispersion coefficient of 17 $ps/nm.km$. Therefore the low dispersion penalties in the G.655 link extend the VCSEL reach. Figure 5.14 (a) summarises the transmission penalties obtained from simulations in figure 5.13. With 4.25 $Gbps$ 1550 nm VCSEL, more penalties are experienced on a G.652. It shows that performance of a fibre is dependent on transmission wavelength of choice. Figure 5.14 (b) shows that the transmission penalty increases with increase in the bit rate and fibre length. The increase in dispersion penalty with fibre length is caused by the cumulative effect of dispersion hence causing more penalties. Similarly, as the bit rate is increased, the bit cycle is reduced. Therefore the effect of dispersion which is constant over a particular fibre length on the bits will lead to more penalty in the transmission.

5.4.3 Wavelength division multiplexing in VCSELs

Experimental set-up used is illustrated in figure 2.4 in chapter 2. Figure 5.15 (a) shows the band pass spectra of the multiplexer (mux) and demultiplexer (demux) used in the study. The multiplexer is a bi-directional device, therefore it can be used to demultiplex signals after the fibre. To characterize the band pass channel spacing, a broadband source, FLS-2300B from EXFO of wavelength range 1480 $nm-1650$ nm was used. Equal optical power of -6 dBm was propagated through each mux/demux and the output spectrum was observed using optical spectrum analyser (OSA), model 86142B from Agilent Company. Each of the multiplexer has one input and eight outputs or vice versa if used as a demultiplexer. For the purpose of illustration, we use a single wavelength on each of the channel spacing. The 50 GHz channel spacing shown is at 1550.02 nm centre wavelength giving about 0.24 nm full width at half maximum (FWHM). The 100 GHz channel spaced is centred 1549.28 nm giving a full width at maximum of 0.62 nm. The difference in FWHM has different effects on the optical power of the signal. The large FWHM allows more power to pass through the band pass filter but the signal has more spectral components as compared to the 50 GHz. It is evident that at equal bandwidths, the 50 GHz spacing can accommodate double the number of channels to that of the 100 GHz spacing. For example, a 800 GHz bandwidth will only accommodate 8 channels of 100 GHz spacing. Similar bandwidth will take 16 channels of 50 GHz. Small channel spacing increase the capacity but suffer more crosstalk and fibre nonlinearities at high power due to the enhanced interaction.

The multiplexer / demultiplexer channels are sh own in figure 5.15 (b). A multiplexer and demultiplexer was used to couple and split the three signals on the same fibre respectively. The marked wavelengths coincide with the 4.25 $Gbps$ 1550 nm VCSEL tuneability used to investigate the wavelength division multiplexing (WDM).

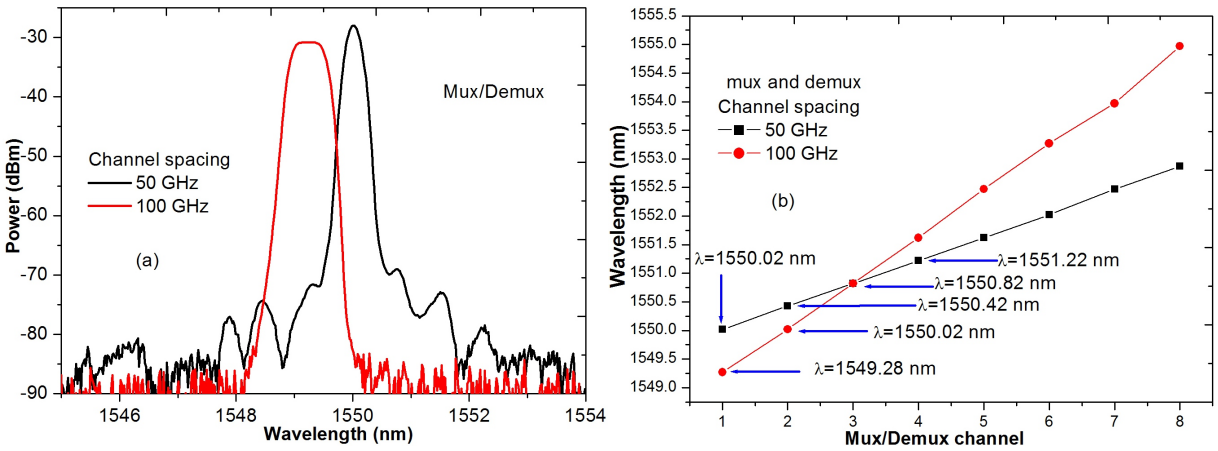

Figure 5.15: Shows (a) the Spectra of 50 GHz and 100 GHz band pass (b) various multiplexer and demultiplexer channels and the corresponding VCSEL wavelengths.

In this transmission, three VCSELs with different wavelengths were used. The wavelengths of the VCSELs used in the transmission were 1549.28 nm, 1550.02 nm and 1550.82 nm giving 100 GHz spacing as depicted in figure 5.15 (b).

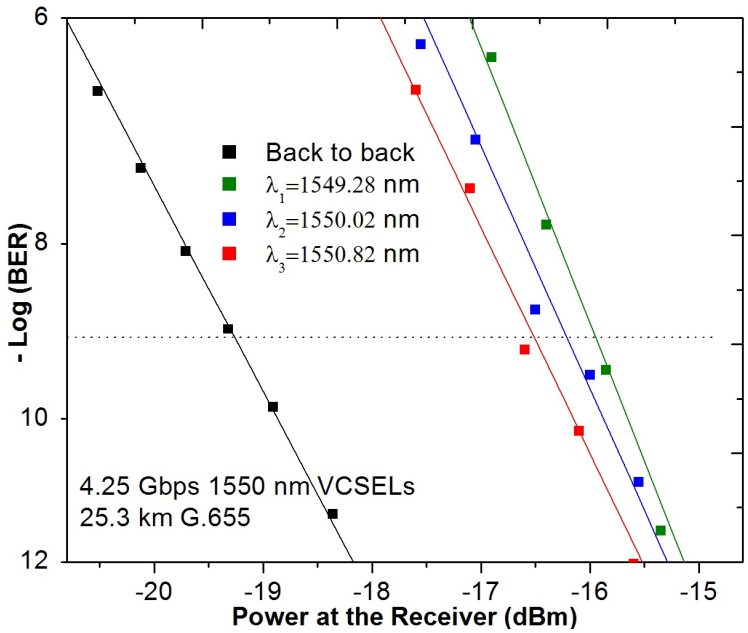

Figure 5.16: Experimental BER measurement obtained from 3x4.25 Gbps 1550 nm VCSELs multiplexed over 25.3 km G.655 fibre.

Each of the three 4.25 $Gbps$ 1550 nm VCSELs was modulated using NRZ-PRBS $(2^7 - 1)$, multiplexed and then transmitted over the 25.3 km G.655 fibre. The multiplexing resulted to 12.75 $Gbps$ of data transmitted over a single fibre. The channels in this transmission are restricted to 3 because of the VCSEL wavelength tuneability range in matching the multiplexer and demultiplexer pass bands specification. On the receiver end, a demultipler was used to

separate the different channels and the BER performed. The channels in this transmission are restricted to 3 because of the VCSEL wavelength tuneability range in matching the multiplexer and demultiplexer pass bands specification. On the receiver end, a demultiplexer was used to separate the different channels and the BER performed on each channel.

Figure 5.16 shows a BER measurement obtained on the different wavelengths corresponding to channel 1, channel 2 and channel 3 on the multiplexer/demultiplexer. The penalties for the different transmission wavelengths are 2.8 dB, 3.1 dB and 3.3 dB respectively. The small difference on the channel performance could be attributed to the difference in bias points which influence the optimal modulation of the device. Note that the different wavelengths are achieved by tuning the bias current of the individual VCSEL device.

This multiplexing demonstration is an important technique for MeerKAT and SKA. In the MeerKAT for example, each dish is expected to have a data flow of about 40 $Gbps$ including the overheads. This experiment demonstrates how 4×10 $Gbps$ VCSELs can be multiplexed enabling the 40 $Gbps$ data rates on a single fibre in the MeerKAT. The multiplexing is inevitable considering SKA's expected data rates. WDM is an elegant solution making effective use of a fibre as opposed to using several fibres dedicated to each wavelength. The cost of the multiplexing and demultiplexing may however be higher than the use of multiple fibres depending on the transmission distances. Multiplexing is suitable for the capacity expansion utilizing an existing deployed fibre but in a new network, use of multiple fibres may be considered as a cheaper option despite complexity arising from the quantity.

5.5 Chromatic dispersion penalties and power budgeting for the MeerKAT

Power budgeting is an issue to be addressed in any fibre network so as to satisfy the bit error rate requirement. Factors that are considered are transmitter, receiver, component losses in the network and fibre penalties which include attenuation, dispersive effects, scattering, crosstalk and nonlinear processes. Components in the network may be splitters, couplers, connectors, multiplexers, demultiplexers, polarization controllers and optical amplifiers for longer reach transmissions. In this case, VCSELs are lower power devices therefore the nonlinear effects are minimized. However, when DWDM technique is employed, high power cause some nonlinearities in a fibre. The 100 GHz channel spacing used has little or minimized interaction resulting in low crosstalk. For MeerKAT telescope array, the distances of concern are relatively short therefore the effect of chromatic dispersion is less problematic. However, for the purpose of link budgeting, we use the worst case scenario to estimate the CD penalty allocations. For longer baselines in the later SKA development phases, dispersion compensation so as to cater for variations and distortions in the transmission may be needed. Typically, about $4 - 6$ dB

is allocated for system margin during the network design [1].

Table 5.1: Shows a MeerKAT power budget example for a 10 Gbps VCSEL transmission

Budget breakdown	**Power Budget (dB)**			
	1310 nm VCSEL G.652 Fibre	**1310 nm VCSEL G.655 Fibre**	**1550 nm VCSEL G.652 Fibre**	**1550 nm VCSEL G.655 Fibre**
Connectors, splices and others	3	3	3	3
Fibre Attenuation (12 km)	3.6	3.6	2.4	2.4
Dispersion penalty allocation	0.1	-	5.2	0.6
Multiplexer and Demultiplexer	5.2	5.2	5.2	5.2
Total budget with WDM	***11.9***	**-**	***15.8***	***11.2***
Total budget without WDM	***6.7***	**-**	***10.6***	***6.0***

Table 5.1 shows a power budget example designed for the 12 km MeerKAT telescope array. With a VCSEL output power of -0.5 dBm and receiver sensitivity of -19 dBm and -26 dBm for PIN and APD respectively, the available power, P_A for budgeting is 18.5 dB and 25.5 dB respectively (refer to equation (3.42) in section 3.9 of chapter 3). Connectors and splices refer to power loss allocation for temporary and permanent fibre joints and others refers to any miscellaneous losses that can be incurred in the link. The dispersion penalty values are obtained from the BER measurements performed in this work. The fibre attenuation constants used in Table 5.1 are 0.2 dB/km and 0.3 dB/km on a G.655 and G. 652 respectively. The link loss used in the calculation excludes the connector losses. The power penalty allocation for a 10 $Gbps$ 1310 nm VCSEL is not included in the table. This is because G.655 fibre is optimized to support long-haul systems therefore using a 1310 nm laser source is not recommended. It basically means that transmission occurs in the anomalous region of dispersion. In fact, if we assume that the fibre dispersion curve for G.655 uniformly follows the G.652 trend, then a 1310 nm laser over a G.655 coincides to about -17 $ps/nm.km$ of dispersion coefficient. However, the anomalous region of dispersion is utilized in dispersion compensation.

Table 5.1 shows the different power budget totals based on single (without WDM) and multiplexed (with WDM) transmission links. From the power budget, it is noted that the PIN receiver can be employed without any constraint. For instance, the total power available on a VCSEL is about 18.5 dB while the budgeted power for the 1550 nm transmission on a G.652 fibre is only 10.6 dB implying an additional transmission distance can be achieved. On the 10 $Gbps$ 1550 nm transmission over a G. 652 fibre, an excess of about 7.9 dB on

a PIN receiver and 14.9 dB on an APD receiver is unallocated. The total budgeted power (from the table) is far off from the available power, P_A even if the worst case scenario of wavelength choice is considered. From equation (3.43) and equation (3.44), additional reach can be attained. The best performance is seen when a 1550 nm VCSEL is used on a G.655 fibre. The 1550 nm VCSEL has the least fibre attenuation of 2.4 dB over the 12 km G.655 fibre. On the other hand, the 1310 nm VCSEL has the least dispersion penalty of 0.1 dB on a G.652 (zero dispersion wavelength) but the attenuation is slightly higher as compared to that of a G.655 fibre. This is the reason for recommending the G.655 fibre for long-haul transmission.

If the WDM technique was to be utilized, then, 5.2 dB loss for the multiplexer and demultiplexer in addition to some nonlinear effects could be incurred in the link. This would still not limit the use of 10 *Gbps* 1550 nm VCSEL on a G.652 fibre with PIN receiver. The use of APD receiver provides additional power for extended reach and is recommended for longer transmissions because of its ability to amplify the signal at the avalanche stage. The APD therefore is suited for SKA 1 and 2 phases where longer transmission distances are to be considered. The amplification at this stage may be needed to compensate for the losses therefore increasing the VCSEL reach. The power budgeting established does not take into consideration the nonlinear effects because of the MeerKAT data rates as well as VCSEL's ability to transmit at low power. For instance, for 40 *Gbps* in the MeerKAT, only four VCSELs transmitting at 10 *Gbps* are needed. This may cause low nonlinearities in the fibre leading to insignificant penalties. If each telescope streams 160 *Gbps* as expected in SKA 1 phase, then 16 VCSELs transmitting at 10 *Gbps* will be needed. This will increase nonlinear effects causing transmission penalties. The issue of nonlinearities will be avoided all together if multiple fibres are used on each telescope dish as implemented in Australian square kilometre array pathfinder (ASKAP).

5.6 Summary

This chapter provides the VCSEL characterization, transmitter-receiver pair optimization and transmissions. We show that VCSEL is a low power device with wavelength tuneability. Differential configuration of a VCSEL offers better performance as compared to single configuration. Acceptable dispersion penalties are attained over the typical MeerKAT telescope distances using a 10 *Gbps* VCSEL and a PIN receiver. Wavelength division multiplexing is successfully demonstrated. The wavelength division multiplexing is vital for telescope fibre network so as to utilize the bandwidth of the fibre in transmitting huge volumes of astronomical data. This technique enables utilization of the optical fibre capacity thus reducing the cost of transmission especially over SKA 1 and beyond distances.

In the subsequent result chapters 6 and 7, we improve the transmission reach by suggesting and demonstrating mechanisms to overcome transmission limitation such as chromatic dispersion and attenuation.

Chapter 6

Chromatic dispersion and its compensation for VCSEL transmission

In addition to attenuation, dispersion in optical fibres limits the distance information can be sent in an optical network as discussed in section 3.8 in chapter 3. The two main types of dispersion in single mode fibres are chromatic dispersion (CD) and polarization mode dispersion (PMD). Dispersion effects are very critical in high speed long distance transmission. With the current development of low PMD modern fibres ($\leq 0.1\ ps/km^{1/2}$) and the rise in coherent transmission technologies [217], PMD which is a secondary effect, has not been of a major concern. The VCSEL performance is mainly limited by the CD. The deterministic nature of CD makes compensation possible. The short MeerKAT distances of up to 12 km are less prone to chromatic dispersion issues. But as the transmission distance increase in the SKA array, the effects of CD should be mitigated so as to boost the efficiency of the VCSEL and reduce the dispersion penalties.

6.1 Chromatic dispersion measurement

In this work, the pulse delay method and phase shift techniques were used to characterize the CD [218, 219]. The two techniques were devised using available components in the NMMU laboratory and used to accurately establish the CD of different fibre types. In figure 6.1 (a), a VCSEL was modulated with a 8.5 GHz sinusoidal clock signal at wavelength, λ_1 and propagated through the fibre under test (FUT) and the resulting waveform captured in the wide bandwidth oscilloscope as the reference. The wavelength, λ_2 was varied by tuning the bias current of the VCSEL and the resulting waveform superimposed on the oscilloscope. The resulting phase variation between reference λ_1 and λ_2 was determined and used to obtain the CD coefficient of the fibre under test by making use of equation (3.33) in chapter 3. For the pulse delay technique illustrated in 6.1 (b), two signals of wavelengths λ_1 and λ_2 from

a WDM Pro 8000 module manufactured by Thorlabs were combined using a 3 dB coupler. The reference wavelength, λ_1 was fixed while the variable wavelength, λ_2 was tuned to the desired wavelength spacing. The combined wavelengths were then simultaneously modulated externally using a Machzehnder modulator (MZM).

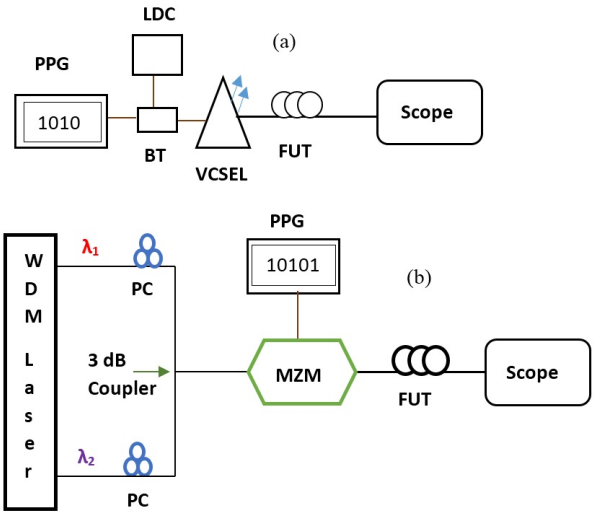

Figure 6.1: Schematic illustration of the experiments used to measure chromatic dispersion (a) Phase shift method (b) Pulse delay technique. PPG is programmable pattern generator, FUT is fibre under test, BT is bias tee, LDC is laser diode controller and PC is polarization controller.

The pulses were propagated through a fibre and the delay between the times of flight of the two pulses corresponding to the wavelengths was used to calculate the dispersion coefficient of the fibre under test. The average of the wavelengths provides the wavelength of which the dispersion is determined. Similarly equation (3.32) in chapter 3 was used.

Table 6.1: Obtained chromatic dispersion coefficients for different fibres at 1547-1553 nm wavelengths measured over different fibre lengths

Fibre type	**Pulse delay method (ps/nm.km)**	**Phase shift method (ps/nm.km)**	**Theoretical/ data sheet (ps/nm.km)**	**Relative Dispersion Slope (RDS) (nm^{-1})**
G.652	17.33±1.66	17.34±0.37	17 [135]	0.00329
G.655 (+)[1]	4.56±0.49	2.81±0.15	2 – 6 [220]	0.0019-0.008
G.655 (-)[2]	-2.93±0.24	-2.95±0.16	-2.8 [221]	-0.016

Table 6.1 summarises the obtained values for different types of fibres. Each of G.655 (+)[1] and G.655 (-)[2] spooled fibres was 25 km while G.652 was a cabled fibre of 18 km. In

[1]G.655 (+) is NZDSF-RS
[2]G.655 (-) is NZDSF-SRS

order to establish the deviation, at least 3 measurements on each fibre length were performed. This was done for the two techniques considered in this study. The different techniques have different resolution as well as measurement range. For instance, pulse delay method has a lower resolution of about $50-100\ ps$ as compared to $10-20\ ps$ for phase shift technique [174]. It thus explains the deviation on the CD coefficients provided in Table 6.1. The measurement on the different techniques however, compare well to the theoretical value provided in the ITU-G recommendations as well as manufacturer's data sheets.

6.2 Chromatic dispersion compensation on a conventional SMF

Owing to the deterministic nature of the chromatic dispersion, it makes it possible for the compensation in a fibre to be easily achieved. This thesis particularly discusses compensation using inverse dispersion fibres (IDFs) [222]. Utilizing anomalous region of dispersion in fibres, the accumulated dispersion can be cancelled. We first begin by simulating an IDFx3 used to compensate for dispersion in a G. 652 fibre. A G.652 fibre has a dispersion coefficient of 17 $ps/nm.km$ and a dispersion slope of 0.056 $ps/nm^2.km$ at 1550 nm while an IDFx3 fibre has a high negative dispersion coefficient of $-54\ ps/nm.km$ and a dispersion slope of $-0.18\ ps/nm^2.km$. The advantage of IDx3 over other dispersion compensating fibres is given in section 3.8.3.3 in chapter 3. Using equation (3.35) in section 3.8, the resulting reduced dispersion slope (RDS) for IDFx3 is $-0.0033\ nm^{-1}$. Clearly, it can be noted that the relative dispersion slope (RDS) value is equal and of opposite sign to the calculated value of RDS of G.652 fibre provided in Table 6.1. The essence of this is to meet the condition for effective compensation of both dispersion and dispersion slope in the fibre as explained in chapter 3 section 3.8.3.3. The matching of the dispersion slope is meant to compensate across a broad range of wavelength. With equation (3.34) we can easily determine the length of an IDF required to achieve sufficient compensation.

The simulation and experimental set-up used in this study is shown in figure 6.2. A VPI simulation software was used. Experimental work was only performed on non-zero dispersion shifted fibre (NZDSF) compensation due to unavailability of the IDF at NMMU lab. This experiment however, clearly illustrates the effect of a negative dispersion fibre in CD compensation. A VCSEL is directly modulated using a NRZ-PRBS sequence and transmitted over the connected fibre sections shown. The BER is then established.

NZDSF-Submarine reduced slope (SRS) fibre is specifically designed for maximum performance in undersea networks, however, we have used to demonstrate the anomolus region in dispersion mitigation.

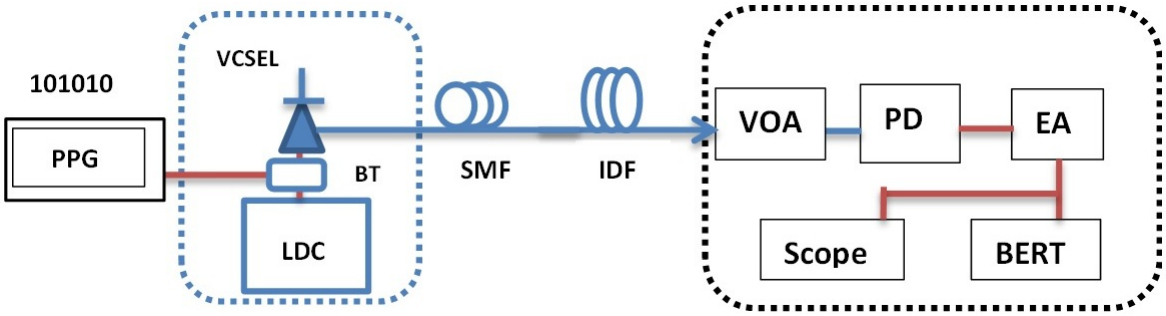

Figure 6.2: Set-up for VCSEL transmission with CD compensation; PPG is pulse pattern generator, LDC is laser diode control, BT is a bias tee, SMF is single mode fibre, IDF is inverse dispersion fibre, VOA is variable optical attenuator, PD is photo detector, EA is electrical amplifier and BERT is bit error rate tester

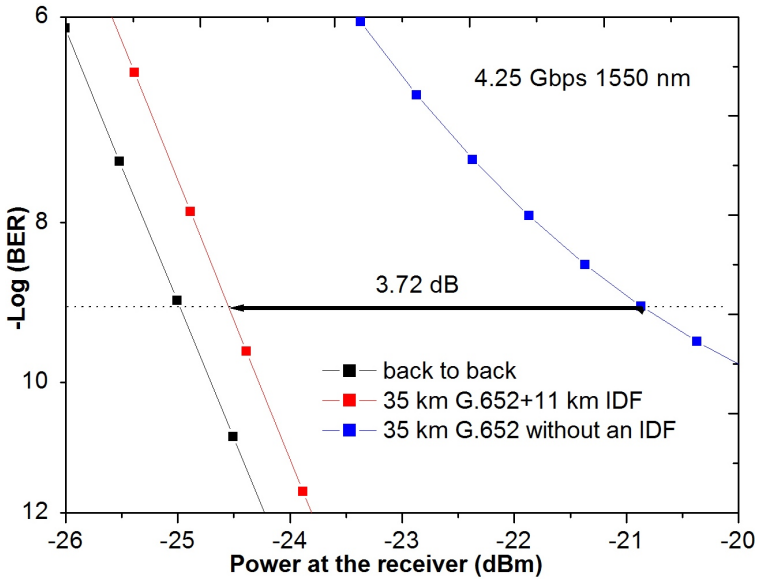

Figure 6.3: Simulated BER measurement showing 4.25 Gbps transmission with IDF compensation.

To bring the clarity on the IDF compensation, we refer to 1550 nm transmissions over G.652 presented in chapter 5 section 5.4 of this thesis. Figures 5.12 and 5.13 (a) in section 5.4 show 10 $Gbps$ and 4.25 $Gbps$ transmissions over G. 652 fibres respectively. It can be evidently noted that the error floor for these transmissions are about 12 km and 42 km respectively. In these transmissions, fibre's dispersion of 17 $ps/nm.km$ contribute to high penalties reducing the reach. The compensated case on a 35 km G.652 SMF is shown in figure 6.3. In this transmission, 3.72 dB of power penalty is compensated using an 11 km IDF fibre.

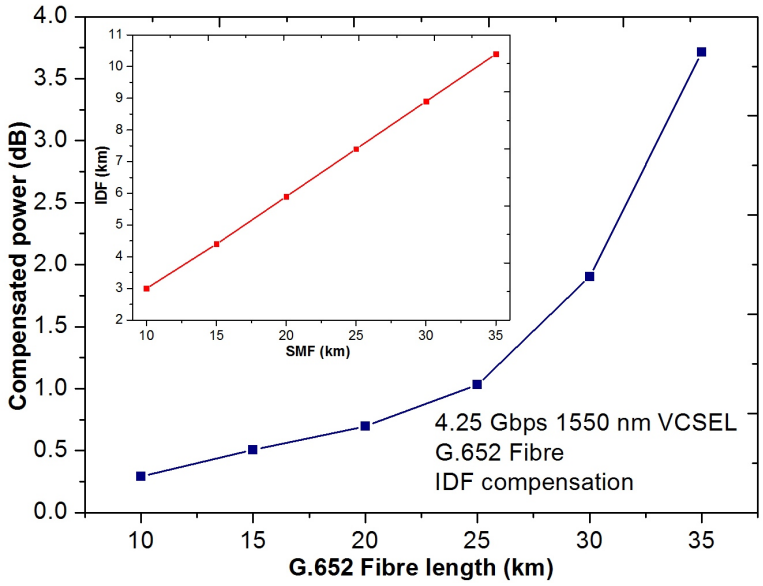

Figure 6.4: Summarised compensated power over the conventional SMF on a 4.25 Gbps simulated transmission. Inset: Relationship between the G.652 and IDF.

The IDF length is derived from equation (3.34) as provided in section 3.8.3.3. The relation is shown on the inset graph in figure 6.4. The gradient of the inset graph is gradient is 3.17. It is equal to the ratio of the dispersion coefficient of the IDF to that of the SMF. The power penalty compensated is seen to increase with increase in the fibre length because of the cumulative dispersion in the fibre. With an IDF, we are able to enhance the reach on a G.652 SMF using the 4.25 *Gbps* 1550 *nm* VCSEL by up to 10 *km* corresponding to 3.72 *dB* of compensated power. This corresponds to a link loss of about 0.3 dB/km. Figure 6.3 shows that the residual dispersion is very small and amount to a penalty of only 0.44 *dB* over the 35 *km* G.652 fibre, hence the compensation is effectively attained. When full compensation is achieved, the transmission limitation is the attenuation which is about 0.3 dB/km on the G.652 fibre. As transmission rates increase the effect of dispersion is expected to increase thus more CD penalties over fibre length. In 10 *Gbps* transmission shown in figure 6.5, a penalty of 7.74 *dB* at 12 *km* is realized. A 5.17 *dB* power is compensated using a 3.78 *km* IDF fibre resulting to residual penalty of 2.57 *dB*. With 5.17 *dB* compensated power an extended transmission of about 16 *km* can be achieved. This implies that with compensation, SKA phase 1 inner baselines data transmissions can be achieved using VCSELs.

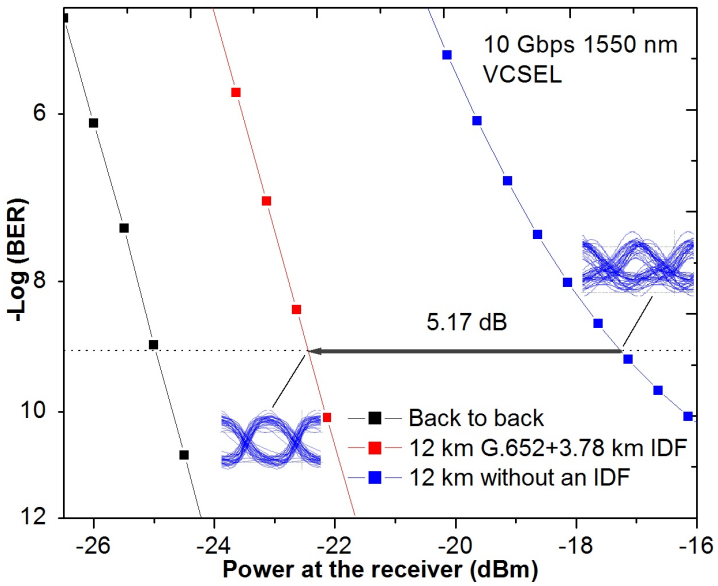

Figure 6.5: Simulated BER measurement showing 10 Gbps transmission with IDF compensation.

6.3 Experimental demonstration of compensation in non-zero dispersion shifted fibres

In this section, we make use of non-zero dispersion shifted fibre (NZDSF) reduced slope (RS) and submarine reduced slope (SRS) True-wave fibres to achieve compensation. The NZDSF-RS and NZDSF-SRS fibres used in the study are manufactured by OFS Furukawa Company.

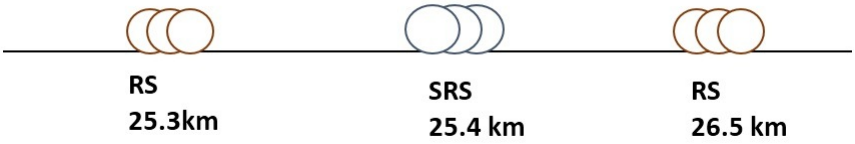

Figure 6.6: Fibre section arrangement for dispersion compensation in NZDSFs.

The properties of these fibres are as presented in Table 6.1. Basically NZDSF-RS has a positive dispersion coefficient while NZDSF-SRS is a negative dispersion fibre. The scheme for compensation is as shown figure 6.6. NZDSF-RS and NZDSF-SRS have dispersion slopes $\leq 0.05\ ps/nm^2.km$ and $< 0.045\ ps/nm^2.km$ respectively. The calculated RDS for RS and SRS fibres are provided in Table 6.1. It is clear that dispersion and dispersion slope compensation can be realized. In order to quantify this compensation, we use the time delay, $\Delta\tau$ during the pulse delay method of CD measurement. We first measure the delay of a NZDSF-RS fibre at 1550 nm region, then combine one NZDSF-RS and one NZDSF-SRS fibres and note the times of flight at a constant wavelength separation of 2.34 nm as shown in figure 6.7.

Evidently, the power levels is attributed to the fibre losses on the different fibre lengths. The delay on the 25.3 km RS fibre is 271 ps, this translates to about 4.5 $ps/nm.km$ of dispersion coefficient. A small shift of 30.7 ps is realized on the 50.7 km fibre. This provides a dispersion coefficient of about 0.24 $ps/nm.km$ clearly implying effective compensation in the system.

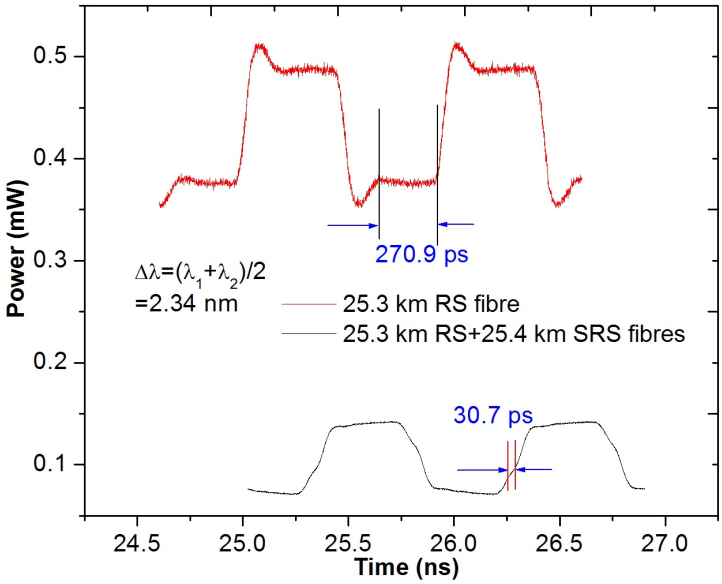

Figure 6.7: Dispersion compensation as measured on a delayed pulse on NZDSF fibres using pulse delay technique.

We further considered the fibre arrangement given in figure 6.6. We establish the overall time delay in the 77.2 km fibre spools and compared it to the delays obtained on NZDSF-RS fibres spools amounting to 76.5 km. The 77.2 km fibre length resulted from a connection of 3 fibre spools of 25.3 km NZDSF-RS, 26.5 km NZDSF-RS and a 25.4 km NZDSF-SRS. Similarly, 76.5 km fibres length comprises of 3 spools but of 25.3 km NZDSF-RS, 26.5 km NZDSF-RS and a 24.7 km NZDSF-RS. In each of the connected fibres, at least three measurements were performed. The resulting time delays is given on Table 6.2. It is noted that the time delay, $\Delta\tau$ increases with increase in the wavelength separation. The reference wavelength, λ_1 is kept constant as λ_2 is varied. Different wavelengths propagate at different speeds. Therefore the higher the wavelength separation, the higher the time delay between the propagated wavelengths.

Table 6.2: Time delay comparison for the 76.5 km and 77.2 km NZDSF fibre spools

Wavelength (nm)	RS+RS+RS Time delay (ps)	RS+SRS+RS Time delay (ps)
1546.70	253.5±30.9	102.0±4
1546.95	415.5±25.3	153.5±4.5
1547.21	653.6±47.3	246.9±8
1547.47	860.4±58.1	356.9±7
1547.74	1078.0±85	436.2±8
1548	1336.1±110.6	527.3±15.8

The overall trend of the effect of negative dispersion fibre is clearly noted on Table 6.2. At each wavelength considered, the time delay for the 77.2 km fibre combination is smaller than that of the 76.5 km fibre link. For instance, at 1546.70 nm, 76.5 km measured a 253.5 ± 30.9 ps of time delay while that of 77.2 km fibre which includes a negative dispersion fibre (NZDSF-SRS) gave 102.0 ± 4 ps. The NZDSF-SRS fibre cancels dispersion therefore reducing the time delay between the respective pulses at different wavelengths. The compensation is not fully achieved as the obtained time delay is not zero. This is also confirmed mathematically by relating the fibre lengths and the corresponding coefficients as provided in equation (3.34) in chapter 3 section 3.8.3.3. The wavelength range considered in this measurement is from 1546.70 nm to 1548 nm. We are limited to this wavelength range due to wavelength tuneability of the VCSEL source used in this experiment.

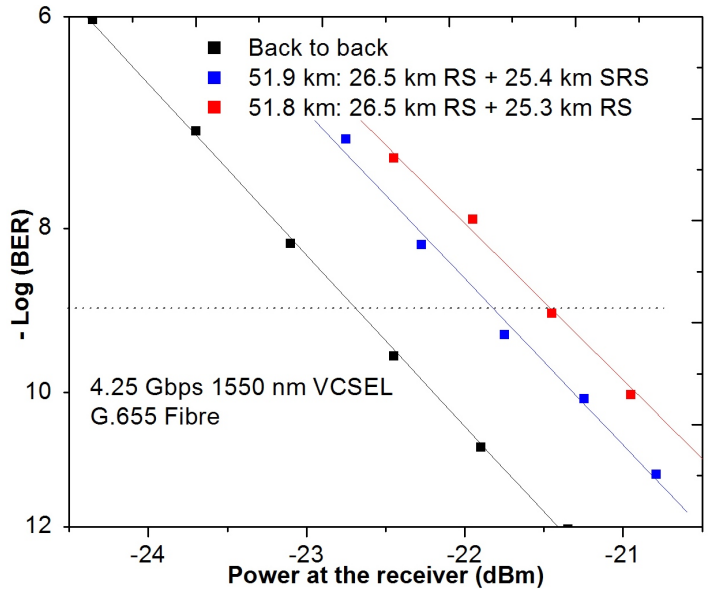

Figure 6.8: Experimental BER of a 4.5 Gbps VCSEL on a compensated NZDSF.

To validate this compensation, we perform BER measurements. A 1550 nm VCSEL was

modulated using a 4.25 *Gbps* NRZ-PRBS and transmitted over two fibre links of about 51 *km* each. The experimental set-up is similar to the one shown in figure 6.2 but the SMF and IDF fibres are replaced with NZDSF-RS and NZDSF-SRS respectively for the CD compensated case. First, two NZDSF-RS spools of 25.3 *km* and 26.5 *km* are connected resulting to a total of 51.8 *km*. Secondly, is the compensated case which comprised of 26.5 *km* of NZDSF-RS fibre joined to a 25.4 *km* NZDSF-SRS fibre giving a total of 51.9 *km* link. A VOA was used to vary the input power on the APD photo detector as the BER measurements were performed. BER measurements are performed so as to compare the transmission performance of the different fibre links.

Figure 6.8 provides the experimental BER measurement of the two transmissions. It is noted that the 4.25 *Gbps* transmission is improved by approximately 0.5 *dB* when compensation is used. The resulting residual penalty for the 51.9 km transmission is 0.8 *dB*. At a data rate of 4.25 *Gbps* on a 1550 *nm* VCSEL, the effect of dispersion on a NZDSF is small therefore reduced penalties. However, it is expected that as the bit rates are increased to 10 *Gbps* or higher, more dispersion penalties corresponding to fibre length should yield more power (*dB*) on effective compensation.

6.4 Summary

A negative dispersion compensating fibre is a promising dispersion management tool for the 1550 *nm* VCSEL transmissions over G.652 fibre. The use of IDF solves the chromatic dispersion limitation in VCSELs by reducing the dispersion penalties over a G.652 fibre at 1550 *nm* transmission. A 3.72 *dB* compensated power has been achieved on a 4.25 *Gbps* over 35 *km* G.652 fibre. On the same note, 5.17 *dB* of power penalty is realized on a 10 *Gbps* improving the reach. This chapter also describes the chromatic dispersion measurement in fibres[3]. We demonstrate how the combination of NZDSF-RS and NZDSF-SRS fibres cancel the CD in a transmission. The CD compensation in NZDSFs reduce penalties and eventually extend the reach. This should help in improving the VCSEL performance in terms of the reach for applications such as long access networks and SKA later phases.

In chapter 7, we extend the reach of the VCSEL by simultaneously using distributed Raman amplifiers while utilizing the dispersion compensation mechanism described in chapter 6.

[3]The author extends his sincere thanks to Wassin Shukree for his contribution in the CD measurement work co-executed and presented in this chapter.

Chapter 7

Raman amplification in VCSEL technology

Raman amplification have been suggested as a potential approach in telecommunication to overcome the fibre attenuation thus increasing the transmission distance [138, 200]. Raman amplifiers have gained popularity both in long haul transmission systems as well as improving the reach in core networks [200]. For instance, its application in passive optical networks (PONs) has been reported [223-225]. In telescope network, distributed Raman amplification remains one of the promising amplification techniques because of its ability to achieve high gain over a wide range of wavelengths and the fact that gain can also be achieved on any fibre.

7.1 Experimental set-up to investigate distributed Raman amplification

A signal at wavelength, $\lambda_s = 1548\ nm$ from an unmodulated VCSEL and a Raman pump (s) of wavelength $\lambda_p = 1448\ nm$ were used to study the Raman gain characteristics. The set-up is shown in figure 7.1. In the forward pumping scheme, only P_1 was used while in the backward scheme only P_2 was used. Polarization controllers were used to vary the orientation signal and pump states so as to ensure best coupling into the fibre. A maximum gain is achieved when the input signal and the pump are co-polarized [199, 200]. In order to avoid the polarization dependent losses, a polarization insensitive Raman amplifier can be designed using a non-polarization maintaining fibre or a polarization diversity pumping [200]. The on-off gain was established for various pump and signal powers over the VCSEL tuneability range. The on-off gain refers to the difference between the signal power when the pump is on and when off. For the bi-directional pumping, both P_1 and P_2 were used. Regarding the gain characterization, 25.3 km and 50.5 km True-wave Reach fibres from OFS Furukawa Company [226, 227] were utilized. The Truewave Reach fibre is fully compliant to both G.655

and G.656 standards and has a chromatic dispersion coefficient of about $5.5 - 8.9 ps/nm.km$ at 1550 nm. The zero dispersion wavelength for the Reach fibre is $\leq$ 1405 nm. The CD is meant to suppress other nonlinear effects such as the four-wave mixing between the pump and the signal in the fibre. The Reach fibre has a low water peak that gives low attenuation at the pump wavelength, i.e. at around 1450 nm. It also has an effective area of 55 μm^2. The effective area is designed to enhance the Raman efficiency by effectively coupling the Raman pump into the optical signal [226]. The VCSEL was then modulated with a 4.25 $Gbps$ $2^7 - 1$ NRZ-pseudorandom bit sequence (PRBS) and the bit error rate (BER) measurements taken for different transmission distances. VOA was used to vary the power getting to an avalanche photodiode (APD) receiver so as to measure BER. EA amplified the received signal for BER measurements. Different lengths of G.655, non-zero dispersion shifted fibres (NZ-DSF (+) / NZDSF (-)) were considered.

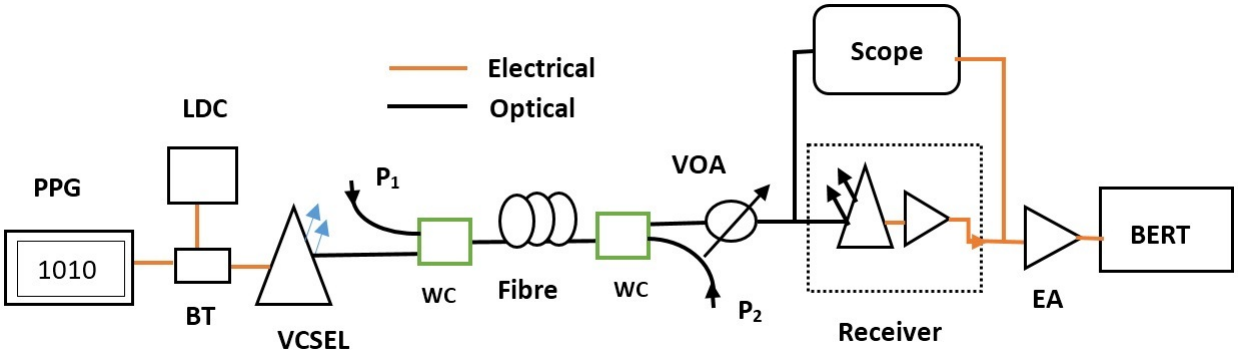

Figure 7.1: Experimental illustration of the set-up used to study Raman amplification. PPG is the programmable pattern generator, LDC is the laser diode controller, BT is the bias tee, P_1 and P_2 are pump 1 and pump 2, WC-wavelength based coupler, VOA is the variable optical attenuator, EA is the electrical amplifier and BERT is the bit error rate tester. PPG generates the sequence, LDC tunes the bias current of the VCSEL and BT couples the DC and data onto the device.

7.2 Raman gain characterization

The Raman gain is dependent on the pump-signal wavelength separation. It is due to this fact that the gain bandwidth tailoring is attained using multiple pumps. Ideally the maximum gain is achieved when the pump is 100 nm (13.2 THz frequency shift) below the signal wavelength as shown in figure 7.2 (a).

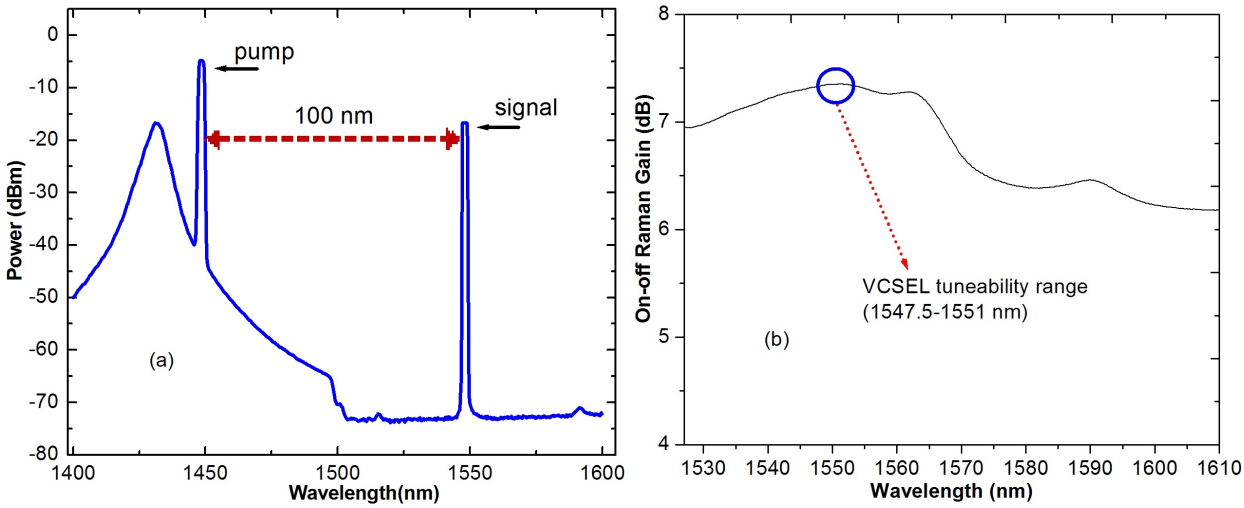

Figure 7.2: (a) Pump-signal wavelength separation (b) Raman gain profile showing VCSEL tuneability range.

For the illustration purposes, the pump power was reduced so as to protect the optical spectrum analyser (OSA) from high intensity. Note that in practice, a pump has a higher intensity relative to that of the signal than as depicted in figure 7.2 (a). Most Raman pumps operate at 1450 nm region providing maximum amplification at 1550 nm window. The VCSEL is a wavelength tuneable source and thus varying on-off gain is realized on tuning the current bias [228]. As the bias current, I_b was tuned from 4 mA to 9 mA the centre wavelength shifted from 1547.5 nm to 1551 nm as illustrated in figure 7.2 (b). To establish the gain relationship shown in figure 7.2 (b), a broadband source FLS-2300B from EXFO was used. The broadband source has a wavelength range of 1480 nm−1650 nm. The on-off gain was measured so as to confirm the optimum signal-pump wavelength separation for maximum gain. This was then used to tune the VCSEL to the optimum wavelength corresponding to the maximum Raman gain. From the Raman profile, it can be concluded that Raman amplifier is a broadband amplifier. The achievable gain varies in accordance with the dynamic range of the VCSEL.

It can be noted that the Raman on-off gain increases with decrease in signal power as depicted in figure 7.3. Amplification is achieved when power is transfered from the pump to the signal as discussed in chapter 3 section 3.8.4. Logically, as the signal power is reduced while maintaining a constant pump power, the relative difference between the pump and the signal is increased hence the pump transfers energy to the weaker signal resulting to more Raman gain. However, certain power levels of the signal are not recommended because of the noise level. At very low signal levels, more noise is amplified thus reducing the optical signal to noise ratio (OSNR). The results presented in this chapter uses signal power of −11 dBm.

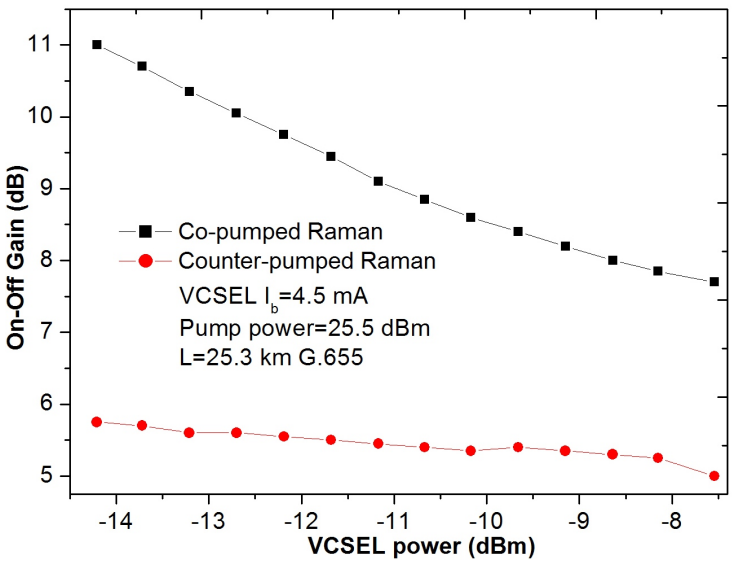

Figure 7.3: On-off gain for different signal powers at I_b = 4.5 mA.

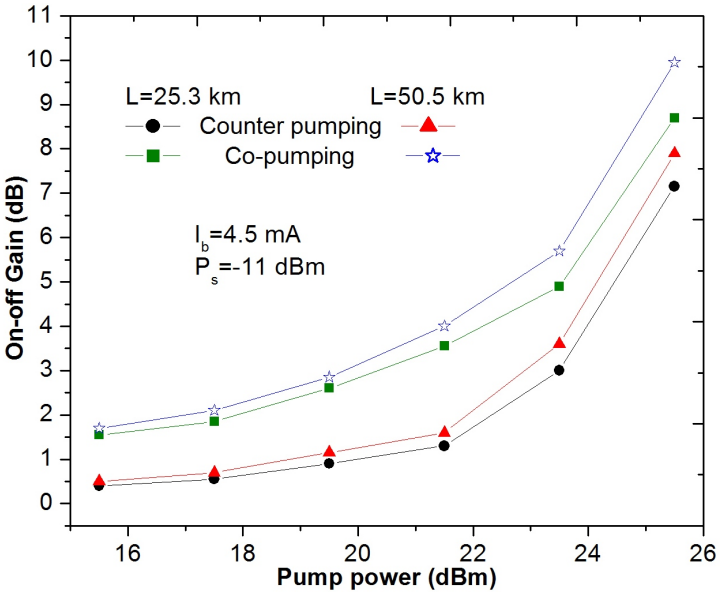

Figure 7.4: Relation between the gain and the pump power for the different schemes.

For both the pumping schemes, Raman on-off gain increases with increase in pump power as noted in figure 7.4. High power provides more energy for transfer to the signal. As discussed in section 3.11, the on-off gain is dependent on the pump power and the fibre length. Raman gain is improved as the length is increased.

Figure 7.5 (a) depicts the wavelength tuneability range of a VCSEL used for investigation of Raman amplification. The arrow points the bias current, $I_b = 4.5\ mA$ corresponding to 1548 nm wavelength that provides highest gain with respect to pump position.

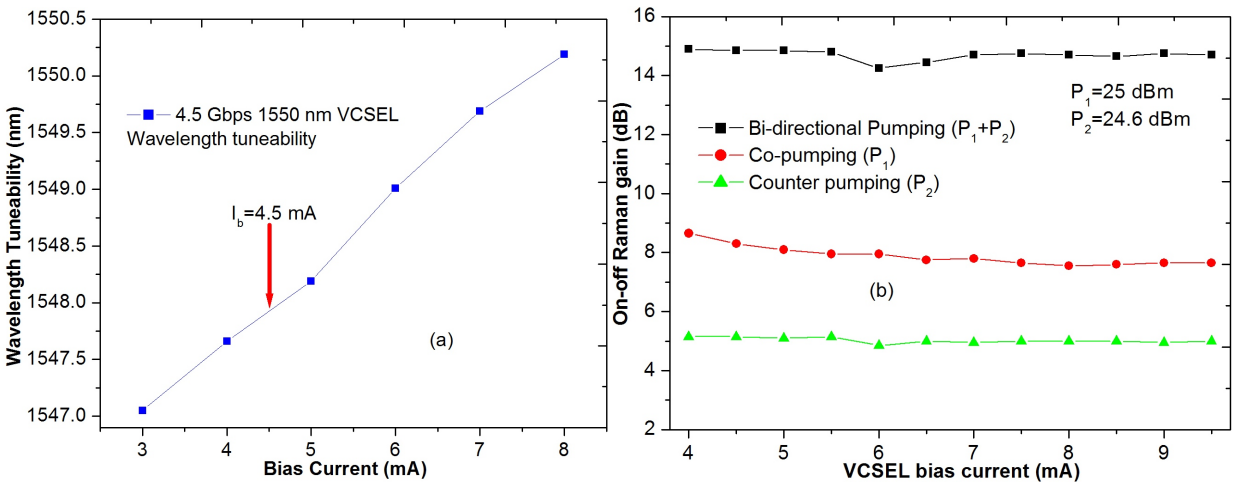

Figure 7.5: (a) VCSEL wavelength tuneability with bias current. (b) On-off gain for different bias currents for different pump configurations over the wavelength tuneability range.

Figure 7.5 (b) shows on-off gain for counter, co- and bi-directional pumps over the VCSEL tuneability range. The input signal power was maintained at $-11\ dBm$ while the pump powers at 25 dBm and 24.6 dBm. The gain spectrum appears flat because of the small wavelength range (see figure 7.2 (b)). In Figure 7. 5 (b), a 25.3 km True-wave Reach fibre optimized for distributed Raman amplification [227] was used. The bi-directional scheme gave the highest on-off gain of about 15 dB while in the forward and the backward pumping schemes[1], 8 dB and 5 dB gains respectively were realized. In a transmission with a link loss of about 0.3 dB/km (fibre and connectors), the obtained gains can increase the reach by up to 50 km, 27 km and 17 km respectively. In the bi-directional scheme, the two pumps provide more energy to be transferred to the signal thus reducing the depletion effect as compared to a single pump. The forward pumping has a higher on-off gain than backward pumping because of the enhanced signal-pump interaction. At the coupling end, the pump and signal are relatively strong and both gets weaker towards the end of the fibre. The energy transfer to a relatively strong signal renders it the advantage of higher optical signal to noise ratio (OSNR) as compared to counter scheme [199]. In the backward configuration, a strong pump in the opposite direction interacts with a weaker signal thus the walk-off effect leads to a lower gain. This is because at the signal coupling end, the signal is relatively strong when the pump is relatively weaker thus reduced power transfer. However, for the counter scheme due to the pump direction, the pump to signal noise transfer is minimized. The bi-directional pumping balances the performance of forward and backward pumping.

[1]Forward and backward pumping schemes has been used interchangeably with co-pumping and counter pumping respectively.

7.3 Transmission performance using distributed Raman amplifier

In this section, we present results on VCSEL transmission with the aid of Raman amplification so as to overcome the fibre losses. To maximize the transmission reach, we use the negative dispersion fibre (NZDSF (-) as discussed in chapter 5. A NZDSF (+) reach fibre optimized for Raman amplification has dispersion of $5.5 - 8.9\ ps/nm.km$ [226]. The fibre spools comprising of 25.3 km NZDSF-RS (+), 25.4 km NZDSF-SRS (-) and 25.3 km NZDSF-Reach (+) were joined giving a total of 76 km.

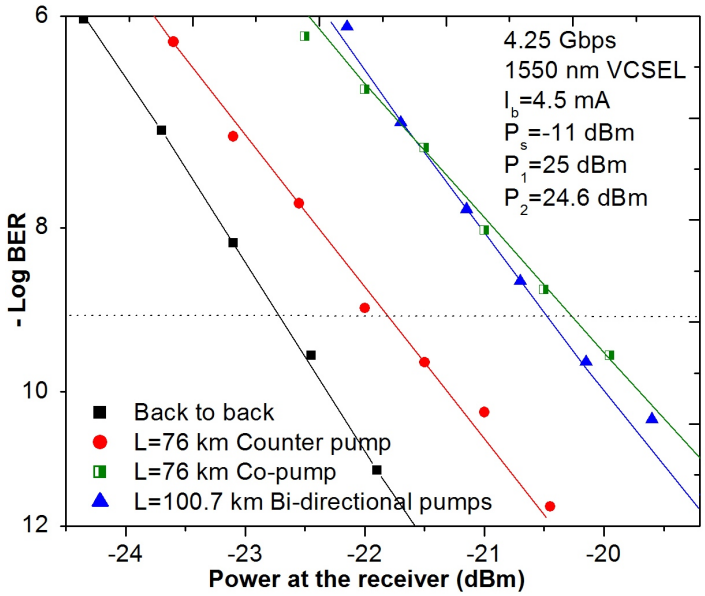

Figure 7.6: Experimental BER measurements of VCSEL transmission with Raman amplification.

A forward and a backward pumping scheme was then used in the 76 km fibre link. The optical power incident on the sampling oscilloscope was $-18.6\ dBm$ for both the 76 km transmissions. For bidirectional pumping, additional 24.7 km NZDSF (+) RS spool giving 100.7 km was used. The choice of an APD photodiode is because of its higher sensitivity of about $-26\ dBm$ as well as its ability to amplify at the Avalanche stage. It is because of this APD properties that makes it suitable for long transmission as discussed in section 3.6. In principle, we employ double amplification namely APD Avalanche stage and distributed Raman amplification to achieve the transmission.

Power penalties of 0.9 dB, 2.5 dB and 2.3 dB for 76 km counter pumped, 76 km co-pumped and 100.7 km bi-directionally pumped transmissions respectively were achieved. The on-off gains of 5 dB, 8 dB and 15 dB for backward, forward and bidirectional schemes are much higher compared to the respective power penalties over the considered distances of transmission. The power penalty difference between the two pumping schemes at 76 km

transmission is 1.6 dB. BER measurements show that the counter pump scheme has a better performance as compared to co-pumped at the 76 km fibre transmission as shown in figure 7.6. This may be attributed to the walk-off effects that may reduce the pump to noise transfer to the signal giving a better performance.

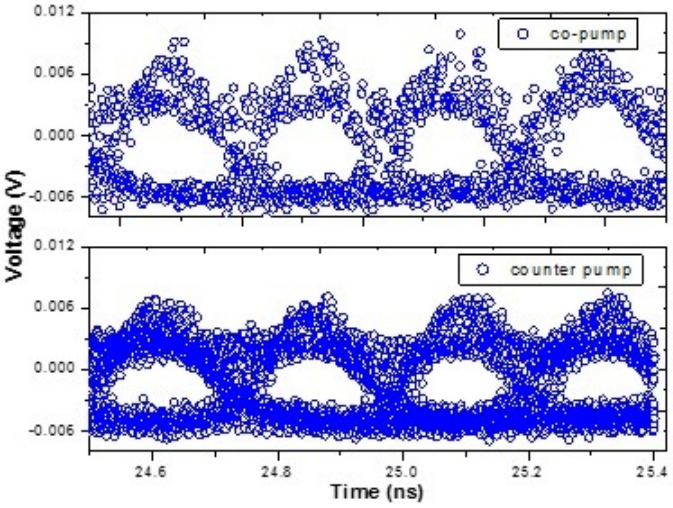

Figure 7.7: Eye diagrams of 76 km transmission with counter and co-pump schemes respectively.

The eye opening in figure 7.7 signify the signal clarity at 76 km transmission. The eye diagrams were taken at telecommunication BER threshold optical powers. The optical powers incident on the sampling oscilloscope were -21.7 dBm and -20.3 dBm for backward and forward pumping respectively. The 100.7 km transmission shows a better performance as compared to 76 km co-pumped configuration. This signifies the advantage of bi-directional pumping in achieving a better signal amplification while balancing the performance of the co-pumped and counter-pumped schemes. Co-pump scheme has a higher gain and OSNR but more noise transferred to the signal. On the other hand, counter-pump scheme has minimized noise transfer from pump to signal but low gain and OSNR. It is expected that power penalties will increase at high transmission rates due to dispersive effects. Generally, the combined transmitter-receiver pair optimization, dispersion management and use of Raman amplification make the VCSEL performance suitable for long reach in telescope networks as well as other applications such as long access networks.

7.4 Simultaneous signal amplification and clock signal distribution employing backward pumping

In this section, we devise an optical link design suitable for a telescope network. Telescope antennas receive astronomical data from objects in space. The received data is then digitized

and transmitted from the remote antennas to the central signal processor. On the other hand, a clock is required at the antenna for the data digitization as well as control and monitoring for proper functioning of the telescope. If the time and frequency reference system is housed at the processor building, then a clock signal is transmitted from the processor building to the each of the remote antennas. We propose a scheme to allow this bi-directional transmission. This scheme is attractive in that a single fibre can be used for both the transmission of the data and clock signals. Secondly, the technique utilizes a Raman pump that serves two purposes, it transmits the clock signal while amplifying the astronomical data propagating in the counter direction.

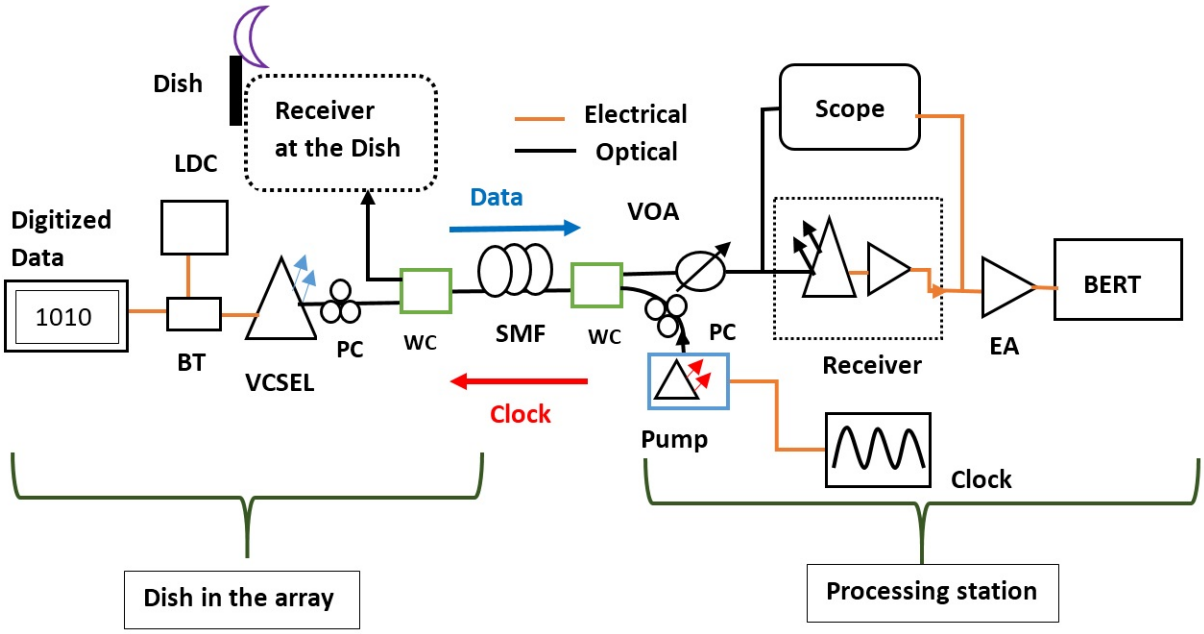

Figure 7.8: Schematic experimental research set-up used to study the bidirectional transmission involving data and clock at NMMU laboratory.

The experimental set-up shown in figure 7.8 illustrates optical fibre link and the bi-directional setting of data and clock transmission between a single dish in the array and the processing station. This is a representation of a typical layout used to clarify the devised scheme. Note that the set-up terms are defined in figure 7.1. A JDSU S34 series Raman pump of wavelength $\lambda_p = 1448\ nm$ was modulated with a 10 kHz clock signal and coupled to the fibre in the counter direction. A JDSU S34 series Raman pump uses LDC 220C laser diode controller that allows a maximum modulation of 50 kHz with a 15 V peak to peak voltage. In order to protect laser module from damage, a low modulation of up to 10 kHz was used. A function generator, FG2 from Circuitmate Electronics Company was used to generate the 1 kHz and 10 kHz clock signal. The received clock signal was viewed on a wide bandwidth oscilloscope. The VCSEL was modulated with a 4.25 $Gbps$ NRZ-PRBS signal and the counter Raman pump modulated with clock signal was used to provide amplification to the VCSEL

signal

A 0.7 dB penalty over 76 km transmission was achieved as shown in figure 7.9. The on-off gain from the backward Raman pump amounted to 5 dB. The 76 km fibre is a combination of 25.3 km NZDSF-RS, 25.4 km NZDSF-SRS and 25.3 km NZDSF- Reach, so as to reduce the dispersion penalties. The inset graph shows an open eye implying error free signal in this transmission.

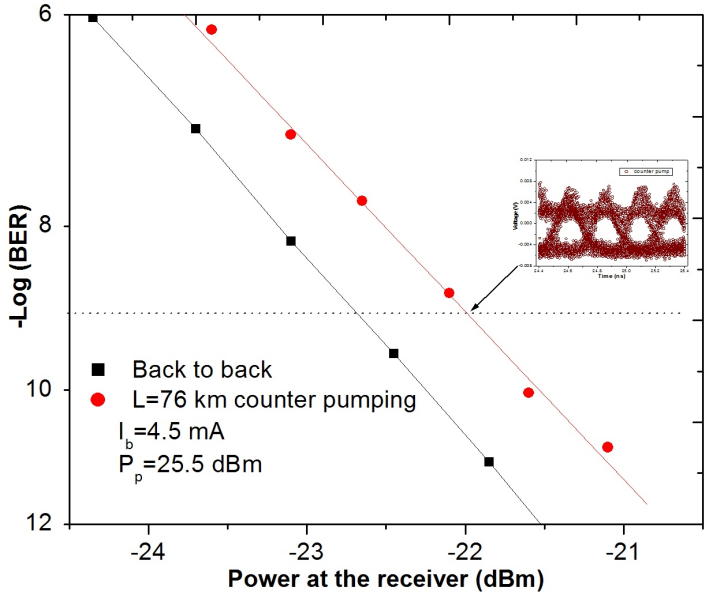

Figure 7.9: BER measurement on a 76 km transmission with counter Raman pumping. Inset: eye diagram for the 76 km transmission.

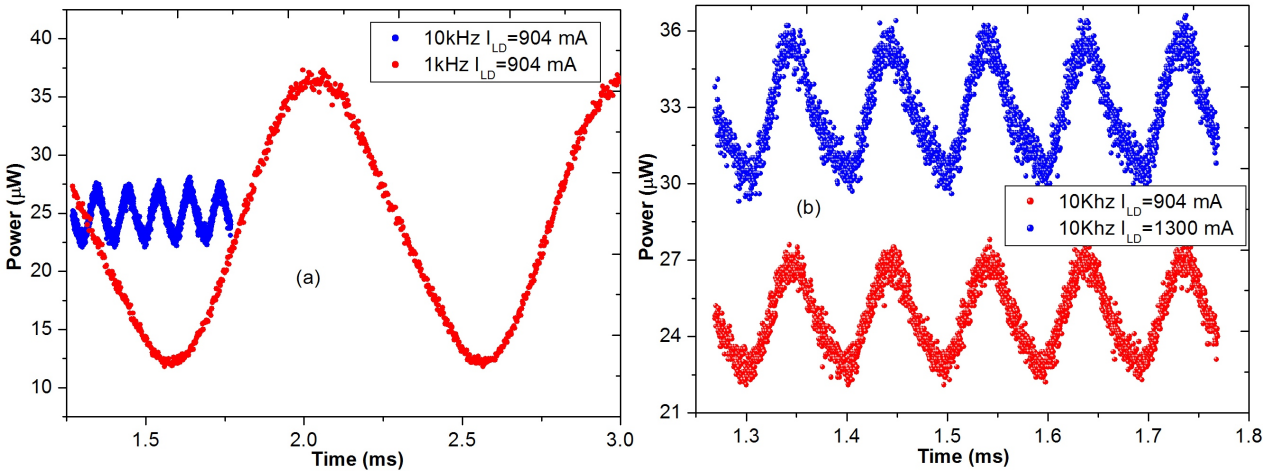

Figure 7.10: (a) Clock signal transmitted using Raman pump at different clock frequencies (b) 10 kHz clock at different pump drive currents.

In this section, clock signal over fibre was achieved using Raman pump as a transmitter. The Raman pump output power depends on the drive current set on the laser diode controller.

To ensure constant and high amplification of the signal, high LDC drive currents are required. The pump drive current, $I_{LD} = 1300\ mA$ was set giving an optical power of about 25.5 dBm. At lower clock frequencies, the LDC bias current limit reduces therefore reducing the pump power and thus amplification. For example at 1 kHz, the LDC limit is 904 mA. Figure 7.10 (a) shows the received clock signals at different frequencies at constant pump drive currents of 904 mA. This yielded 23 dBm power enabling about 2 dB gain in the counter scheme. The output power of received clock signal is seen to increase with increase in drive current as shown in figure 7.10 (b). The pump residue after amplification was high and therefore an attenuator was used to reduce the optical power before receiving. Signal averaging on the scope was performed so as to minimize the noise effect resulting from high residual Raman pump power transporting the clock signal. This work basically introduces and demonstrates a cost effective concept for a telescope optical network with transmission distances demanding signal amplification. However, some more work needs to be done to ascertain the phase noise or jitter of the transmitted clock. The phase noise measurements were not performed due to limitation of the necessary equipment.

Considering SKA 1 baselines extending up to 100 km, amplification is inevitable for the VCSEL technology. The VCSELs would be used to transmit digitized astronomy data from the antennas to the Karoo processing station. To achieve the bi-directional transmission for these baselines, appropriate Raman pump modulation frequencies may be employed. For example, if the MeerKAT clock frequencies of 1.088 GHz and 1.712 GHz [23] are to be used, Raman pumps with modulation inputs of about 2 GHz can be used. With such Raman pumps, the signal amplification enabling increased reach as well as simultaneous clock distribution will be achieved hence giving a cost effective solution to the SKA.

7.5 Summary

Raman amplification has been tested successfully on VCSELs. High on-off gains of 15 dB, 8 dB and 5 dB in the bi-directional, forward and backward pumping schemes respectively enabling error free transmission were achieved. Transmission extending to about 80 km can be obtained using a single Raman pump in either scheme. Bi-directional scheme is an excellent configuration for longer reach extending beyond 100 km. Therefore, Raman amplification proves vital and appropriate for VCSEL use in long reach telescope networks.

We have also successfully demonstrated a novel idea involving a bi-directional transmission over 76 km optical fibre employing a VCSEL and a Raman pump. Raman pump in the counter scheme was used to successfully transmit a 10 kHz clock signal while providing a 5 dB amplification to the the VCSEL signal. The bi-directional approach is vital for SKA application where the clock signal is to be distributed to remote telescopes as the collected astronomical data is transmitted for processing.

Chapter 8

Conclusions

Optical fibre transport in the Square kilometre Array is an essential solution for the collection and transmission of the streaming astronomical data in addition to antenna monitoring and control. The main goal of this thesis was to develop and characterize a high speed optical fibre network suitable for telescope application. This work proves the feasibility of VCSEL application beyond MeerKAT distances while addressing other optical effects paramount in the telescope array.

In the first part of this work, field characterization of KAT-7 optical fibre network is performed so as to estimate the contribution of the fibre to the deterioration of the synchronisation and timing signal in the MeerKAT telescope array. The fibre link comprised of buried section and the exposed sections forming the riser cable. A mean differential group delay (DGD) of 84.8 fs over the wavelength $1530 - 1560$ nm for the deployed 10.25 km single mode fibre was measured. From the DGD of the buried section amounting to 60.1 fs, it revealed that additional DGD is contributed by the riser cable. To ascertain this, we monitored the state of polarization (SOP) of the buried fibre section and compared it to the SOP of the entire section. After 15 hour monitoring period, a maximum polarization fluctuation of 14^o on the buried section and up to 180^o was obtained on the entire section. This polarization fluctuation is directly related to the phase drift between birefringent axes of the fibre. Polarization fluctuation is a deleterious effect on the clock distribution in the telescope array. The obtained DGD values attained are low (fs range) and within the allocated budget in the MeerKAT telescope array. Proper fibre deployment with minimized fibre stresses and the use of polarization maintaining fibre on the riser cable is recommended in reducing the polarization effects thus ensuring stable and accurate clock signal over fibre. A polarization maintaining fibre but which can maintain light polarization is however more costly than a single mode fibre.

In this work, telescope optical fibre network for astronomical data transport has been successfully designed and tested using the high speed VCSEL technology. This thesis derives the VCSEL potential for this application from the telecommunication access network perspective.

For the MeerKAT distances $\leq 12\ km$, 10 *Gbps* VCSEL transmission was achieved error free with a maximum acceptable power penalty of 5.2 dB in the worst case scenario of chromatic dispersion in the fibre. In order to achieve the 40 *Gbps* expected in the MeerKAT antenna, wavelength division multiplexing utilizing the wavelength tuneability in a device is employed. In SKA 1 and SKA 2 longer distances extending up to 100 km and 3000 km will call for dispersion compensation mechanisms as well as signal amplification. To extend the VCSEL use to SKA 1 inner baselines, selection of fibre type at different transmission windows so as to reduce the dispersion effects is suggested. As noted on the performed transmissions, minimized dispersion penalty is realized when a 1550 nm source is used on a G.655 fibre and a1310 nm source on a zero dispersion wavelength over a G.652 fibre. For specialized dispersion management, this work demonstrates the use of negative dispersion fibre for application in the telescope network. Inverse dispersion fibre (IDF) designed for compensation on a conventional single mode fibre, G. 652 in cabled system is studied. Up to 5.2 dB of power was compensated on a 10 *Gbps* transmission 1550 nm VCSEL over 12 km fibre link. This compensated power can increase the transmission reach of the VCSEL. Similarly, we experimentally achieve the dispersion compensation on a non-zero dispersion shifted fibre (NZDSF) through the combination of NZDSF (+) fibre and NZDSF (-). We use the pulse delay approach to measure the effect of compensation, with this combination 4.25 *Gbps* on 1550 nm VCSEL over 52 km was achieved a penalty less than 1 dB. Negative dispersion fibre is an effective and convenient compensation management tool for use in VCSEL technology for telescope array network. To further improve the transmission reach, the use of distributed Raman amplifier with dispersion compensation was applied. In this case, high gains of 15 dB, 8 dB and 5 dB for bidirectional, co-pumping and counter pumping respectively are attained. With increased pump powers, more gain can be achieved. We also propose a cost effective approach involving the simultaneous signal amplification and clock distribution using a backward Raman pump. A backward Raman pump providing an on-off gain of 5 dB while transmitting a 10 kHz clock signal over a 76 km G.655 fibre was demonstrated. This Raman amplification concurrently enabled 4.25 *Gbps* data transmission over 76 km G.655 fibre.

In essence the research and development work provided in this thesis is very vital for Square Kilometre Array optical transport and other applications such as extended access networks. It gives an insight of sensitive issues to address in improving transmissions for timing and synchronization in addition to providing a possible technology for transmission of enormous data rates streaming from the individual antennas in the array.

Appendix A

Research outputs in journals, conferences and other reports

Published/accepted/presented articles

2015:

1. T. B. Gibbon, E. K. Rotich Kipnoo, R. R. G. Gamatham, A. W. R. Leitch, R. Siebrits, R. Julie, S. Malan, W. Rust, F. Kapp, T. L. Venkatasubramani, B. Wallace, A. Peens-Hough, P. Herselman, "Fibre-to-the-telescope: MeerKAT, the South African precursor to Square Kilometre Telescope Array (SKA)", *SPIE J. of astronomical telescopes, measurement and systems- Accepted.*

2014:

1. E. K. Rotich Kipnoo, D. Waswa, G. Amolo and A.W. R. Leitch, "Gain analysis for a 2-pump fibre optical parametric amplifier", *African Review of Physics Journal* (2014) 9:0008, pp. 47- 52.

2. G. M. Isoe, K. M. Muguro, D. W. Waswa, E. K. Rotich Kipnoo, T. B. Gibbon and A.W. R. Leitch, "Analysis of optical signal to noise ratio in modern transmission fibres during Raman amplification", *Proc. of the 17th annual Southern Africa telecommunication networks and applications conference (SATNAC)*, Boardwalk, Port Elizabeth, South Africa, pp. 161-164, 31st Aug. to 3rd Sept. 2014. ISBN: 978-0-620-61965-3.

3. D. Kiboi Boiyo, E. K. Rotich Kipnoo, R. R. G. Gamatham, A.W. R. Leitch and T. B. Gibbon, "Towards investigating transmission penalties in a flexible spectrum optical

network", *Proc. of the 17th annual Southern Africa telecommunication networks and applications conference (SATNAC)*, Boardwalk, Port Elizabeth, South Africa, pp. 459-460, 31st Aug. to 3rd Sept. 2014. Work in progress paper. ISBN: 978-0-620-61965-3.

4. S. Wassin, E. K. Rotich Kipnoo, R. R. G. Gamatham, A. W. R. Leitch and T. B. Gibbon, "A performance analysis of the phase shift and pulse delay techniques for chromatic dispersion measurements and compensation in single mode fibre", *Proc. of the 17th annual Southern Africa telecommunication networks and applications conference (SATNAC)*, Boardwalk, Port Elizabeth, South Africa, pp. 155-159, 31st Aug. to 3rd Sept. 2014. ISBN: 978-0-620-61965-3.

5. E. K. Rotich Kipnoo, T. V. Chabata, R. R. G. Gamatham, A. W. R. Leitch and T. B. Gibbon, "Experimental demonstration of Raman amplification in vertical cavity surface emitting lasers for extended reach access networks" *Proc. of the 17th annual Southern Africa telecommunication networks and applications conference (SATNAC)*, Boardwalk-Port Elizabeth, South Africa, pp. 21-24, 31st Aug. to 3rd Sept. 2014. ISBN: 978-0-620-61965-3.

6. E. K. Rotich Kipnoo, R. R. G. Gamatham, A. W. R. Leitch, T. B. Gibbon, S. Malan, H. Kriel and F. Kapp, "Phase noise analysis of a 1.712 GHz clock signal transmitted over optical fibre for MeerKAT time and frequency reference (TFR)", *Presented at 59th annual conference of the South African institute of physics (SAIP)*, University of Johannesburg, 7th - 11th Jul. 2014. Poster

7. G. M. Isoe, K. M. Muguro, D. W. Waswa, E. K. Rotich Kipnoo, T. B. Gibbon and A. W. R. Leitch , "Performance comparison of SMF-Reach and SMF-RS optical fibres for Raman amplification", *Presented at 59th annual conference of the South African institute of physics (SAIP)*, University of Johannesburg, 7th - 11th Jul. 2014. Poster.

8. D. Kiboi Boiyo, E. K. Rotich Kipnoo, T. B. Gibbon and A. W. R. Leitch, "Flexible spectrum and the effects of crosstalk on a 20 Gbps signal over a 12 km optical fibre", *Presented at 59th annual conference of the South African institute of physics (SAIP)*, University of Johannesburg, 7th - 11th Jul. 2014. Poster

9. S. Wassin, E. K. Rotich Kipnoo, R. R. G. Gamatham, A. W. R. Leitch and T. B. Gibbon, "Using a VCSEL to accurately measure chromatic dispersion in single mode fibre by the phase shift technique", *Presented at 59th annual conference of the South African institute of physics (SAIP)*, University of Johannesburg, 7th - 11th Jul. 2014.

10. T. V. Chabata, E. K. Rotich Kipnoo, R. R. G. Gamatham, A. W. R. Leitch and T. B. Gibbon, "A single DFB laser with multilevel directly modulated signal for high speed

optical fibre communication system," *Presented at 59th annual conference of the South African institute of physics (SAIP)*, University of Johannesburg, 7th - 11th Jul. 2014.

2013:

1. T. B. Gibbon, E. K. Rotich, H. Y. S. Kourouma, R. R. G. Gamatham, A. W. R. Leitch, R. Siebrits, R. Julie, S. Malan, W. Rust, F. Kapp, T. L. Venkatasubramani, B. Wallace, A. Peens-Hough and P. Herselman, "Fibre-to-the-telescope: MeerKAT, the South African precursor to square kilometre telescope array (SKA)," *Proc. SPIE 9008*, Optical metro networks and short-haul systems VI, 90080P (Dec. 20th, 2013).

2. E. K. Rotich Kipnoo, H. Y. S. Kourouma, R. R. G. Gamatham, A. W. R. Leitch and T. B. Gibbon, "Chromatic dispersion compensation for VCSEL transmission for applications such as square kilometre array South Africa," *Proc. 58th annual conference of the South African institute of physics (SAIP)*, University of Zululand, pp. 490-495, 8-12th Jul 2013. ISBN: 978-0-620-62819-8.

3. E. K. Rotich Kipnoo, H. Y. S. Kourouma, R. R. Gamatham, A. W. R. Leitch and T.B. Gibbon. R. Julie, R. Siebrits and F. Kapp., "Characterization of the polarization mode dispersion of single mode fibre in KAT-7 telescope array network, South Africa", *Africon 2013*, vol., no., pp.1-4, 9th- 12th Sept. 2013.

4. E. K. Rotich Kipnoo, H. Kourouma, T. V. Chabata, R. R. G. Gamatham, A. W. R. Leitch and T. B. Gibbon, "Optimizing VCSEL transmission for longer reach in optical access networks", *Proc. 16th annual Southern Africa telecommunication networks and applications conference (SATNAC),* Spier, Stellenbosch, Western Cape, South Africa, pp 27-30, 1st- 4th Sept. 2013.

5. H. Kourouma, E. Rotich, T. Gibbon, A. Leitch, R. Siebrits, R. Julie and F. Kapp, "Birefringence and polarization fluctuations as a result of optical fibre bending during scanning of a KAT-7 riser cable", *Africon 2013*, vol., no., pp.1-5, 9th- 12th Sept. 2013.

6. Romeo Gamatham, Enoch Rotich, Andrew Leitch and Timothy Gibbon, "Fibre-to-the-hut: Research into tailored FTTH solutions for Africa", *Africon 2013*, vol., no., pp.1-5, 9th- 12th Sept. 2013.

7. D. Kiboi Boiyo, S. Kuja, D. Waswa, G. Amolo, ,R. R. G. Gamatham, E. K. Rotich Kipnoo, T. B. Gibbon and A. W.R. Leitch, "Effects of polarization mode dispersion (PMD) on Raman gain and PMD measurement using an optical fibre Raman amplifier", *Africon 2013*, vol., no., pp.1-5, 9th- 12th Sept. 2013.

8. Hamed Y. S. Kourouma, Enoch K. Rotich Kipnoo, Romeo Gamatham, Andrew W.R. Leitch, Tim B. Gibbon, "Phase instabilities of a reference signal for timing and frequency distribution of the square kilometre array (SKA)", *Proc. 16th annual Southern Africa telecommunication networks and applications conference (SATNAC)*, Spier, Stellenbosch, Western Cape, South Africa, pp. 15-20, 1st- 4th Sept. 2013.

9. S. Wassin, E. K. Rotich Kipnoo, R. R. G. Gamatham, A. W. R. Leitch and T. B. Gibbon, "Pulse delay chromatic dispersion measurements in single mode fibre", *Proc. 58th annual conference of the South African institute of physics (SAIP)*, University of Zululand, pp. 507-512, 8th- 12th Jul. 2013.

10. S. Wassin, E. K. Rotich Kipnoo, R. R. G. Gamatham, A. W. R. Leitch and T. B. Gibbon, "Chromatic dispersion measurements of optical fibre using the pulse delay technique", *Proc. 16th annual Southern Africa telecommunication networks and applications conference (SATNAC)*, Spier, Stellenbosch, Western Cape, South Africa, pp. 137-140, 1st- 4th Sept. 2013. ISBN: 978-0-620-62819-8.

11. T. V. Chabata, R. R. G. Gamatham, H. Y. S. Kourouma, E. K. Rotich Kipnoo, A. W. R. Leitch, and T. B. Gibbon, "Digital signal processing algorithm for signal analysis and performance monitoring in an optical communication link", *Proc. 58th annual conference of the South African institute of physics (SAIP)*, University of Zululand, pp. 460-463, 8th-12th Jul. 2013. ISBN: 978-0-620-62819-8.

12. T.V. Chabata, R. R. G. Gamatham , H. Y. S. Kourouma, E. K. Rotich Kipnoo, A. W. R. Leitch, and T. B. Gibbon, "Digital signal processing algorithm for signal reconstruction and performance measurement for a single photo detector optical communication system", *Proc. 16th annual Southern Africa telecommunication networks and applications conference (SATNAC)*, Spier, Stellenbosch, Western Cape, South Africa 1st- 4th Sept. 2013.

13. E. K. Rotich Kipnoo, R. R. G. Gamatham, A. W. R. Leitch and T. B. Gibbon, "1310 nm VCSELs enabling error-free transmission at 10 Gbps over 23 km fibre link for applications such as square kilometre array," *The NMMU/Telkom centre of excellence 34th Steering committee meeting and project presentations*, NMMU, 12th Nov. 2013.

14. S. Kuja, D. Boiyo, D. Waswa, G. Amolo, E. Kipnoo, T. Gibbon, and A. Leitch, "Comparison of PMF and LEAF as optical fibre stress and temperature sensing elements," in *advanced photonics 2013*, K. Ewing and M. Ferreira, eds., OSA technical digest (online) (OSA 2013), paper,JT3A.32.

15. E. K. Rotich Kipnoo, H. Y. S. Kourouma, R. R. G. Gamatham, A. W. R. Leitch, T. B. Gibbon, R. Julie, R. Siebrits and F. Kapp, "Polarization mode dispersion (PMD)

in KAT-7 optical fibre network," *The South African SKA project post graduate bursary conference*, 2013.

2012:

1. E. K. Rotich Kipnoo, D. Waswa, A. W. R. Leitch and T. B Gibbon, "VCSEL technology for square kilometre array (SKA) optical fibre network," *Proc. of the 57th annual conference of South African institute of physics (SAIP)*, Pretoria, South Africa, 2012. Poster

2. E. K. Rotich Kipnoo, H. Kourouma, D. Waswa, A. W. R. Leitch and T. B. Gibbon, "Analysis of VCSEL transmission for the square kilometre array (SKA) in South Africa," *Proc. 15th annual Southern Africa telecommunication networks and applications conference (SATNAC)*, Fancourt, George, South Africa, 2$^{\text{nd}}$ to 5$^{\text{th}}$ Sept. 2012. Work in progress paper.

3. Hamed Y.S. Kourouma, Enoch K. Rotich, David Waswa, Romeo Gamatham, Tim B. Gibbon, Andrew W. Leitch, "Polarization effects on the phase of a 4.25 GHz reference clock signal transmitted over optical fibre for applications such as the square kilometre array (SKA)," *Proc. 15thannual Southern Africa telecommunication networks and applications conference (SATNAC)*, Fancourt, George, South Africa, 2$^{\text{nd}}$ to 5$^{\text{th}}$ Sept. 2012. Work in progress paper.

4. T.V. Chabata, E. K. Rotich Kipnoo, R. R. G. Gamatham, A. W. R. Leitch, and T. B. Gibbon, "Performance comparison of OOK NRZ and DPSK modulation formats in an optical transmission system," *5th ALC student workshop,* Windhoek, Namibia, 14-18 Nov. 2012.

5. E. K Rotich Kipnoo, H. Kourouma, D. Waswa, R. Gamatham, A. W. R. Leitch and T. B. Gibbon, "Simulation and laboratory demonstration of vertical cavity surface emitting lasers (VCSELs) for data collection in the square kilometre array, (SKA) project," *The South African SKA project postgraduate bursary conference*, Stellenbosch, 2012.

Appendix B

SKA timeline and data rate calculation

Table B.1: SKA project timeline [16]

Time/Year	Particulars
1991	SKA Concept
2006	Site short listing
2008-2012	Telescope system design
2011	Establishment of SKA as a legal entity
2012	Site selection
2013	**Proposal evaluation**: Request for proposals, Proposal responses and cost ceiling establishment and Design consortia start. Work groups - (Assembly and integration, Science data processor, Wide band pixel feeds, Telescope manager, Dish, Signal data transport, Central signal processor, Mid frequency aperture array, Low frequency aperture array, Infrastructure)
2014-2016	Development of SKA organization governance, SKA 1 funding and preliminary design review.
2016	System prototyping deployment, critical design review and SKA 1 construction approval.
2017	Tender and procurement for construction –SKA 1
2018-2023	SKA 1 construction and detailed SKA 2 design
2020-2030	SKA 1 Early science and SKA 2 construction

Antenna/Dish Array

10 bits x1 GHz x 2 (Nyquist) x 2 (H and V polarizations) x 3000 (Antennae) = 120 $Tbps$

Aperture Array-Phase 1

50 (Stations) x 11200 (dipoles) x $\sim$ 10 bits x 2 (Nyquist) x 2 (H and V Polarizations) x $\sim$ 500 MHz = 11 $Pbps$.

Bibliography

[1] G.P. Agrawal, *Fibre-optic Communication Systems,* 3rd ed., John Wiley & Sons, Inc., New York, 2002.

[2] N. Massa, *Fibre optic telecommunication*, fundamentals of photonics, module 1.8, University of Connecticut, 2000, pp. 293-347.

[3] E. Ip, P. Ji, E. Mateo, H. Yue-Kai, X. Lei, Q. Dayou, B. Neng and W. Ting, 100G and beyond transmission technologies for evolving optical networks and relevant physical-layer issues, *Proceedings of the IEEE*, 100 (2012) 1065-1078.

[4] M. Nakazawa, S. Okamoto, T. Omiya, K. Kasai and M. Yoshida, 256-QAM (64 Gbps) coherent optical transmission over 160 km with an optical bandwidth of 5.4 GHz, *IEEE Photonics Technology Letters*, 22 (2010) 185-187.

[5] S. Okamoto, K. Toyoda, T. Omiya, K. Kasai, M. Yoshida and M. Nakazawa, 512 QAM (54 Gbit/s) coherent optical transmission over 150 km with an optical bandwidth of 4.1 GHz, *36th European Conference and Exhibition on Optical Communication (ECOC)*, 2010, pp. 1-3.

[6] Y. Koizumi, K. Toyoda, M. Yoshida and M. Nakazawa, 1024 QAM (60 Gbit/s) single-carrier coherent optical transmission over 150 km, *Optics Express*, 20 (2012) 12508-12514.

[7] C. Konstantinos and E.M. Varvarigos, Static and dynamic spectrum allocation in flexi-grid optical networks, *14th International Conference on IEEE Transparent Optical Networks (ICTON)*, 2012.

[8] A. N. Patel, P. N. Ji, J. P. Jue and T. Wang, Routing, Wavelength assignment, and spectrum allocation in transparent flexible optical WDM (FWDM) networks, *Photonics in Switching*, Monterey, California, United States, 2010, Paper PDPWG1.

[9] C. Politi, C. Matrakidis, T. Orphanoudakis, V. Anagnostopoulos and A. Stavdas, Planning and operation of elastic flex-grid optical networks with OFDM variable band-

width capabilities, *15th International Conference Transparent Optical Networks (ICTON)*, 2013, pp. 1-4.

[10] R. Spencer, L. Hu, B. Smith, M. Bentley, I. Morison, B. Anderson, D. Moodie, M. Robertson and D. Nesset, The use of optical fibres in radio astronomy, *Journal of Modern Optics*, Vol. 47, Iss. 11 (2000) 2015-2020.

[11] T. Morioka, Ultrahigh capacity optical communications beyond Pb/s, in: B.C.S.K.M. Boulanger and W. Knox (Eds.) Nonlinear Optics, *Optical Society of America*, Kohala Coast, Hawaii, United States, 2013, pp. NM2B.1.

[12] One petabit per second fibre transmission over 50km, *Phys.org*, http://phys.org/news/2012-09-petabit-fibre-transmission-km.html, 2012. Accessed 14th October 2014.

[13] J. Sakaguchi, B. J. Puttnam, W. Klaus, Y. Awaji, N. Wada, A. Kanno, T. Kawanishi, K. Imamura, H. Inaba, K. Mukasa, R. Sugizaki, T. Kobayashi and M. Watanabe, 19-core fibre transmission of 19x100x172-Gbps SDM-WDM-PDM-QPSK signals at 305Tb/s, *Optical fibre Communication Conference*, *Optical Society of America*, Los Angeles, California, 2012, pp. PDP5C.1.

[14] A. Sano, T. Kobayashi, S. Yamanaka, A. Matsuura, H. Kawakami, Y. Miyamoto, K. Ishihara and H. Masuda, 102.3-Tb/s (224 x 548-Gbps) C- and extended L-band all-Raman transmission over 240 km using PDM-64QAM single carrier FDM with digital pilot tone, *Optical fibre Communication Conference*, *Optical Society of America*, Los Angeles, California, 2012, pp. PDP5C.3.

[15] Alcatel-Lucent, 31 Tbps over a single fibre optic cable, http://www.ispreview.co.uk/index.php/2013/07/ alcatel-lucent-breaks-record-with-31tbps-over-a-single-fibre-optic-cable.html, 2013. Accessed 24th June 2014.

[16] Square kilometre array (SKA) website; http://www.ska.ac.za/index.php and https://www.skatelescope.org/project/, Accessed 10th October 2014.

[17] ASKAP Science Update, Vol. 1, CSIRO, in, http://www.atnf.csiro.au/projects/askap/ASKAP_Science_Update_1.pdf, 2009. Accessed 28th August 2014.

[18] R. Schilizzi, SKA-SADT technical development plan, No. SKA-TEL.SADT-PROP_Tech-RED-001, https://www.skatelescope.org/wp-content/uploads/2013/09/SKA-TEL-SADT-PROP_TECH-001_Redacted_final_24Sept13.pdf 2013. Accessed 18th July 2014.

[19] South Africa's MeerKAT radio telescope, technical fact sheet, in, http://www.ska.ac.za/download/fact_sheet_meerkat_2014.pdf, March 2014. Accessed 17th July 2014.

[20] A. J. Mullavey, B. J. J. Slagmolen, D. A. Shaddock and D. E. McClelland, Stable transfer of an optical frequency standard via a 4.6 km optical fibre, *Optics Express,* 18, (2010) 5213–5220.

[21] K. G. Baldwin, Y. He, M. Hsu, M. Wouters, M. Gray, B. J. Orr, A. Luiten, S. Schediwy, J. Chow, D. Shaddock, G. Aben, P. Fisk, and B. Warrington, Analog and all-digital frequency distribution via optical fibre links, *Conference on Lasers and Electro-Optics 2012*, *Optical Society of America* Technical Digest (online) (2012), paper CTh4A.2., 2012.

[22] S. Wang, D. Sun, Y. Dong, W. Xie, H. Shi, L. Yi and W. Hu, Distribution of high-stability 10 GHz local oscillator over 100 km optical fibre with accurate phase-correction system, *Optics Letters*, Vol. 39, Issue 4, (2014) 888-891.

[23] A. Peens-Hough, T. Küsel, S. Malan, F. Kapp and W. Esterhuyse, MeerKAT system preliminary design, *memo series M0000-0000V1-42 TM Revision 1A*, 2012.

[24] R. McCool, S. Garrington and R. Spencer, Signal transport and networks for the SKA, *General Assembly and Scientific Symposium*, 2011 XXXth URSI, 2011, pp. 1-4.

[25] ASKAP update, CSIRO astronomy and space, in, http://www.atnf.csiro.au/projects/askap/askap_update_3_web.pdf and http://www.atnf.csiro.au/projects/askap/data_transport.html, 2012. Accessed 28th August 2014.

[26] R. Beresford, ASKAP photonic requirements, *International topical meeting on Microwave photonics, 2008.* jointly held with the *2008 asia-pacific microwave photonics conference. mwp/apmp 2008.* 2008, pp. 62-65.

[27] R. Perley, P. Napier, J. Jackson, B. Butler, B. Carlson, D. Fort, P. Dewdney, B. Clark, R. Hayward, S. Durand, M. Revnell and M. McKinnon, The expanded very large array, *Proceedings of the IEEE*, 97 (2009) 1448-1462.

[28] S. Durand and D. Gerrard, *EVLA project book*, chapter 7, Fibre optic system, version 5 in, http://www.aoc.nrao.edu/evla/admin/projbook/chap7.pdf. 2006. Accessed 17th July 2014.

[29] S. Durand, J. Jackson and K. Morris, Phase coherence of the EVLA radio telescope, *Proc. SPIE 6267*, Ground-based and Airborne Telescopes, 62673Y, Orlando, FL 2006.

[30] A. Wootten, The Atacama large millimetre array (ALMA), *Proc. SPIE*, vol. 4837, 2003, pp. 110-118.

[31] W. Shillue, Fibre Distribution of local oscillator for Atacama large millimetre array, *Optical Fibre communication/National Fibre Optic Engineers Conference, 2008. OFC/NFOEC 2008*, 2008, pp. 1-3.

[32] A. Baudry, F. B. Marchet, H. Kurlandcyk and S. Rossi, The ALMA back end, telescopes and instrumentation, *The messenger 125*, 37-40, in, https://www.eso.org/sci/publications/messenger/archive/no.125-sep06/messenger-no125-37-40.pdf, 2006. Accessed 18th July 2014.

[33] R. Spencer, R. McCool, B. Anderson, D. Brown and M. Bentley, ALMA and E-MERLIN data transmissions systems: Lessons for SKA, *Experimental Astronomy,* 17, (2004) 221-228.

[34] e-MERLIN Web site, in, http://www.e-merlin.ac.uk/, 2014. Accessed 15th July 2014.

[35] A.K. Somani, *Survivability and traffic grooming in WDM PON networks*, Cambridge university press, Cambridge, UK, 2011.

[36] R. Ramaswami, K. N. Sivarajan and G. H. Sasaki, *Optical networks: A practical perspective*, 3rd ed., Morgan Kaufmann, Burlington, MA, 2010.

[37] A. Banerjee, Y. Park, F. Clarke, H. Song, S. Yang, G. Kramer, K. Kim and B. Mukherjee, Wavelength-division-multiplexed passive optical network (WDM-PON) technologies for broadband access: a review, *Journal of Optical Networking*, Vol. 4 Issue 11 (2005) 737-758.

[38] E. Wong, Next-generation broadband access networks and technologies, *Journal of Lightwave Technology*, 30 (2012) 597-608.

[39] J. A. Lázaro, J. Prat, P. Chanclou, G. M. Tosi Beleffi, A. Teixeira, I. Tomkos, R. Soila and V. Koratzinos, Scalable extended reach PON, *Optical fibre Communication Conference/National fibre Optic Engineers Conference*, *Optical Society of America*, San Diego, California, 2008, pp. OThL2.

[40] ITU-T, G.694.1: Spectral grids for WDM applications: DWDM frequency grid, in, http://www.itu.int/rec/T-REC-G.694.1-201202-I/en, 2012. Accessed 28th July 2014.

[41] B. Zhu, Entirely passive reach extended GPON using Raman amplification, *Optics Express*, 18, (2010) pp. 23428-23434.

[42] K. Jeung-Mo and H. Sang-Kook, A novel hybrid WDM/SCM-PON sharing wavelength for up- and down-link using reflective semiconductor optical amplifier, *IEEE Photonics Technology Letters*, 18 (2006) 502-504.

[43] T. B. Gibbon, K. Prince, T. T. Pham, A. Tatarczak, C. Neumeyr, E. Rönneberg and M. Ortsiefer, VCSEL transmission at 10 Gbps for 20 km single mode fibre WDM-PON without dispersion compensation or injection locking, *Optical Fibre Technology*, 17 (2011) 41-45.

[44] C. J. Chang-Hasnain, Optically-injection locked tunable multimode VCSEL for WDM passive optical networks, *International Nano-Optoelectronics Workshop, 2008. i-NOW 2008*. 2008, pp. 98-99.

[45] W. Hofmann, E. Wong, G. Bohm, M. Ortsiefer, N. H. Zhu and M. C. Amann, 1.55-μm VCSEL Arrays for high-bandwidth WDM-PONs, I*EEE Photonics Technology Letters*, 20 (2008) 291-293.

[46] D. Lei, Z. Ying, P. Xiaodan, T. Ming, S. Ping and L. Deming, All-VCSEL transmitters with remote optical injection for WDM-OFDM-PON, *IEEE Photonics Technology Letters*, 26 (2014) 461-464.

[47] K. H. Han, E. S. Son, H. Y. Choi, K. W. Lim and Y. C. Chung, Bidirectional WDM PON using light-emitting diodes spectrum-sliced with cyclic arrayed-waveguide grating, *IEEE Photonics Technology Letters*, 16 (2004) 2380-2382.

[48] Z. Xu, Y. J. Wen, W.-D. Zhong, C.-J. Chae, X.-F. Cheng, Y. Wang, C. Lu and J. Shankar, High-speed WDM-PON using CW injection-locked Fabry-Pérot laser diodes, *Optics Express*, 15 (2007) 2953-2962.

[49] P. J. Winzer and R. Essiambre, Advanced optical modulation formats, *Proceedings of the IEEE*, 94 (2006) 952-985.

[50] M. Daikoku, I. Morita, H. Taga, H. Tanaka, T. Kawanishi, T. Sakamoto, T. Miyazaki, T. Fujita, 100Gbit/s DQPSK transmission experiment without OTDM for 100G ethernet transport, *Optical fibre Communication Conference and Exposition and The National fibre Optic Engineers Conference*, *Optical Society of America*, Anaheim, California, 2006, pp. PDP36.

[51] X. Zhou, J. Yu, D. Qian, T. Wang, G. Zhang and P. Magill, 8x114 Gbps, 25-GHz-spaced, PolMux-RZ-8PSK transmission over 640 km of SSMF employing digital coherent detection and EDFA-only amplification, *Optical fibre Communication Conference/National fibre Optic Engineers Conference*, *Optical Society of America*, San Diego, California, 2008, pp. PDP1.

[52] J. Renaudier, G. Charlet, O. Bertran-Pardo, H. Mardoyan, P. Tran, M. Salsi and S. Bigo, Transmission of 100Gbps coherent PDM-QPSKover 16x100km of standard fibre with all Erbium amplifiers, *Optics Express*, 17 (2009) 5112-5119.

[53] P. J. Winzer and A. H. Gnauck, 112-Gbps polarization-multiplexed 16-QAM on a 25-GHz WDM grid, *34th European Conference on Optical Communication, 2008. ECOC 2008.* 2008, pp. 1-2.

[54] F. Koyama, Recent advances of VCSEL photonics, *Journal of Lightwave Technology*, 24 (2006) 4502-4513.

[55] Princeton Optronics http://www.newmetals.co.jp/pdf/234.pdf, in, 2013. Accessed 30th July 2014.

[56] Finisar, http://www.myvcsel.com/designing-with-vcsels/, in, 2013. Accessed 28th Aug. 2014.

[57] K. Iga, Surface-emitting laser-its birth and generation of new optoelectronics field, *IEEE Journal Selected Topics Quantum Electron*, 6 (2000) 1201-1215.

[58] K. Iga, Surface emitting laser, *Trans. IEICE C-I*, 1998, pp. 483-493.

[59] VertilasGmbH, Communications VCSEL product catalog. Rev. 5.0 in, http://www.vertilas.com/pdf/VERTILAS_Communications_V5_0.pdf, 2007. Accessed 28th August 2014.

[60] H. Soda, K.-i. Iga, C. Kitahara and Y. Suematsu, GaInAsP/InP surface emitting injection lasers, *Japanese Journal of Applied Physics*, 18 (1979) 2329-2330.

[61] K. Iga, S. Kinoshita and F. Koyama, Microcavity GalaAs/GaAs surface-emitting laser with I_{th} = 6 mA, *Electronics Letters*, 23 (1987) 134-136.

[62] F. Koyama, S. Kinoshita and K. Iga, Room-temperature continuous wave lasing characteristics of a GaAs vertical cavity surface-emitting laser, *Applied Physics Letters*, 55 (1989) 221-222.

[63] J. L. Jewell, S. L. McCall, A. Scherer, H. H. Houh, N. A. Whitaker, A. C. Gossard and J. H. English, Transverse modes, waveguide dispersion, and 30 ps recovery in submicron GaAs/AlAs microresonators, *Applied Physics Letters*, 55 (1989) 22-24.

[64] R. S. Geels, S. W. Corzine and L. A. Coldren, InGaAs vertical-cavity surface-emitting lasers, *IEEE Journal of Quantum Electronics*, 27 (1991) 1359-1367.

[65] D. L. Huffaker, D. G. Deppe, K. Kumar and T. J. Rogers, Native-oxide defined ring contact for low threshold vertical-cavity lasers, *Applied Physics Letters*, 65 (1994) 97-99.

[66] K.D. Choquette, K.M. Geib, C.I.H. Ashby, R.D. Twesten, O. Blum, H.Q. Hou, D.M. Follstaedt, B.E. Hammons, D. Mathes and R. Hull, Advances in selective wet oxidation of AlGaAs alloys, *IEEE Journal of Selected Topics in Quantum Electronics*, 3 (1997) 916-926.

[67] Y. Hayashi, T. Mukaihara, N. Hatori, N. Ohnoki, A. Matsutani, F. Koyama and K. Iga, Lasing characteristics of low-threshold oxide confinement InGaAs-GaAlAs vertical-cavity surface-emitting lasers, *IEEE Photonics Technology Letters*, 7 (1995) 1234-1236.

[68] K. L. Lear, K. D. Choquette, R. P. Schneider, S. P. Kilcoyne and K. M. Geib, Selectively oxidised vertical cavity surface emitting lasers with 50% power conversion efficiency, *Electronics Letters*, 31 (1995) 208-209.

[69] R. Jager, M. Grabherr, C. Jung, R. Michalzik, G. Reiner, B. Weigl and K. J. Ebeling, 57% wallplug efficiency oxide-confined 850 nm wavelength GaAs VCSELs, *Electronics Letters*, 33 (1997) 330-331.

[70] M. Muller, C. Grasse and M. C. Amann, InP-based 1.3 µm and 1.55 µm short-cavity VCSELs suitable for telecom- and datacom-applications, *14th International Conference on Transparent Optical Networks (ICTON)*, 2012, pp. 1-4.

[71] W. Hofmann, M. Müller, P. Wolf, A. Mutig, T. Gründl, G. Böhm, D. Bimberg and M. C. Amann, 40 Gbit/s modulation of 1550 nm VCSEL, *Electronics Letters*, 47 (2011) 270-271.

[72] A. Gatto, A. Boletti, P. Boffi, E. Ronneberg, C. Neumeyr, M. Ortsiefer and M. Martinelli, 1.3 µm VCSEL transmission performance up to 12.5 Gbit/s for metro access networks, *IEEE Photonics Technology Letters*, 21 (12) (2009) 778–780.

[73] T. Suzuki, S. Imai, S. Kamiya, K. Hiraiwa, M. Funabashi, Y. Kawakita, H. Shimizu, T. Ishikawa and A. Kasukawa, Reliability study of 1060 nm 25 Gbps VCSEL in terms of high speed modulation, *Proc. SPIE 8276*, Vertical-Cavity Surface-Emitting Lasers XVI, 827604, 2012, pp. 04-01 to 04-08.

[74] P. Wolf, P. Moser, G. Larisch, M. Kroh, A. Mutig, W. Unrau, W. Hofmann and D. Bimberg, High-performance 980 nm VCSELs for 12.5 Gbit/s data transmission at 155 degrees C and 49 Gbit/s at-14 degrees C, *Electronics Letters*, 48(7) (2012) 389-390.

[75] D. M. Kuchta, A. V. Rylyakov, C. L. Schow, J. E. Proesel, C. Baks, C. Kocot, L. Graham, R. Johnson, G. Landry, E. Shaw, A. MacInnes and J. Tatum, A 55 Gbps

directly modulated 850nm VCSEL-based optical link, *2012 IEEE Photonics Conference (IPC)*, 2012, pp. 1-2.

[76] D. Kuchta, A. V. Rylyakov, C. L. Schow, J. Proesel, C. Baks, P. Westbergh, J. S. Gustavsson and A. Larsson, 64 Gbps transmission over 57m MMF using an NRZ modulated 850 nm VCSEL, *Optical fibre Communication Conference*, *Optical Society of America*, San Francisco, California, 2014, pp. Th3C.2.

[77] O.F.S. Furukawa, Understanding fibre optics-Attenuation, http://www.ofsoptics.com/resources/UFO-ATT.pdf, 2007. Accessed 4th June 2014.

[78] C. Cole, Beyond 100G client optics, *IEEE Communications Magazine*, 50 (2012) s58-s66.

[79] E. Lach and W. Idler, Modulation formats for 100G and beyond, *Optical Fibre Technology*, 17 (2011) 377-386.

[80] R. Rodes, J. Estaran, B. Li, M. Muller, J. B. Jensen, T. Gruendl, M. Ortsiefer, C. Neumeyr, J. Rosskopf, K. J. Larsen, M. C. Amann and I. T. Monroy, 100 Gbps single VCSEL data transmission link, *Optical fibre Communication Conference and Exposition* and the *National fibre Optic Engineers Conference*, *(OFC/NFOEC)*, 2012, pp. 1-3.

[81] C. Xie, S. Spiga, P. Dong, P. J. Winzer, A. Gnauck, C. Gréus, C. Neumeyr, M. Ortsiefer, M. Müller and M. Amann, Generation and transmission of 100-Gbps PDM 4-PAM using directly modulated VCSELs and coherent detection, *Optical fibre Communication Conference*; OSA Technical Digest (online), San Francisco, California, 2014.

[82] C. Xie, P. Dong, P. Winzer, C. Gréus, M. Ortsiefer, C. Neumeyr, S. Spiga, M. Müller and M. C. Amann, 960-km SSMF transmission of 105.7-Gbps PDM 3-PAM using directly modulated VCSELs and coherent detection, *Optics Express*, 21 (2013) 11585-11589.

[83] C. S. Wang, J. Geske, G. Berdin, F. Talantov, T. Cardellino, H. Garrett, D. Millenheft, V. Kumsomboone and D. Renner, Recent advances in high-power VCSEL arrays, *2012 IEEE Photonics Society Summer Topical Meeting Series*, 2012, pp. 3-4.

[84] J.-F. Seurin, V.K. Guoyang Xu, A. Miglo, J.D. Wynn, P. Pradhan, C.L. Ghosh and L.A. D'Asaro, Progress in high-power high-efficiency VCSEL arrays in: *Proc. SPIE 7229*, Vertical-Cavity Surface-Emitting Lasers XIII, 722903, 2009.

[85] D. Zhou, J.-F. Seurin, G. Xu, A. Miglo, D. Li, Q. Wang, M. Sundaresh, S. Wilton, J. Matheussen and C. Ghosh, Progress on vertical-cavity surface-emitting laser arrays for infrared illumination applications in: *Proc. SPIE 9001*, Vertical-Cavity Surface-Emitting Lasers XVIII, 90010E San Francisco, California, 2014.

[86] M.-C. Amann and W. Hofmann, InP-based long-wavelength VCSELs and VCSEL Arrays, *IEEE Journal of Selected Topics in Quantum Electronics*, 15 (2009) 861-868.

[87] M. Gobet, H. P. Bae, T. Sarmiento and J. S. Harris, GaInNAsSb/GaAs vertical cavity surface-emitting lasers (VCSELs): current challenges and techniques to realize multiple-wavelength laser arrays at 1.55 μm in: C. Lei, J.K. Guenter (Eds.), *Proc. SPIE 6908*, Vertical-Cavity Surface-Emitting Lasers XII, 69080N, San Jose, CA 2008.

[88] C. Chase, Y. Rao, M. Huang and C. Chang-Hasnain, 1550-nm wavelength-tunable HCG VCSELs, *Proc. SPIE 8995*, High Contrast Metastructures III, 89950A, San Francisco, California, United States, 2014.

[89] T. Gruendl, M. Mueller and M.-C. Amann, New standards in high-speed and tunable long wavelength VCSELs, *Proc. SPIE 8432*, Semiconductor Lasers and Laser Dynamics V, Vol. 843203 2012.

[90] C. Gierl, T. Gruendl, P. Debernardi, K. Zogal, C. Grasse, H. A. Davani, G. Böhm, S. Jatta, F. Küppers, P. Meißner and M. C. Amann, Surface micromachined tunable 1.55 μm-VCSEL with 102 nm continuous single-mode tuning, *Optics Express*, 19 (2011) 17336-17343.

[91] M.-C. Amann, E. Wong and M. Mueller, Energy-efficient high-speed short-cavity VCSELs, *Optical fibre Communication Conference*, *Optical Society of America*, Los Angeles, California, 2012, pp. OTh4F.1.

[92] P. Westbergh, R. Safaisini, E. Haglund, B. Kogel, J. S. Gustavsson, A. Larsson, M. Geen, R. Lawrence and A. Joel, High-speed 850 nm VCSELs with 28 GHz modulation bandwidth operating error-free up to 44 Gbit/s, *Electronics Letters*, 48 (2012) 1145-1147.

[93] T. Gruendl, M. Mueller, C. Grasse, K. Vizbaras and M. Amann, Recent results on long-wavelength VCSELs: Device structures, performance and applications, *2012 IEEE Photonics Conference (IPC)*, 2012, pp. 112-113.

[94] M. Mueller, T. Gruendl, M. Horn, R. Nagel, W. Wiedmeier, E. Roenneberg, G. Boehm and M. C. Amann, Small-signal analysis of high-temperature stable 1550 nm high-speed VCSELs, *6th Joint Symposium Opto- Microelectronic Devices Circuits*, Berlin, Germany, 2010.

[95] M. Muller, W. Hofmann, T. Grundl, M. Horn, P. Wolf, R .D. Nagel, E. Ronneberg, G. Bohm, D. Bimberg and M.-C. Amann, 1550-nm high-speed short-cavity VCSELs, *IEEE Journal of Selected Topics in Quantum Electronics*, 17 (2011) 1158-1166.

[96] M. Ortsiefer, B. Kögel, J. Rosskopf and C. Neumeyr, Long Wavelength High Speed VCSELs for Long Haul and Data Centers, *Optical fibre Communication Conference, Optical Society of America*, San Francisco, California, 2014, pp. W4C.2.

[97] R. Gamatham, E. Rotich, A. Leitch and T. Gibbon, Fibre-to-the-hut: Research into tailored FTTH solutions for Africa, *AFRICON 2013*, 2013, pp. 1-5.

[98] T. B. Gibbon, K. Prince, C. Neumeyr, E. Ronneberg, M. Ortsiefer and I. T. Monroy, 10 Gbps 1550 nm VCSEL transmission over 23.6 km single mode fibre with no dispersion compensation and no injection locking for WDM PONs, *Optical fibre Communication (OFC), collocated National fibre Optic Engineers Conference, 2010 Conference on (OFC/NFOEC)*, 2010, pp. 1-3.

[99] K. Prince, M. Ma, T. B. Gibbon and I.T. Monroy, Demonstration of 10.7-Gbps transmission in 50-km PON with uncooled free-running 1550-nm VCSEL, *2010 Conference on Lasers and Electro-Optics (CLEO) and Quantum Electronics and Laser Science Conference (QELS)*, 2010, pp. 1-2.

[100] L. Deng, Z. Ying, P. Xiaodan, Y. Xianbin, J.B. Jensen, L. Deming and I. T. Monroy, Colorless ONU based on all-VCSEL sources with remote optical injection for WDM-PON, *2011 IEEE Photonics Conference (PHO)*, 2011, pp. 220-221.

[101] E. Wong, X. Zhao, C.J. Chang-Hasnain, W. Hofmann and M.C. Amann, Optically injection-locked 1.55-um VCSELs as upstream transmitters in WDM-PONs, *IEEE Photonics Technology Letters*, Vol. 18, No. 22. (2006) 2371-2373.

[102] Y. Matsui, D. Mahgerefteh, Z. Xueyan, C. Liao, Z.F. Fan, K. McCallion and P. Tayebati, Chirp-managed directly modulated laser (CML), *IEEE Photonics Technology Letters*, 18 (2006) 385-387.

[103] Z. Bo, Z. Xiaoxue, L. Christen, D. Parekh, W. Hofmann, M. C. Wu, M.-C. Amann, C. J. Chang-Hasnain and A. E. Willner, Adjustable chirp injection-locked 1.55-μm VCSELs for enhanced chromatic dispersion compensation at 10-Gbit/s, *Optical fibre communication/National fibre Optic Engineers Conference, 2008. OFC/NFOEC*, 2008, pp. 1-3.

[104] K.Y. Kim, (Ed), *Advances in Optical and Photonic Devices*, INTECH, Croatia, 2010.

[105] W. W. Chow, K. D. Choquette, M. H. Crawford, K. L. Lear and G. R. Hadley, Design, fabrication, and performance of infrared and visible vertical-cavity surface-emitting lasers, *IEEE Journal of Quantum Electronics*, 33 (1997) 1810-1824.

[106] C. W. Wilmsen, H. Temkin and L. A. Coldren, (Eds), *Vertical-cavity surface-emitting lasers: Design, fabrication, characterization, and applications*, Cambridge University press, Cambridge, UK, 1999.

[107] R. Michalzik, (Ed.), *VCSELs: Fundamentals, technology and applications of vertical-cavity surface-emitting lasers*, Springer, Berlin Heidelberg, 2013.

[108] J. K. Guenter, R. A. Hawthorne, D. N. Granville, M. K. Hibbs-Brenner and R. A. Morgan, Reliability of proton-implanted VCSELs for data communications, *SPIE, Vol. 2683* No. 1, 1996, pp. 102-113.

[109] N. Suzuki, T. Anan, H. Hatakeyama and M. Tsuji, Low resistance tunnel junctions with type-II heterostructures, *Applied Physics Letters*, 88 (2006) 231103.

[110] Raycan, 1310 nm / 1550 nm VCSEL structure in RayCan http://www.raycan.com/tech_7.html, 2007. Accessed 7th August 2014.

[111] Raycan, VCSEL data sheets: 10 Gbps 1310 nm, 100615 Rev 1.0 (RC24xxx1-F) and 4.5 Gbps 1550 nm (RC33xxx1-F), 090115 Rev 4.0, 2013. Accessed 29th May 2014.

[112] Finisar, Designing with the AOC 10 Gbps TOSA and ROSA, Application note. http://www.finisar.com/sites/default/files/pdf/Application_Note_Designing_with_the_AOC_10Gbps_TOSA_and_ROSA.pdf, 2007. Accessed 29th May 2014.

[113] P. J. Winzer, *Optical transmitters, receivers, and noise: Wiley Encyclopaedia of Telecommunications*, J. G. Proakis (Ed), pp 1824-1840, 2002.

[114] I. Kaminow, T. Li, *Optical fibre telecommunications IV A: Components*, 4th ed., Academic Press, San Diego, CA, 2002.

[115] K. Sung Kee, O. Mizuhara, Y. K. Park, L. D. Tzeng, Y. S. Kim and J. Jichai, Theoretical and experimental study of 10 Gbps transmission performance using 1.55 μm LiNbO3-based transmitters with adjustable extinction ratio and chirp, *Journal of Lightwave Technology*, 17 (1999) 1320-1325.

[116] E. L. Wooten, K. M. Kissa, A. Yi-Yan, E. J. Murphy, D.A. Lafaw, P. F. Hallemeier, D. Maack, D. V. Attanasio, D. J. Fritz, G. J. McBrien and D. E. Bossi, A review of lithium niobate modulators for fibre-optic communications systems, *IEEE Journal of Selected Topics in Quantum Electronics*, 6 (2000) 69-82.

[117] K. Goi, K. Oda, H. Kusaka, Y. Terada, K. Ogawa, T.-Y. Liow, X. Tu, G.-Q. Lo and D.-L. Kwong, 11-Gbps 80-km transmission performance of zero-chirp silicon Mach-Zehnder modulator, *Optics Express*, 20 (2012) B350-B356.

[118] T. L. Koch and R. A. Linke, Effect of nonlinear gain reduction on semiconductor laser wavelength chirping, *Applied Physics Letters*, 48 (1986) 613-615.

[119] L. Bjerkan, A. Royset, L. Hafskjaer and D. Myhre, Measurement of laser parameters for simulation of high-speed fibreoptic systems, *Journal of Lightwave Technology*, 14 (1996) 839-850.

[120] C. H. Henry, Theory of the linewidth of semiconductor lasers, *IEEE Journal of Quantum Electronics, QE-*, 18(2) (1982) 259–264.

[121] S. R. Forrest, Optical detectors: Three contenders: Depending on the application, the photoconductor, p-i-n diode, or avalanche photodiode may prove the best choice, *IEEE Spectrum*, 23 (1986) 76-85.

[122] J. C. Campbell, *Heterojunction photodetectors for optical communications*, in: N.G. Einspruch, W.R. Frensley (Eds.) *Heterostructures and quantum devices*, Academic, New York, 1994.

[123] J. C. Campbell, Recent advances in telecommunications Avalanche photodiodes, *Journal of Lightwave Technology*, 25 (2007) 109-121.

[124] S. M. Sze, *Physics of semiconductor devices*, Wiley-Interscience, New York, 1969.

[125] K. Taguchi, *P-I-N photodiodes* in: A. K. Dutta, N. K. Dutta, M. Fujiwara (Eds.) *WDM technologies; Active optical components*, Elsevier Science, Academic, San Diego, California, USA, 2002.

[126] G. Keiser, *Optical fibre communication*, 3rd ed., Mc-Graw-Hill, Singapore, 2000.

[127] M. Kobayashi and T. Mikawa, *Avalanche photodiodes*, in: A. K. Dutta, N. K. Dutta, M. Fujiwara (Eds.) *WDM technologies; Active optical components*, Elsevier Science, Academic, San Diego, California, USA, 2002.

[128] L. Kazovsky, N. Cheng, W. Shaw, D. Gutierrez and S. Wong, *Broadband optical access networks*, Wiley, Hoboken, New Jersey, 2011.

[129] Discovery Semiconductors, PIN and APD data sheets; http://discoverysemi.com/Product%20Pages/DSCR402 PIN.php and http://discoverysemi.com/Product%20Pages/DSCR402APD.php., 2012. Accessed 15th Aug 2014.

[130] J. Hecht, *Understanding fibre optics*, 3rd ed., Prentice-Hall, Inc, Upper Saddle River, New Jersey, 1999.

[131] R. C. Neat and G. Kuyt, Optical fibre standards-people, places and products of IEC, *54^{th} IWCS/FOCUS Conference: Proceedings of the International Wire & Cable Symposium (IWCS),* Providence, Rhode Island, USA, 2005.

[132] W. B. Gardner and A. H. Cherin, The status of international fibre measurement tests, *Technical Digest Symposium on Optical Fibre Measurement, National institute of standards and technology*, 2000, pp. 73-76.

[133] J. Ainslie and C. R. Day, A review of single-mode fibres with modified dispersion characteristics, *Journal of Lightwave Technology*, LT-4 No. 8 (1986) 967-979.

[134] ITU-T, Recommendations G.651.1: Characteristics of a 50/125 µm multimode graded index optical fibre cable for the optical access network, 2011.

[135] ITU-T, Recommendations G.652: Characteristics of a single-mode optical fibre cable, 2009.

[136] ITU-T, Recommendations G.655: Characteristics of a non-zero dispersion shifted, single-mode optical fibre and cable, 2009.

[137] ITU-T, Recommendations G.657: Characteristics of a bending-loss insensitive single-mode optical fibre and cable for the access network, 2012.

[138] G. P. Agrawal, *Nonlinear fibre optics*, 4^{th} ed., Academic Press, San Diego, CA, 2007.

[139] Invocom website: http://www.invocom.et.put.poznan.pl/~invocom/C/P1-9/swiatlowody_en/p1-1_2_2.htm. Accessed 23^{rd} May 2014.

[140] L. N. Binh, *Optical fibre communication systems: theory with matlab and simulink models*, CRC press, Boca Raton, FL, 2010.

[141] E. Collett, *Field guide to polarization*, SPIE Press, Bellingham, WA 2005.

[142] M. Born and E. Wolf, *Principles of optics*, 7^{th} Ed., Cambridge University press, Cambridge, UK, 2003.

[143] D. Derickson, (Ed.), *Fibre optic test and measurement*, Prentice-Hall, Upper Saddle River, NJ, 1998.

[144] M. Karlsson, Polarization mode dispersion induced pulse broadening in optical fibres, *Optics Letters*, 23 (1998) 688-690.

[145] J. Cameron, C. Liang, B. Xiaoyi and J. Stears, Time evolution of polarization mode dispersion in optical fibres, *IEEE Photonics Technology Letters*, 10 (1998) 1265-1267.

[146] W. T. Ireeta, V. Musara and A. W. R. Leitch, Monitoring FO-PMD and SO-PMD over time with respect to environmental conditions, *Applied Physics Research,* Vol. 6, No. 4 (2014).

[147] C. D. Poole and J. Nagel, *Polarization effects in lightwave systems*, in *Optical Fibre Telecommunications, vol. III A*, in: I.P. Kaminov, T.L. Koch (Eds.), Academic Press, San Diego, 1997.

[148] F. Kapron, A. Dori, J. Peters and H. Knehr, Polarization-mode dispersion: Should you be concerned?, *NFOEC'96*, Denver, 1996, pp. 757-768.

[149] H. Paul, *Polarization mode dispersion measurement by Jones matrix Eigen analysis and wavelength scanning methods*, Hewlett Packard Lightwave Operations Technical Report, Santa Rosa, CA, USA, 1997.

[150] C. Shen, C. Zhong, Y. You, J. Chu, X. Zou, X. Dong, Y. Jin, J. Wang and H. Gong, Polarization-dependent curvature sensor based on an in-fibre Mach-Zehnder interferometer with a difference arithmetic demodulation method, *Optics Express*, 20 (2012) 15406-15417.

[151] F. Liu, C. J. Lee, J. Chen, E. Louis, P. J. M. van der Slot, K. J. Boller and F. Bijkerk, Ellipsometry with randomly varying polarization states, *Optics Express*, 20 (2012) 870-878.

[152] J. Fatome, S. Pitois, P. Morin and G. Millot, Observation of light-by-light polarization control and stabilization in optical fibre for telecommunication applications, *Optics Express*, 18 (2010) 15311-15317.

[153] A. Galtarossa, L. Palmieri, M. Schiano and T. Tambosso, Statistical characterization of fibre random birefringence, *Optical Letters*, Vol. 25 No. 18 (2000) 1322-1334.

[154] J. Cameron, L. Cheng, X. Bao and J. Stears, Time evolution of polarization mode dispersion in optical fibres, *IEEE Photonics Technology Letters*, Vol. 10 No. 9 (1998) 1265-1267.

[155] S. C. Rashleigh, Origins and control of polarization effects in single-mode fibres, *Journal of Lightwave Technology*, 1 (1983) 312-331.

[156] B. Xiaoyi, D. S. Waddy and C. Liang, Polarization fluctuations in field fibres, *The 17th Annual Meeting of the IEEE Lasers and Electro-Optics Society, 2004. LEOS 2004*, 2004, pp. 82-83.

[157] T. Imai and T. Matsumoto, Polarization fluctuations in a single-mode fibre, *Journal of Lightwave Technology*, 6 No. 9 (1988) 1366-1375.

[158] G. D. VanWiggeren and R. Roy, Transmission of linearly polarized light through a single-mode fibre with random fluctuations of birefringence, *Applied Optics*, 38 (1999) 3888-3892.

[159] S. Yao, *Polarization in fibre systems: Squeezing out More bandwidth*, The Photonics Handbook, http://www.generalphotonics.com/Old_Website/pdf/PSReprint.pdf, in, Laurin Publishing, 2003. Accessed 1st August 2014.

[160] M. Martinelli, P. Martelli and S. M. Pietralunga, Polarization stabilization in optical communications systems, *Journal of Lightwave Technology*, 24 (2006) 4172-4183.

[161] G. B. Xavier, G. Vilela de Faria, G. P. Temporão and J. P. von der Weid, Full polarization control for fibre optical quantum communication systems using polarization encoding, *Optics Express*, 16 (2008) 1867-1873.

[162] J. Noda, K. Okamoto and Y. Sasaki, Polarization-maintaining fibres and their applications, *Journal of Lightwave Technology*, 4 (1986) 1071-1089.

[163] FibrePulse, Polarization maintaining fibre optic technology, http://www.fibrepulse.com/html/polar1.html, Accessed 1st Aug 2014.

[164] Y. He, B. J. Orr, K. G. H. Baldwin, M. J. Wouters, A. N. Luiten, G. Aben and R. B. Warrington, Stable radio-frequency transfer over optical fibre by phase-conjugate frequency mixing, *Optics Express*, 21 (2013) 18754-18764.

[165] B. Costa, D. Mazzoni, M. Puleo and E. Vezzoni, Phase shift technique for the measurement of chromatic dispersion in optical fibres using LED's, *IEEE Journal of Quantum Electronics*, 18 (1982) 1509-1515.

[166] L. Cohen and C. Lin, Pulse delay measurements in the zero material dispersion wavelength region for optical fibres, *Applied Optics*, 16 (1977) 3136-3139.

[167] J. Hult, R. S. Watt and C. F. Kaminski, Dispersion measurement in optical fibres using supercontinuum pulses, *Journal of Lightwave Technology*, 25 (2007) 820-824.

[168] M. Tateda, N. Shibata and S. Seikai, Interferometric method for chromatic dispersion measurement in a single-mode optical fibre, *IEEE Journal of Quantum Electronics*, 17 (1981) 404-407.

[169] L. Thevenaz, J. Pellaux and J. V. D. Weid, All fibre interferometer for chromatic dispersion measurements, *Journal of Lightwave Technology*, Vol. 6, No.1 (1988) 1-7.

[170] J. Y. Lee and D. Y. Kim, Versatile chromatic dispersion measurement of a single mode fibre using spectral white light interferometry, *Optics Express*, 14 (2006) 11608-11615.

[171] P. A. Merritt, R. P. Tatam and D. A. Jackson, Interferometric chromatic dispersion measurements on short lengths of monomode optical fibre, *Journal of Lightwave Technology*, 7 (1989) 703-716.

[172] K.S. Abedin, M. Hyodo and N. Onodera, Measurement of the chromatic dispersion of an optical fibre by use of a Sagnac interferometer employing asymmetric modulation, *Optics Letters*, 25 (2000) 299-301.

[173] L. Zong, F. Luo, S. Cui and X. Cao, Rapid and accurate chromatic dispersion measurement of fibre using asymmetric Sagnac interferometer, *Optics Letters*, 36 (2011) 660-662.

[174] L. G. Cohen, Comparison of single-mode fibre dispersion measurement techniques, *Journal of Lightwave Technology*, 3 (1985) 958-966.

[175] A. Gumaste and T. Antony, *DWDM network designs and engineering solutions*, Cisco Press, Indianapolis, IN 46290 USA, 2002.

[176] M. M. E. Said, J. Sitch and M. I. Elmasry, An electrically pre-equalized 10-Gbps duobinary transmission system, *Journal of Lightwave Technology*, 23 (2005) 388-400.

[177] J. A. P. Morgado and A. T. Cartaxo, Dispersion supported transmission technique: comparison of performance in anomalous and normal propagation regimes, *IEEE Proceedings of Optoelectronics*, 148 (2001) 107-116.

[178] A. Sano, Y. Miyamoto, S. Kuwahara and H. Toba, A 40-Gbps/ch WDM transmission with SPM/XPM suppression through prechirping and dispersion management, *Journal of Lightwave Technology*, 18 (2000) 1519-1527.

[179] T. Mizuochi, Forward error correction in next generation optical communication systems, *2009 Conference on Lasers and Electro-Optics and Quantum electronics and Laser Science Conference. CLEO/QELS,* 2009, pp. 1-2.

[180] S. Kaneko, J.-I. Kani, K. Iwatsuki, A. Ohki, M. Sugo and S. Kamei, Scalability of spectrum-sliced DWDM transmission and its expansion using forward error correction, *Journal of Lightwave Technology*, 24 (2006) 1295-1301.

[181] S. Huan, K. Byoung-Whi and B. Mukherjee, Long-reach optical access networks: A survey of research challenges, demonstrations, and bandwidth assignment mechanisms, *IEEE Communications Surveys & Tutorials*, 12 (2010) 112-123.

[182] X. Li, X. Chen, G. Goldfarb, E. Mateo, I. Kim, F. Yaman and G. Li, Electronic post-compensation of WDM transmission impairments using coherent detection and digital signal processing, *Optics Express*, 16 (2008) 880-888.

[183] M. G. Taylor, Coherent detection method using DSP for demodulation of signal and subsequent equalization of propagation impairments, *IEEE Photonics Technology Letters*, 16 (2004) 674-676.

[184] E. M. Ip and J. M. Kahn, Fibre impairment compensation using coherent detection and digital signal processing, *Journal of Lightwave Technology*, 28 (2010) 502-519.

[185] S. J. Savory, G. Gavioli, R. I. Killey and P. Bayvel, Electronic compensation of chromatic dispersion using a digital coherent receiver, *Optics Express*, 15 (2007) 2120-2126.

[186] G. S. He, Optical phase conjugation: principles, techniques, and applications, *Prog. in Quantum Electronics,* 26, (2002) 131–191.

[187] S. Ramachandran, *Fibre based dispersion compensation*, Springer, New York USA, 2007.

[188] K. Aikawa, J. Yoshida, S. Saitoh, M. Kudoh and K. Suzuki, Dispersion compensating fibre module, *Fujikura Technical review.* http://www.fujikura.co.jp/eng/products/tele/o_device/data/td5000b.pdf, (2011) 16-22.

[189] G. Prabhakar, A. Peer, V. Rastogi and A. Kumar, Large-effective-area dispersion-compensating fibre design based on dual-core microstructure, *Applied Optics*, 52 (2013) 4505-4509.

[190] S. Knudsen and T. Veng, Large effective area dispersion compensating fibre for cabled compensation of standard single mode fibre, *Optical fibre Communication Conference*, *Optical Society of America*, Baltimore, Maryland, 2000, pp. TuG5.

[191] L. Gruner-Nielsen, T. Veng, S. N. Knudsen, C. C. Larsen and B. Edvold, New dispersion compensating fibres for simultaneous compensation of dispersion and dispersion slope of non-zero dispersion shifted fibres in the C or L band, *Optical fibre Communication Conference*, 2000, pp. 101 - 103.

[192] C. Peucheret, I. Munoz, F. Liu, A. Buxens and S. N. Knudsen, L-band transmission over 1000 km using standard and dispersion-compensating fibres in pre-compensation scheme optimised at 1550 nm, *Electronics Letters*,Volume 35 , Issue 20 (1999) 1759 - 1761.

[193] S. N. Knudsen, M.O. Pedersen and L. Gruner-Nielsen, Optimisation of dispersion compensating fibres for cabled long-haul applications, *Electronics Letters*, Volume 36, Issue 25 (2000) 2067 - 2068.

[194] C. Peucheret, T. Tokle, S. N. Knudsen, C. J. Rasmussen and P. Jeppesen, System performance of new types of dispersion compensating fibres, *Lasers and Electro-Optics, CLEO '01*. Technical Digest, 2001.

[195] T. Tokle, C. Peucheret and P. Jeppesen, System Optimisation of dispersion maps using new cabled dispersion compensating fibres, *Journal of Optical Communications*, Vol. 25(2) (2004) 41-80.

[196] L. Gruner-Nielsen, S. N. Knudsen, T. Veng, B. Edvold and C. C. Larsen, Design and manufacture of dispersion compensating fibre for simultaneous compensation of dispersion and dispersion slope, in: *Optical fibre Communication Conference 1999,* and *the International Conference on Integrated Optics and Optical fibre Communication. OFC/IOOC '99*. Technical Digest, 1999, Vol.232, pp. 232-234.

[197] E. J. Woodbury and W. K. Ng, First demonstration of stimulated Raman scattering, *Proc. IRE* 50, 2347, 1962.

[198] J. I. Gersten, R. R. Alfano and M. Belic, Combined stimulated Raman scattering and continuum self-phase modulation, *Physical Reviews A*, Vol. 21 (1980) 1222-1224.

[199] C. Headley and G. P. Agrawal, *Raman amplification in fibre optical communication systems*, Elsevier Academic press, San Diego, CA, 2005.

[200] M. N. Islam, Raman amplifiers for telecommunications, *IEEE Journal of Selected Topics in Quantum Electronics*, Vol. 8, No. 3 (2002) 548-559.

[201] D. B. M. Pereira, A. L. J. Teixeira, M. J. N. Lima, P. S. B. André, H. C. C. Fernandes and J. R. F. d. Rocha, Raman amplifiers for use in WDM Systems, *Revista Do Detua*, 2003.

[202] Finisar, White paper, Applications for distributed Raman amplification, in, http://www.finisar.com/sites/default/files/pdf/Applications_for_Distributed_ Raman_Amplification.pdf, 2012. Accessed 5th August 2014.

[203] R. H. Stolen and E. P. Ippen, Raman gain in glass optical waveguides, *Applied Physics Letters,* 22, (1973) 276–281.

[204] Q. Lin and G. P. Agrawal, Vector theory of stimulated Raman scattering and its application to fibre-based amplifiers, *Optical Society of America B20*, (2003) 1616-1631.

[205] C. R. S. Fludger, V. Handerek and R. J. Mears, Pump to signal RIN transfer in Raman fibre amplifiers, *Journal of Lightwave Technology*, 19 (2001) 1140-1148.

[206] P. Gallion, J. Zhou, S. Jiang, J. Chen and Y. Jaouën, Noise in distributed Raman Amplification, *Proc. of SPIE*, Vol 6781, 6781U, 2007.

[207] R. Roberge, Case study: PMD measurement on aerial fibre under wind-induced oscillations and vibrations, in, *EXFO Electro Optical Engineering Inc. Technical Note* 039, 2009.

[208] T. B. Gibbon, E. K. Rotich, H. Y. S. Kourouma, R. R. G. Gamatham, A. W. R. Leitch, R. Siebrits, R. Julie, S. Malan, W. Rust, F. Kapp, T. L. Venkatasubramani, B. Wallace, A. Peens-Hough and P. Herselman, Fibre-to-the-telescope: MeerKAT, the South African precursor to square kilometre telescope array (SKA), *Proc. SPIE 9008*, Optical Metro Networks and Short-Haul Systems VI, 2003, pp. 90080P-90080P-90086.

[209] E. K. R. Kipnoo, H. Y. S. Kourouma, R. R. Gamatham, A. W. R. Leitch, T. B. Gibbon, R. Julie, R. Siebrits and F. Kapp, Characterization of the polarization mode dispersion of single mode fibre in KAT-7 telescope array network, South Africa, *Africon 2013*, 2013, pp. 1-4.

[210] VPI transmission Maker/VPI component Maker, VPI photonics, 2013.

[211] P. Westbergh, *Design, fabrication, and evaluation of high-speed vertical-cavity surface-emitting lasers*, Thesis for the degree of licentiate of engineering, Chalmers University of Technology, Göteborg, Sweden, 2009.

[212] C. Gierl, T. Gründl, S. Paul, K. Zogal, M. T. Haidar, P. Meissner, M. C. Amann and F. Küppers, Temperature characteristics of surface micromachined MEMS-VCSEL with large tuning range, *Optics Express*, 22 (2014) 13063-13072.

[213] E. K. R. Kipnoo, H. Kourouma, T. V. Chabata, R. R. G. Gamatham, A. W. R. Leitch and T. B. Gibbon, Optimizing VCSEL transmission for longer reach in optical access networks, *16th annual Southern Africa telecommunication networks and applications conference (SATNAC)*, Spier, Stellenbosch, Western Cape, South Africa, 2013, pp. 27-30.

[214] Modulating VCSELs, Application sheet, Honeywell. http://www.imedea.uib.es/~salvador/coms_optiques/addicional/app_notes/ honeywell_1.pdf, Accessed 29th May 2014.

[215] K. Petermann, *Laser diode modulation and noise*, Kluwer Academic, Dordrecht, 1988.

[216] B. R. Bennett, R. A. Soref and J. A. D. Alamo, Carrier-induced change in refractive index of InP, GaAs and InGaAsP, *IEEE Journal of Quantum Electronics*, 26 (1), (1990).

[217] Infinera Website, www.infinera.com/pdfs/whitepapers/Infinera_Coherent_Tech.pdf, CA 94089 USA, 2012. Accessed 30$^{\text{th}}$ July 2014.

[218] S. Wassin, E. K. Rotich Kipnoo, R. R. G. Gamatham, A. W. R. Leitch, T. B. Gibbon, A performance analysis of the phase shift and pulse delay techniques for chromatic dispersion measurements and compensation in single mode fibre, R. Volkwyn (Ed.) *Proceedings of the 17*$^{\text{th}}$ *annual Southern Africa Telecommunication Networks and Applications Conference (SATNAC)*, Boardwalk-Port Elizabeth, South Africa, 31$^{\text{st}}$ Aug. to 3$^{\text{rd}}$ Sept . 2014, pp. 155-159.

[219] S. Wassin, E. K. Rotich Kipnoo, R. R. G. Gamatham, A. W. R. Leitch, T. B. Gibbon, Using a VCSEL to accurately measure chromatic dispersion in single mode fibre by the phase shift technique, *Proceedings of the 59*$^{\text{th}}$ *Annual Conference of the South African institute of physics (SAIP)*, University of Johannesburg, 7-11$^{\text{th}}$ Jul. 2014. In press.

[220] O.F.S. Truewave, RS fibre low water peak data sheet, http://www.gatelsupply.com/index.cfm/feature/285_54/truewavers-low-water- peak-fibre—-ofs.cfm, 2009. Accessed 30$^{\text{th}}$ July 2014.

[221] O.F.S. Truewave, Ocean fibres SRS data sheet, http://fibre-optic-catalog.ofsoptics.com/Asset/TrueWaveSRS fibre-121-web.pdf, 2013. Accessed 30$^{\text{th}}$ July 2014.

[222] E. K. Rotich Kipnoo, H. Y. S. Kourouma, R. R. G. Gamatham, A. W. R. Leitch and T. B. Gibbon, Chromatic dispersion compensation for VCSEL transmission for applications such as Square Kilometre Array South Africa, R. Botha, T. Jili (Eds.) *Proceedings of the 58*$^{\text{th}}$ *Annual Conference of the South African institute of physics (SAIP)*, University of Zululand, 8-12$^{\text{th}}$ Jul. 2013, pp. 490-495.

[223] R. Kjær, I. T. Monroy, L. K. Oxenløwe, P. Jeppesen and B. Palsdottir, Impairments due to burst-mode transmission in a Raman-based long-reach PON link, *IEEE Photonics Technology Letters*, Vol. 19, No. 19 (2007) 1490-1492.

[224] I. T. Monroy, R. Kjær, F. Öhman, K. Yvind and P. Jeppesen, Distributed fibre Raman amplification in long reach PON bidirectional access links, Optical Fibre Technology, 14 (2008) 41–44.

[225] R. Kjaer, I. T. Monroy, L. K. Oxenloewe, P. Jeppesen and B. Palsdottir, Bi-directional 120 km long-reach PON link based on distributed Raman amplification, *19th Annual*

Meeting of the IEEE Lasers and Electro-Optics Society, 2006. LEOS 2006, 2006, pp. 703-704.

[226] O.F.S. Truewave, Truewave Reach fibre, low water peak. http://fibre-optic-catalog.ofsoptics.com/Asset/TrueWaveREACHfibre-124-web.pdf, 2013. Accessed 7$^{\text{th}}$ August 2014.

[227] T. Geisler and B. Pálsdóttir, Selecting the right NZDF fibre for distributed Raman amplification . http://fibre-optic-catalog.ofsoptics.com/Asset/NZDF-for-Distributed-Raman-Amplification.pdf, 2006. Accessed 7$^{\text{th}}$ August 2014.

[228] E. K. Rotich Kipnoo, T. V. Chabata, R. R. G. Gamatham, A. W. R. Leitch and T. B. Gibbon, Experimental demonstration of Raman amplification in vertical cavity surface emitting lasers for extended reach access networks, R. Volkwyn (Ed.) *Proceedings of the 17$^{\text{th}}$ annual Southern Africa Telecommunication Networks and Applications Conference (SATNAC)*, Boardwalk-Port Elizabeth, South Africa, 31$^{\text{st}}$ Aug. to 3$^{\text{rd}}$ Sept. 2014, pp. pp. 21-24.